

Master Thesis

Three-Dimensional Finite Element Analysis of Offshore Jack-Up Structures Accounting for Non-linear Soil-Structure Interaction

Author: Robbin Schipper



MASTER THESIS

Three-Dimensional Finite Element Analysis of Offshore Jack-Up Structures Accounting for Non-Linear Soil-Structure Interaction

by

Robbin Schipper

Delft, 24 November 2016

Final report

Faculty of Civil Engineering and Geosciences - Delft University of Technology

Student

Robbin Schipper

Van Hasseltlaan 558
2625 JJ Delft
Tel. +31 (0)6 20180087
R.H.J.Schipper@student.tudelft.nl
4394011

Assessment committee

Chair

Prof. dr. C. Jommi

TU Delft , Faculty of Civil Engineering and Geosciences
Department of Geo-Engineering
Tel. +31(0) 15 27 84173
C.Jommi@tudelft.nl

Daily supervisor TU Delft

Dr. F. Pisano

TU Delft , Faculty of Hydraulic Engineering
Department of Offshore Engineering
Tel. +31 (0)15 27 88030
F.Pisano@tudelft.nl

Daily supervisor TNO DIANA BV

Dr. G. Schreppers

TNO DIANA BV
Tel. +31 (0)6 51534867
G.Schreppers@tnodiana.com

Supervisor TU Delft

Dr. A. Tsouvalas

TU Delft, Faculty of Hydraulic Engineering
Department of Offshore Engineering
Tel. +31 (0)15 27 89225
A.Tsouvalas@tudelft.nl

Three-dimensional finite element analysis of offshore jack-up structures accounting for non-linear soil-structure interaction

November 17, 2016

Robbin Schipper¹

Abstract

Jack-up structures are widely used in the offshore industry. Not only in the field of oil and gas, but also in the installation for offshore wind turbines. These jack-up structures typically consist of three trusswork legs, where the foundation is formed by inverted conical cones that are penetrated into the soil, called spudcans. The spudcans transfer the combination of weight and environmental loading to the underlying soil. Jack-up structures are assessed for each particular offshore site, where their stability is checked for a 50 year return period storm as prescribed by the current guidelines. The behaviour of the jack-up structures is strongly influenced by the restraint given by the spudcan footings. This phenomenon is generally described as fixity and is a complicated effect, governed by the interaction between soil and structure. To properly take into account this effect, computational models are needed that incorporate the complicated non-linear behaviour of the jack-up foundation in a structural framework. This paper describes the three-dimensional finite element modelling of a generic jack-up structure, that takes into account the interaction of soil and structure. Through calibration, the complicated non-linear behaviour of the soil is captured in the model. A benchmark study is performed, where the prediction of the finite element model is compared to experimental tests, as well as a macroelement model. This comparison shows that the finite element model is capable of describing the global behaviour of the jack-up unit under loading, as well as the behaviour of the individual spudcan footings. Furthermore, it has been shown through parametric analyses that emphasis should be placed on the calibration of soil parameters under compression, especially at high stresses. The dilative behaviour of the soil has a positive influence on both the global capacity and stiffness, as does an increase of preloading of the structure. The loading direction along the axis of symmetry provides the highest global capacity and stiffness of the rig during loading. Torsional loading of the structure predicts a significant torsional moment at the spudcan footings and predicts a rotation of these footings in the soil. The incorporation of a large-deformation finite element framework has shown to be crucial in the proper prediction of the behaviour of the jack-up structure during push-over loading.

Keywords: Jack-up structure; Shallow foundation; Offshore engineering; Finite element modelling; Soil-structure interaction

¹Corresponding author. E-mail: R.H.J.Schipper@student.tudelft.nl

1 Introduction

1.1 General aspects

Mobile jack-up units are widely used in the offshore industry for drilling in shallow to moderate water depths as well as being used as a structure in the installment of offshore wind turbines. Due to their simple and quick installation procedure, jack-up platforms are cost effective platforms that can be used in the offshore oil and gas exploration (Randolph and Gourvenec, 2011; Bienen and Cassidy, 2006). Modern jack-up units (Figure 1) used for exploratory drilling typically consist of a triangular hull and three independent trusswork legs (Bienen and Cassidy, 2009). Jack-up units can be self propelled or towed to the installation site. Several consecutive steps are then taken to install the jack-up structure (Figure 2). The jack-up unit is first afloat, after which its legs are lowered onto the seabed. The weight of the topside of the jack-up is then used to allow for the jack-up footings to penetrate the seabed. After penetration, the jack-up is preloaded by pumping water in ballast tanks, located at the topside. The preloading typically results in a larger penetration, after which the load on the spudcan is carried by its area. The preloading also prestresses the foundation to ensure that the bearing capacity exceeds the anticipated extreme load during storm conditions ((Ng and Lee, 2002)). After preloading, the water is removed from the ballast tanks and the topside is jacked up to its final air gap height, after which drilling operations can commence (Randolph and Gourvenec (2011); Zhang et al. (2014); Houlsby (2016)).

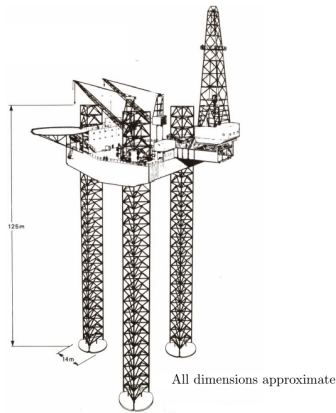


Figure 1: Typical jack-up geometry (adapted from Reardon (1986))

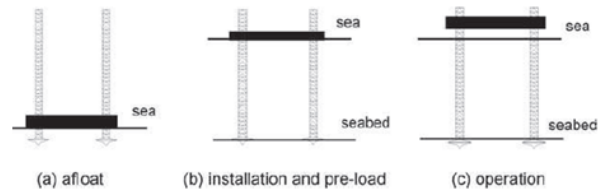


Figure 2: Simplified installation procedure for jack-up units (after Randolph and Gourvenec (2011))

The foundation of a jack-up unit is formed either by large inverted cones, also known as spudcans, or large mat structures (Martin, 1994). The mat structures are typically applied in very soft clay and silt deposits, whilst spudcans are applied in sandy and more stiff clay soils and are the most commonly applied foundation type (Cassidy et al., 2010; Martin, 1994; Randolph and Gourvenec, 2011; Zhang et al., 2014). Spudcans have a typically conical shape, most commonly combined with a sharp, protruding spigot and are applied to the end of each jack-up leg (Figure 3). The spudcan spigot allows for the spudcan to penetrate into the seabed, whilst the sloped walls of the spudcan allow for a significant bearing area under a relatively small penetration. Spudcans are fabricated from steel and are attached to the legs of the jack-up by use of welds. Spudcan shapes and sizes depend on the size and the manufacturer of the jack-up unit. Large jack-up structures can have spudcans in excess of 20 m in diameter.

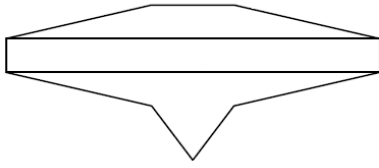


Figure 3: Typical spudcan geometry

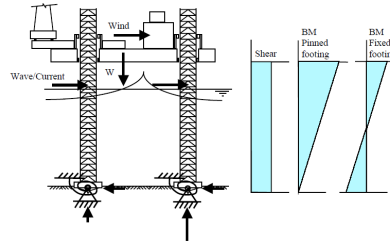


Figure 4: Influence of foundation fixity (after Hoyle et al. (2006))

1.2 Foundation fixity in jack-up foundation modelling

An important aspect in the modelling of jack-up structures is the 'fixity' of the foundation. Fixity is defined by ISO (2012) as "the rotational restraint offered by the soil supporting the spudcan". The amount of fixity at the foundation has a significant influence on the moments in the jack-up's legs, and thus the member stresses (Figure 4). Especially the critical member stresses, such as stresses at the leg-to-hull connection are strongly influenced by the foundation fixity.

For the assessment of a jack-up unit, it is therefore important that this foundation fixity is accounted for properly. The guidelines issued by the ISO (see ISO (2012)) account for the effects of fixity by introducing springs that represent the foundation. Researches on the behavior of jack-up units under loading (see for example (Vlahos et al. (2008); Bienen and Cassidy (2009); Cassidy et al. (2010))) have shown that the fixity of the foundation changes during loading. This means that, although the proposed springs in the ISO standards are reduced in stiffness according to a yield surface, they are not well capable of describing the behavior of a jack-up unit under loading. The springs used in the ISO guidelines typically result in a conservative capacity of the jack-up unit.

An alternative to the use of springs, is the use of a so-called macroelement approach. This approach describes the foundation in terms of force resultants in the (V,H,M) space. For an accurate description, these models have complicated yield surfaces and hardening rules that are capable of describing the nonlinear behavior of a jack-up unit under loading. These models, however, are created for a single, site specific jack-up unit. The parameters that are used have to be calibrated for the specific structural and environmental conditions, making them hard to use for a wider variety of situations.

An alternative to both methods is the use of a finite element model that uses continuum elements. Such a model would model the structure and the soil as a continuum, where the soil-structure interaction is implicitly described by the soil material model. There is very limited literature on the integrated three-dimensional modelling of a jack-up unit, as of yet.

1.3 Research goal

Jack-up structures are not only applied in the offshore oil and gas industry, but are also increasingly utilized in the offshore wind industry for the installment of wind turbines. Jack-up units are therefore not only important in the exploration and production of hydrocarbons, but can also be used in the production of sustainable energy. The stability of a jack-up unit is strongly influenced by its foundation and more specifically the fixity of this foundation. This foundation fixity is a complicated phenomenon, being determined by the soil-spudcan interaction and typically non-linear in behaviour. The current guidelines use spring models to capture the behaviour of the foundation. From experimental tests it is known that these spring models do not give an accurate description of the foundation behaviour. Macroelement models have recently been developed that give a better description, although these models are very case-specific and not entirely accurate, as of yet. It is therefore that there is a need to research both the behaviour of jack-up units under loading, as well as to develop numerical models to describe the jack-up behaviour. It is the goal of this research to investigate the capabilities of a three-dimensional finite element model in describing the behavior of a jack-up unit under loading. For the future development of numerical models that are capable of describing the behaviour of jack-up units, finite element models can aid in the calibration and development of these models.

The capabilities of the finite element model will be researched by:

- Benchmarking the finite element model to small-scale tests by Bienen et al. (2009)
- Performing parametric analyses to study the influence of preloading, loading angle and soil material model on the jack-up's performance
- Studying the influence of geometrical nonlinearities in finite element modelling of jack-up units

2 Modelling of spudcan fixity in soil–jack-up interaction analyses

The different methods in modelling the foundation fixity is discussed here. The standards by the ISO, as well as models from literature will be discussed.

2.1 Industry design guidelines: the ISO 19905-1 code

The ISO standards are widely used in the offshore industry for the site-specific assessment of jack-up structures. The main aspects of the guidelines will be discussed. The reader is referred to ISO (2012) as a reference.

Historical developments of the ISO code

In the late 1980s, Shell commissioned an industry wide study on the site specific assessment of jack-up units. Companies were requested to complete a questionnaire on the site assessment. Fourteen companies undertook analyses of a prescribed jack-up unit. An immediate conclusion was the difference between the expectations of companies. The study also showed a large spread in calculations. The results of the study commissioned by Shell led to an industry wide collaboration to harmonize assessment guidelines. The result of the extensive collaborative work that took place in a period of five years was the first SNAME document SNAME (2002), describing the full assessment process of a jack-up unit at a specific site. The SNAME documents have been updated throughout the years as research and computational capacity in jack-up unit assessment increased. In the mid 1990s, an initiative was formed to develop an ISO standard for the site specific assessment of jack-up units. The previously developed SNAME guidelines were adopted as a basis for the ISO standard. A workgroup within the ISO was formed to develop the new ISO standards. The ISO standards are perceived to have a more prescriptive approach when compared to the originally developed SNAME guidelines (Hoyle et al. (2006)). ISO 199905-1 (ISO (2012)) is the respective guideline that is used today in site specific jack-up assessments.

ISO guidelines on foundation fixity

The ISO guidelines give a thorough description of the steps taken in the site specific assessment of jack-up units. The guidelines propose several options for modelling the foundation fixity:

- Pinned foundation model (i.e. no foundation fixity)
- Secant foundation model with linear vertical and horizontal stiffnesses and a secant rotational stiffness that is reduced based on a yield interaction surface
- Yield interaction model with nonlinear vertical, horizontal and rotational stiffnesses where the nonlinear behavior is based on compliance with a yield interaction surface (typically referred to as macroelement models)
- Continuum model using a nonlinear foundation model, coupled to the structure which also accounts for the load-penetration behavior beyond penetration achieved by preloading

These foundation models are then used to check the jack-up structure for acceptance. The ISO guidelines have three levels of acceptance checks, with increasing complexity and reducing conservatism:

Level 1: Foundation capacity check of the wind- and leeward legs based on the preloading capability, using a pinned foundation model

Level 2: Foundation capacity checks with one of the following steps:

1. Foundation capacity check and sliding resistance check based on the vertical and horizontal reactions assuming a pinned spudcan, or;
2. Foundation capacity check and sliding resistance check based on the vertical, horizontal and moment reactions from a spudcan model that includes vertical, horizontal and rotational stiffness with a rotational stiffness reduction, or;
3. Foundation capacity check based on the vertical, horizontal and moment reactions from a spudcan model that includes vertical, horizontal and rotational foundation stiffness with a reduction of vertical, horizontal and rotational stiffnesses, together with a level 3 displacement check.

Level 3: Displacement check using one of the following steps:

1. Simple check using the leg-penetration curve based on the results of a level 2 check when the foundation capacity check fails and/or a check of the effects of windward leg sliding when the level 2 sliding check fails, or;
2. Numerical analysis of the complete jack-up and non-linear foundation coupled in vertical, horizontal and rotational degrees of freedom, e.g. finite element approach.

The basic philosophy of the ISO guidelines is that the simpler models are typically more conservative. For this reason, the foundation capacity is checked using a pinned case. If the acceptance checks are not passed, a spring model will be used instead. The spring models differ in terms of stiffness formulation. Where a linear spring model can be used, a stiffness reduction is also described for the spring model. The guidelines describe in detail the capacity and sliding resistance checks for the pinned and spring models. The use of a macroelement or continuum model is only suggested in the case that these acceptance checks are not passed for a pinned or spring foundation. Where the guidelines give a thorough description of the acceptance checks for the simpler models the nonlinear models are described to have these checks implicitly built in. The ISO guidelines do not give a thorough description of the macroelement or continuum models, or their acceptance checks.

It is mentioned in the ISO guidelines that the described checks do not cover all loading cases of the foundation. Some of the cases that are not covered in the checks are:

- Cases for which the long-term drained soil bearing capacity is less than the short-term undrained bearing capacity.
- Cases where a reduction of soil strength occurs due to cyclic loading.
- Cases where an increase in spudcan penetration occurs and a punch-through potential is present.

Although the lack of inclusion of these cases in the assessment is mentioned, the ISO guidelines do not give a thorough guidance on the inclusion of these effects. The guidelines do state that analyses should be carried out when one of these cases is expected to be present.

2.2 Macroelement plasticity models

Macroelement plasticity models have been developed by several authors as a way of combining the structural and foundation behavior of a jack-up unit through numerical modelling. As the structural design of jack-up units is performed by structural engineers, ideally the foundation of the jack-up would be described by the use of linear springs. This would allow the assessment of the structure to be performed by linear analyses in a structural framework. It is well known, however, that the foundation of a jack-up structure does not behave in a linear fashion. The foundation fixity is strongly influenced by the soil response, which is known by geotechnical engineers to be a typically nonlinear problem. To allow for a proper description of the foundation behavior in a structural framework, the response of the foundation is described in force resultants at the foundation. A sign convention was proposed by Butterfield et al. (1997), which is used to describe the force resultants in (V, H, M) space (Figure 5). The foundation model describes the behavior of the foundation for elastic loading situations, as well as cases for which plasticity (or foundation yielding) occurs. The foundation model can be attached to a structural node to achieve an integrated simulation of the foundation and structural system (Bienen and Cassidy, 2009).

Failure at the foundation is caused by an interaction of the different load resultants. The concept here, is that the application of different loads leads to a different failure capacity as compared to a single load failure. This concept can be explained by considering a flat foundation on sand that is loaded two-dimensionally in (V, H) space. The failure of the foundation in (V, H) space could be described by a sliding failure and a bearing capacity failure. Understandably, the sliding failure will be strongly dependent on the vertical load applied at the foundation, as a larger normal pressure typically results in a larger friction. Similarly, a horizontal load will influence the bearing capacity, as the application of a horizontal load will reduce the vertical capacity of the foundation.

As the foundation of a jack-up unit experiences loading from different directions, a yield surface is defined in a (V, H, M) space to describe the loading combinations for which yielding occurs. The yield surfaces in three-dimensional plane are investigated by so-called experimental swipe tests. A loading apparatus was designed by Martin (1994) to investigate the load combinations for which yielding occurs. The designed loading apparatus allowed for different loading combinations of vertical, horizontal and moment loading of a shallow foundation. Different expressions have since been developed for the yield surface of a six-degrees-of-freedom loading of a jack-up structure foundation on sand. Bienen and Cassidy (2009) have further developed the yield surface proposed by Martin (1994) and describe the yield surface as

$$\begin{aligned}
 f = 0 = & \left(\frac{H_3}{h_0 V_0} \right)^2 + \left(\frac{M_2/2R}{m_0 V_0} \right)^2 - \frac{2aH_3 M_2/2R}{h_0 m_0 V_0^2} + \left(\frac{H_2}{h_0 V_0} \right)^2 + \left(\frac{M_3/2R}{m_0 V_0} \right)^2 \\
 & + \frac{2aH_2 M_3/2R}{h_0 m_0 V_0^2} + \left(\frac{Q/2R}{q_0 V_0} \right)^2 - \left[\frac{(\beta_1 + \beta_2)^{(\beta_1 + \beta_2)}}{\beta_1^{\beta_1} \beta_2^{\beta_2}} \right]^2 \left(\frac{V}{V_0} \right)^{2\beta_1} \left(1 - \frac{V}{V_0} \right)^{2\beta_2} \quad (1)
 \end{aligned}$$

Where V_0 is the preload magnitude, h_0 , m_0 and q_0 describe the dimension of the yield surface, a is the excentricity of the yield surface and β_1 and β_2 are the curvature factors. The yield surface is typically elliptical and, in shape, looks like a rugby ball (Figure 6).

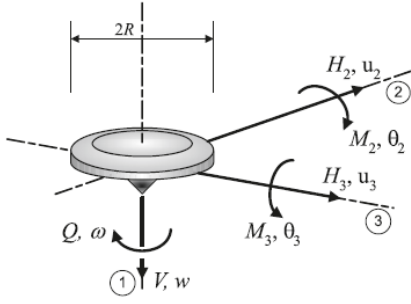


Figure 5: Sign convention as proposed by Butterfield et al. (1997) (after Bienen and Cassidy (2009))

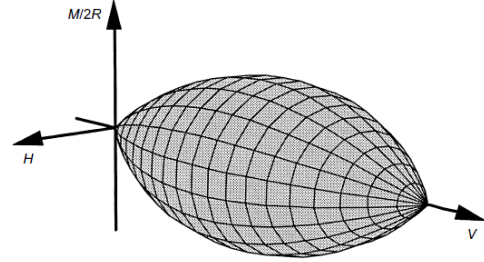


Figure 6: Yield surface in planar loading (after Houlsby and Cassidy (2002))

The elastic response within the yield surface can be described in six-degrees-of-freedom as (Bienen and Cassidy (2009))

$$\begin{pmatrix} dV \\ dH_2 \\ dH_3 \\ dQ/2R \\ dM_2/2R \\ dM_3/2R \end{pmatrix} = 2GR \begin{bmatrix} k_1 & 0 & 0 & 0 & 0 & 0 \\ 0 & k_3 & 0 & 0 & 0 & -k_4 \\ 0 & 0 & k_3 & 0 & k_4 & 0 \\ 0 & 0 & 0 & k_5 & 0 & 0 \\ 0 & 0 & k_4 & 0 & k_2 & 0 \\ 0 & -k_4 & 0 & 0 & 0 & k_2 \end{bmatrix} \begin{pmatrix} dw^e \\ du_2^e \\ du_3^e \\ 2Rd\omega^e \\ 2Rd\theta_2^e \\ 2Rd\theta_3^e \end{pmatrix} \quad (2)$$

Where G is the shear modulus and k_1, k_2, k_3, k_4 are dimensionless stiffness factors and k_5 is a torsional constant.

The macroelement model is then supplied with a hardening law and a flow rule to describe the behavior of the model during yielding. The hardening law is generally stated as a semi-empirical formulation, which takes into account the spudcan geometry and roughness, as well as the soil parameters Bienen and Cassidy (2009); Gottardi et al. (1999). The macroelement models are supplied with a large number of parameters that are calibrated, usually on the basis of experimental tests.

Advantages and disadvantages of macroelement models

Macroelement models are complicated, nonlinear models that have their specific advantages and disadvantages. The main advantages of macroelement are:

- Macroelement models are easily implemented in structural numerical codes.
- The plasticity and nonlinear behavior of a jack-up foundation under loading is better captured using macroelement models, as compared to spring models.

Some disadvantages of macroelement models are:

- Many parameters need calibration, requiring swipe tests or finite element models.
- Macroelement models are case-specific, meaning they can not reproduce results for other situations without recalibration.

2.3 Three-dimensional finite element modelling of nonlinear soil-spudcan interaction

The concept of applying a three-dimensional finite element model to model the interaction between soil and spudcan for jack-up analyses has not yet been explored. As this research will focus on applying this method, a brief and general description will be given.

Three-dimensional finite element models, using continuum elements are widely used in the area of geotechnics. Groen (1997) developed a material model for sand, using a double hardening rule, where the plastic behaviour in shear is independent from the plastic behaviour in compression. The model by Groen (1997) has since been used in many commercially available finite element models to describe the behaviour of sandy soils. Typically, the parameters in the material model are calibrated by simulating real tests, such as oedometer and triaxial tests. When calibrated properly, the finite element model is capable of describing the behaviour of the real soil. When combining these soil models with a structural model, the soil-structure interaction is typically given by the behaviour of the soil model and therefore obtained automatically. A large advantage of these finite element models is the analyses that they can be used for. Virtually every type of analysis can be performed, given that the material model that describes the soil is correct. This means that the model can be used to model static situations, but is also capable of modeling cyclic or dynamic behaviour. When used in conjunction with a large deformation framework, installation effects can also be modeled. Another advantage of finite element models is that they can provide a basis for the calibration of macroelement models.

Although there are many advantages to employing finite element models, they also have their specific disadvantages. Calculations can become computationally heavy, especially when large geometries are being modelled. Finite element models are also typically mesh dependent. The size and refinement of the mesh influences directly the degrees of freedom of the model, and thus influences results.

As of yet, very little literature exists on the integral three-dimensional modelling of soil-spudcan-jackup interaction.

3 3D finite element modelling of soil-spudcan-jack-up interaction

The research is performed by making use of the commercially available DIANA finite element software. To allow for benchmarking of the finite element model, a comparison will be made with experimental tests on a small-scale jack-up. The experimental tests that are used as a reference have been described by Bienen and Cassidy (2009). The model jack-up used in these experimental tests represents an average field jack-up structure. The experimental tests are performed in a geotechnical centrifuge, allowing for the size of the experimental set-up to be scaled back, by use of a 200*g* gravitational field. The experimental set-up represents a jack-up with a leg length of 89 meters, a spudcan diameter of 10 meters and a center-to-center distance of the legs of approximately 25 meters. The experimental set-up has been constructed from aluminium, for proper mass scaling of the structure. The finite element model in DIANA software will model the average field jack-up structure, to allow for a comparison with the experimental tests.

3.1 Structural modelling

The structural aspects, together with the element types in DIANA software will be discussed for the jack-up structure as well as the spudcan footings.

3.1.1 Jack-up structure

The jack-up structure is formed by three legs and the hull. Emphasis was placed on modelling the jack-up using structural properties that correspond to the experimental set-up by Bienen and Cassidy (2009), as this research will serve as a benchmark. Analogous to Bienen and Cassidy (2009), the topside was modelled as very stiff, compared to the legs. Six rectangular beam elements are interconnected to form the topside structure. The legs are modelled in a similar way, using hollow circular beam elements and are attached to the topside (Figure 7). The entire structure is constructed from aluminium, analogous to the research by Bienen and Cassidy (2009). Emphasis here has been placed on a proper modelling of the structural properties. As the experimental set-up uses a solid triangular hull, the mass of the topside will be adjusted in the finite element model to allow for proper mass scaling of the structure. This leads to a larger density of the topside, when compared to the jack-up legs. The finite element model size is that of an average field jack-up structure. The structural properties of the jack-up structure are displayed in Table 1, the axes of the structural properties as well as the set-up are displayed in Figure 7.

Table 1: Structural properties of modelled jack-up in DIANA software

Description	Value	Dimension
Leg length	89	<i>m</i>
Center of forward leg to centerline of aft legs	25	<i>m</i>
Center to center of aft legs	27	<i>m</i>
Young's modulus	200	<i>GPa</i>
Shear modulus	81	<i>GPa</i>
Cross-sectional area of leg (x,y)	2.9	<i>m</i> ²
Second moment area of leg (x,y)	7.04	<i>m</i> ⁴
Cross-sectional area of hull beam (x,y)	30	<i>m</i> ²
Second moment area of hull beam (x,y)	71.6	<i>m</i> ⁴
Density of spudcans and jack-up legs	2700	<i>kg/m</i> ³
Density of topside beams	3400	<i>kg/m</i> ³

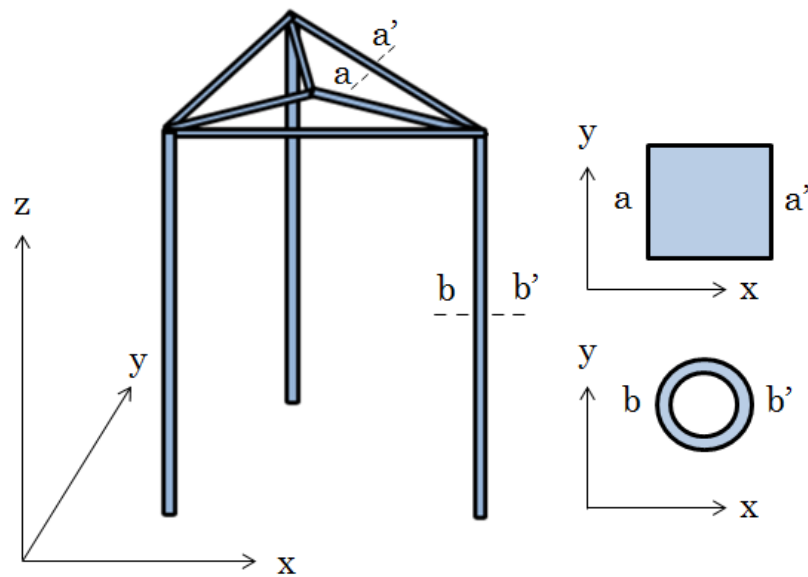
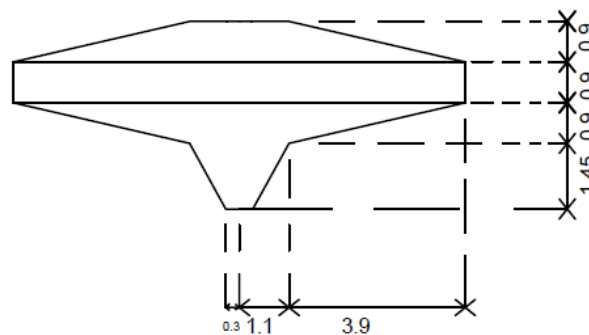


Figure 7: Structural set-up in DIANA

3.1.2 Spudcans

The spudcans are modelled in DIANA software using solid elements that are tetra- and hexahedrons in shape, with quadratic shape functions. The spudcans are considered to be entirely solid by the finite element model, having no internal rotational freedom. The spudcans can, however, rotate as a whole, under influence of moment loading. The spudcan geometry (Figure 8) has been selected to be close to the geometry as described by Bienen and Cassidy (2009). For this research, however, it has been decided to flatten the spudcan underside. The geometry as proposed by Bienen and Cassidy (2009) shows a pointed underside of the spudcans. This has been verified to lead to difficulties in the finite element model, as large stress concentrations are observed, that lead to non-convergence or divergence. The flattened underside that is modelled in the finite element model is still small in area, relative to the overall size of the spudcan. The influence of this point on the overall modelling response is expected to be negligible.

Figure 8: Spudcan geometry and sizing in DIANA (in m)

3.1.3 Connections

An important aspect in the modelling of jack-up structures is the connection between the legs and the hull, and the connection between the legs and the spudcans. It is recognized that a jack-up

structure typically has a stiffness at the leg-to-hull connection, which is defined by the jacking system. This stiffness has been disregarded in this research, leading to a clamped connection between legs and hull (also displayed in Figure 7). The same assumption has been made for the leg-to-spudcan connection, although it can be stated that this assumption is somewhat closer to reality.

3.2 Soil modelling

The soil can be modelled in DIANA software by making use of the available material models, although user-supplied routines are also possible. The material models that will be used in this research will first be discussed, after which the applied parameters are discussed and motivated.

3.2.1 The Modified Mohr–Coulomb soil plasticity model

The Modified Mohr–Coulomb (hereafter abbreviated as MMC) is the material model that is typically used for the modelling of sandy soils. The model is capable of capturing the complicated nonlinear behaviour of sandy materials through a double-hardening mechanism. A short description of the model will be given, comprising the main features of the model. For further details, the reader is referred to Groen (1997) and Manie (2016a). The cohesionless model formulation is expressed in terms of isotropic and deviatoric stress invariants, p' and q (Nova, 2012).

The MMC model features a nonlinear elastic law, with a constant Poisson's ratio ν and a pressure-dependent bulk modulus:

$$K_t = K_{ref} \left(\frac{p'}{p'_{ref}} \right)^{1-n} \quad (3)$$

where n and K_{ref} are the constitutive parameters and the reference pressure p_{ref} is such that $K_t(p' = p'_{ref}) = K_{ref}$. The oedometric Young's modulus is defined similarly:

$$E_d = E_{d,ref} \left(\frac{p'}{p'_{ref}} \right)^{1-n} \quad \text{where } E_{d,ref} = \frac{3(1-\nu)}{1+\nu} K_{ref} \quad (4)$$

The yielding surface of the MMC model is a so-called double-mechanism yielding. Two yielding loci are defined, one for shear yielding, $f_1 = 0$ and one for radial loading paths², $f_2 = 0$:

$$f_1 = \frac{q}{R_1(\theta)} - \frac{6 \sin \phi}{3 - \sin \phi} p' = 0 \quad f_2 = p'^2 + \alpha \left(\frac{q}{R_2(\theta)} \right)^2 - p_c^2 = 0 \quad (5)$$

where α is a cap shape parameter, and functions R_1 and R_2 determine the π -section of both yield loci and are dependent on the lode angle:

$$R_1(\theta) = \left(\frac{1 - \beta_1 \sin 3\theta}{1 - \beta_1} \right)^b \quad R_2(\theta) = 1 \quad (6)$$

where β_1 and b are constitutive parameters, while R_2 is assumed to not depend on the load angle θ . The mobilised friction angle during yielding evolves as a function of the equivalent deviatoric plastic strain according to:

$$\sin \phi = \sin \phi_f - (\sin \phi_0 - \sin \phi_f) e^{-a\gamma_{eff}^p} \quad (7)$$

²Radial loading paths are straight curves in $p - q$ space, intersecting through the origin (e.g. oedometer test)

where ϕ_0 and ϕ_f are the mobilised friction angle at first yielding and failure, respectively, γ_{eff}^p is the equivalent deviatoric plastic strain and a is a hardening parameter that determines the shape of the hardening function. This hardening function can be user-defined in DIANA software, allowing for the soil parameters to be calibrated, typically to a triaxial test.

The cap locus $f_2 = 0$ hardens through the evolution of the hardening parameter p_c , which depends on the incremental volumetric plastic strain $\dot{\epsilon}_{vol}^p$, a hardening parameter δ and the current void ratio e :

$$\frac{\dot{p}_c}{p_c} = \frac{1+e}{\delta} \dot{\epsilon}_{vol}^p \quad (8)$$

Analogous to the double yielding mechanism, two plastic flow mechanisms are introduced through two expressions for the plastic potential g_1 and g_2 :

$$g_1 = q - \frac{6 \sin \psi}{3 - \sin \psi} p', \quad g_2 = p'^2 + \alpha q^2 - (p_c^q)^2 \quad (9)$$

both plastic potentials have a circular deviatoric π -section (i.e. no θ dependence, assuming $\beta_1 = 0$) and with $g_2 = f_2$ (associated plasticity along the cap). The dilatancy is controlled by Rowe's relationship (Rowe, 1962):

$$\sin \psi = \frac{\sin \phi - \sin \phi_{cv}}{1 - \sin \phi \sin \phi_{cv}} \quad (10)$$

where ϕ is the current friction angle (influenced by the hardening rule) and ϕ_{cv} is the constant volume friction angle that can be related to a triaxial test.

Soil parameters

The soil parameters that are applied for the MMC model are displayed in table 2. These parameters have been based on a calibration in DIANA software. As a conservative assumption, the dilatancy angle of the soil is taken as 0° , with the friction angle of the soil being modelled at constant volume. For more detail on the specifics of the calibration and the data used for the calibration the reader is referred to Appendix A.

Table 2: Calibrated MMC soil parameters

K_{ref} [MPa]	p_{ref} [kPa]	m [-]	ν [-]	ϕ_0 [-]	ϕ_f [-]	α [-]	γ [-]	$\gamma_{soil,dry}$ [kN/m ³]
110	100	0.5	0.3	18.5	33.75	120	0.0008	17.36

3.2.2 Soil–spudcan interface modelling

The soil-structure interaction is modelled in DIANA software by making use of interface elements. Interface elements are inserted between continuum elements to allow for relative displacements and to avoid interpenetration of nodes (Figure 9).

In the modeling of soil-structure interaction, a difference can be made between compression and tension behavior. As a sandy type soil generally has no tension capacity, this should be taken into account by the finite element model. The interface elements allow for the distinction between compression and tension. There are many different interfaces available in DIANA software. They range from perfectly linear elastic interfaces, to interfaces that have a gap opening under tension, to interfaces that allow for sliding.

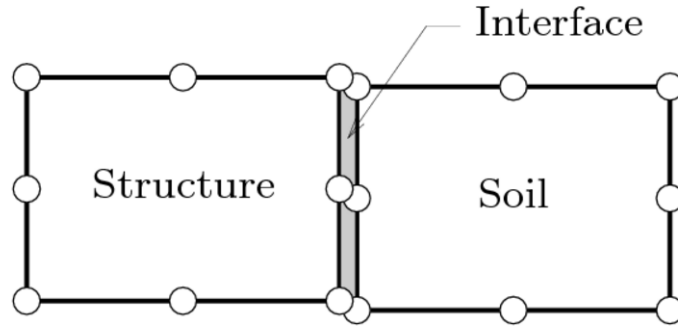


Figure 9: Interface elements in DIANA software (after (Manie, 2016a))

The spudcans present in the finite element model should be capable of showing a gap opening under a horizontal pushover. There are two interface element types in DIANA software that are suitable for this type of application:

- Linear no-tension interfaces: linear stiffness under compression with a stiffness reduction controlled by a reduction factor under tension (typically 0).
- Coulomb-friction interfaces: linear stiffness under compression with a sliding capacity and a stiffness reduction under tension according to a material model.

A selection between both elements has been made, based on both numerical stability and the proper prediction of results. The reader is referred to Appendix B for a more detailed description of the interfaces, as well as their comparison.

The interface parameters are displayed in Table 3. The interface that has been selected from

Table 3: Properties of interface elements

Parameter	Value	Dimension	Description
Normal stiffness modulus z	4E+9	N/m^3	Vertical stiffness modulus
Shear stiffness modulus x	4E+8	N/m^3	Stiffness modulus for shearing in x-direction
Shear stiffness modulus y	4E+8	N/m^3	Stiffness modulus for shearing in y-direction
Critical interface opening	0	m	Interface opening distance for stiffness reduction in linear no-tension interfaces
Normal stiffness reduction factor	0	-	Reduction factor for vertical stiffness modulus in linear no-tension interfaces

the comparison in Appendix B is the linear no-tension interface. It can be observed that the normal and shear stiffness moduli are high. An interface opening distance and factor is given to the interfaces, to allow for separation of structure and soil under tension conditions.

3.3 Finite element model set-up and numerical aspects

The different aspects of the finite element set-up will be discussed, showing the numerical solution procedure that is performed. Special emphasis has been placed on the mesh that is used, together with geometrical nonlinearities.

3.3.1 Domain size

The domain size (Figure 10) has been selected, such that the boundaries do not have an influence on the stresses in the soil. This leads to a size that is related to the width of the topside. As the center-to-center of the aft legs is 27 meters, a general rule of thumb is that the area of influence is roughly twice this width in the horizontal plane. The same goes for the geometry sizing in depth, which requires a minimum of twice the topside width. The soil mass below the jack-up structure is 60 meters deep, to avoid any boundary effects. The domain size has been verified based on soil stresses in DIANA software.

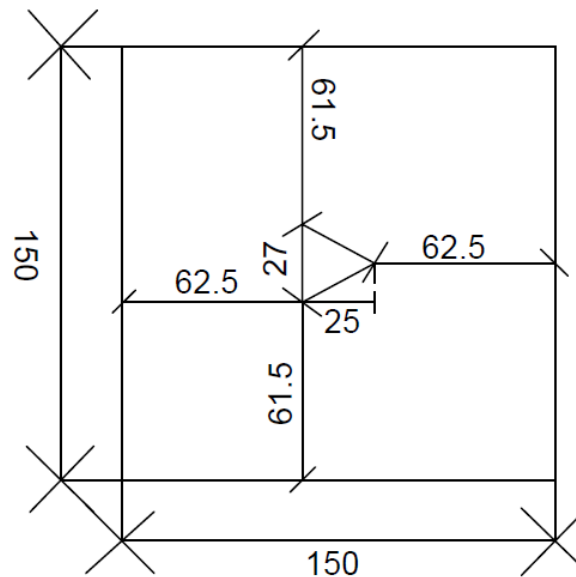


Figure 10: Space discretization of finite element model, topside view (in m)

3.3.2 Mesh discretization

An important aspect in finite element modelling is the mesh size. The size of the mesh can not be too large, due to a limit on the computational efforts and should still give an accurate result. For this reason, a mesh refinement is applied. This refinement is concentrated at the spudcan footings, as the foundation is expected to have the largest influence on results. A circular coarsening is applied to ensure that the computational efforts do not become too large. The selected mesh can be observed in Figure 11. It should be noted here that different mesh refinements have been tested and compared. The mesh displayed in Figure 11 has been selected based on computational efforts and numerical accuracy. For a detailed description of the comparison of different mesh types, the reader is referred to Appendix C.

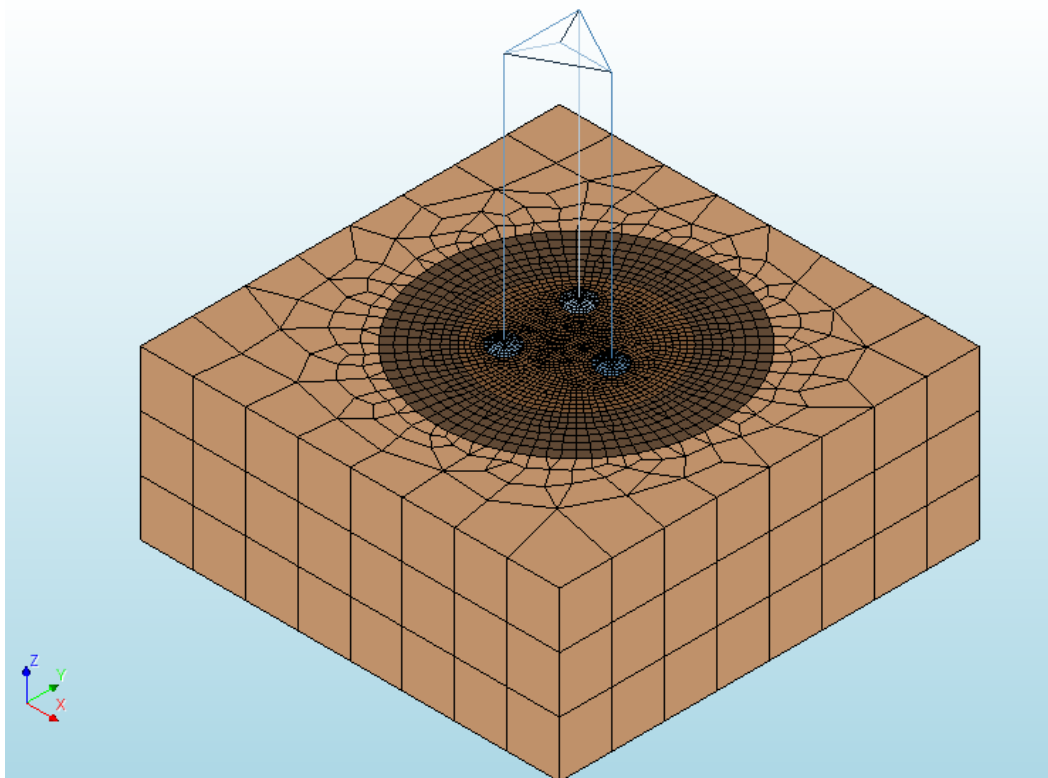


Figure 11: Finite element mesh in DIANA

Next to the size and refinement of the mesh, the symmetry condition of the mesh is an important factor. The mesh has been constructed so, that an axis of symmetry is present in the model. This allows for the numerical solution to produce a pure symmetrical response during loading. The axis of symmetry can be observed in Figure 12 and is located along the symmetry axis of the topside structure.

The entire mesh uses quadratic shape functions. The element types differ between tetra- and hexahedrons, where the hexahedrons are mostly observed in the outer soil mesh and the tetrahedrons can be observed close to the spudcan geometry, due to the pointed shape of the spudcans. The mesh is automatically generated in the DIANA software package. The program selects the proper element types, based on the original geometry, allowing for the mesh of the soil to follow the complex shape of the spudcans. A slice of the finite element mesh shows the different element types and the meshing connection, which can be observed in Figure 13.

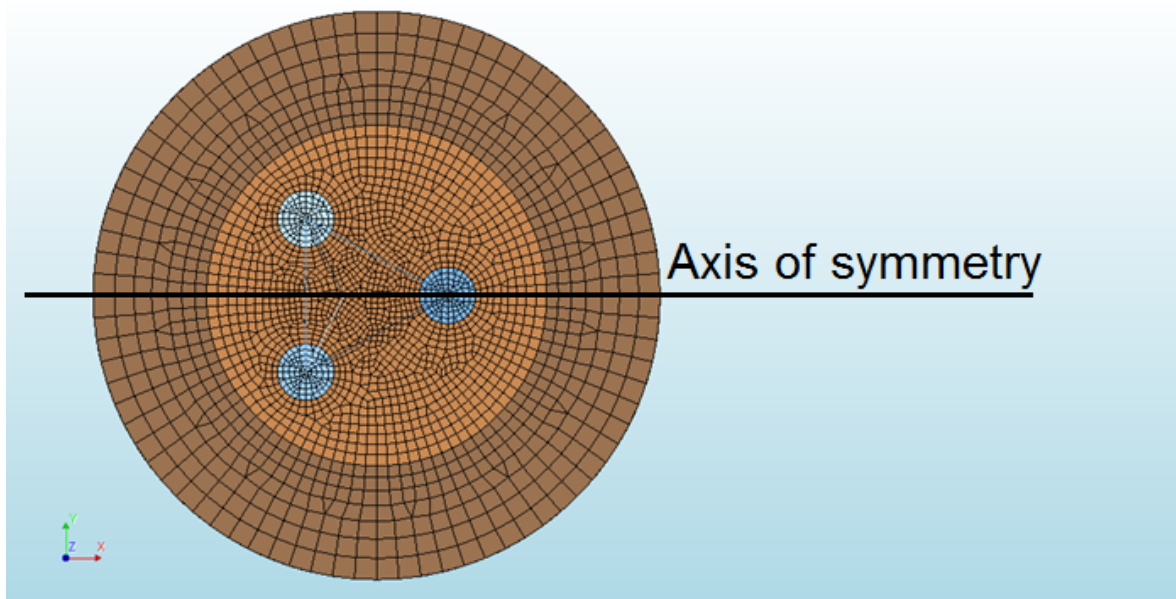


Figure 12: Symmetricality of finite element mesh in DIANA

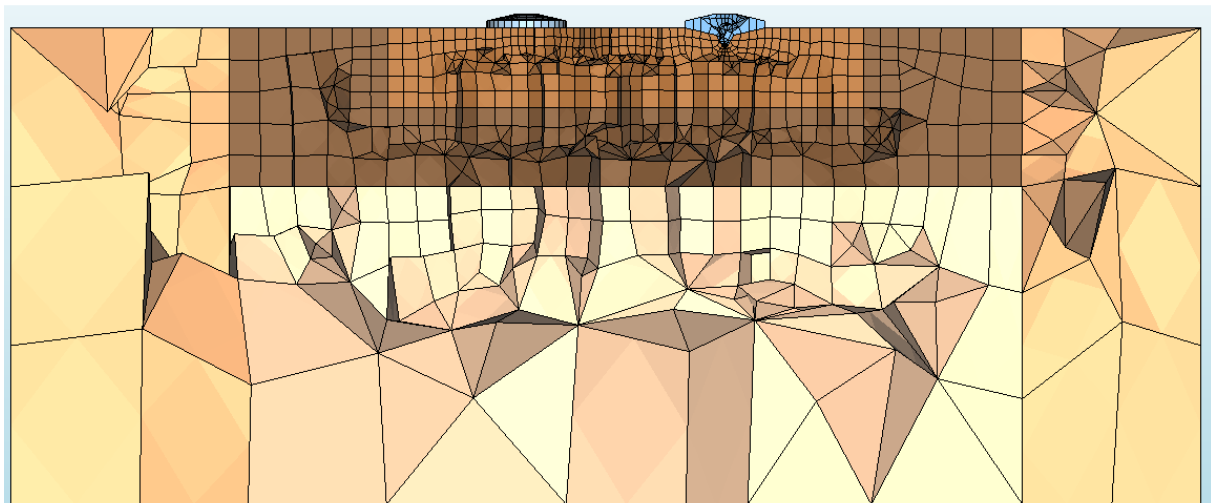


Figure 13: Slice of finite element mesh along spudcan geometry in DIANA

3.3.3 Boundary conditions and loading stages

The finite element model used in the description of the behaviour of a jack-up structure has specific boundary conditions and initial conditions. The geometrical boundary conditions of the soil mass below the jack-up structure ensure that the soil mass does not move normal to the respective direction. Displacements are therefore fixed along these boundaries. These boundary conditions are displayed in Figure 14 where the bottom boundary condition is not visible, but also applied in the finite element model.

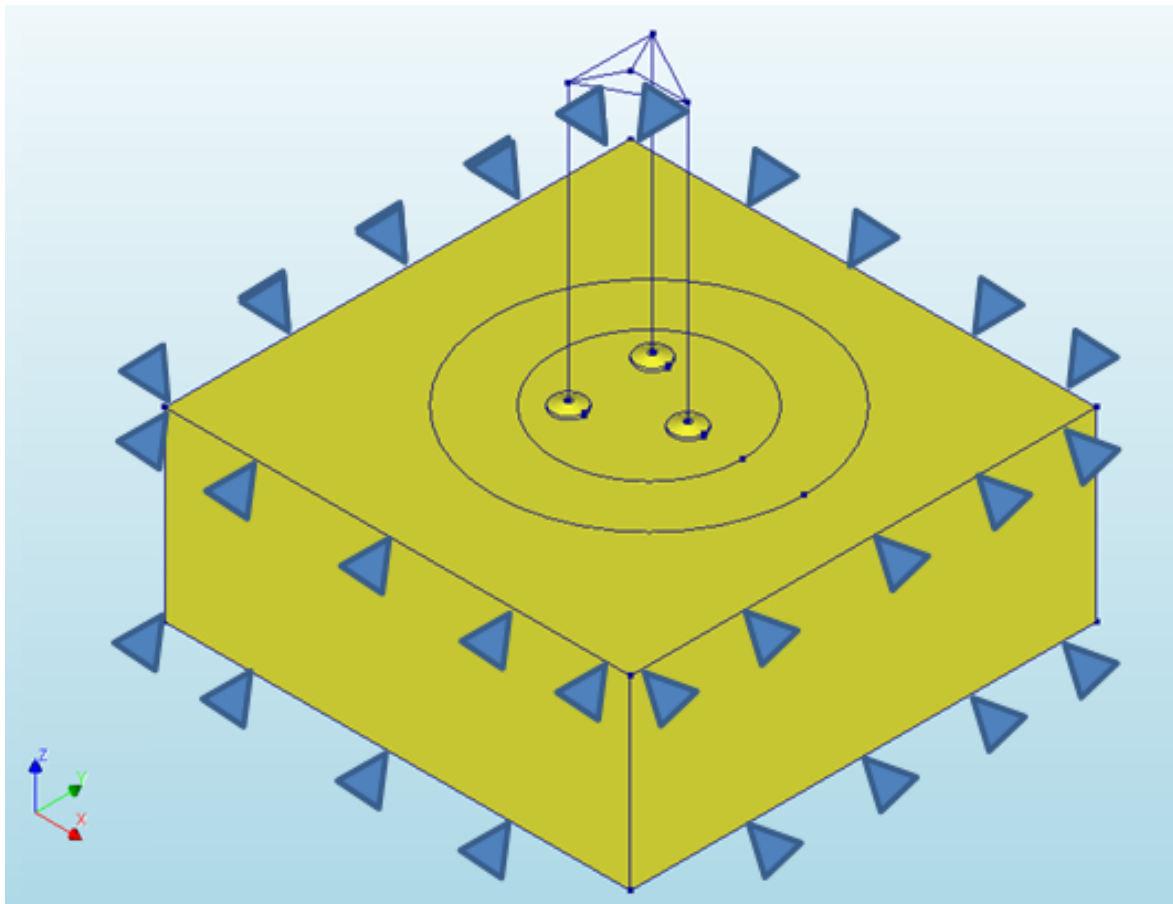


Figure 14: Geometrical boundary conditions of finite element model in DIANA

Next to the geometrical boundary conditions of the soil mass, the initial condition is a wished-in-place structure. This effectively means that the installation effects of the structure are not taken into account by the finite element model. Although these installation effects can be of particular interest, this is outside the scope of this research and therefore not accounted for. The initial stress condition of the finite element model is a result of the gravity loads of both the soil and the structure. For this initial condition, no displacements are allowed and stresses are computed in this phase. The stress state in the initial stage is displayed in Figure 15, where the slice of the model for which the stress is shown is displayed in Figure 16.

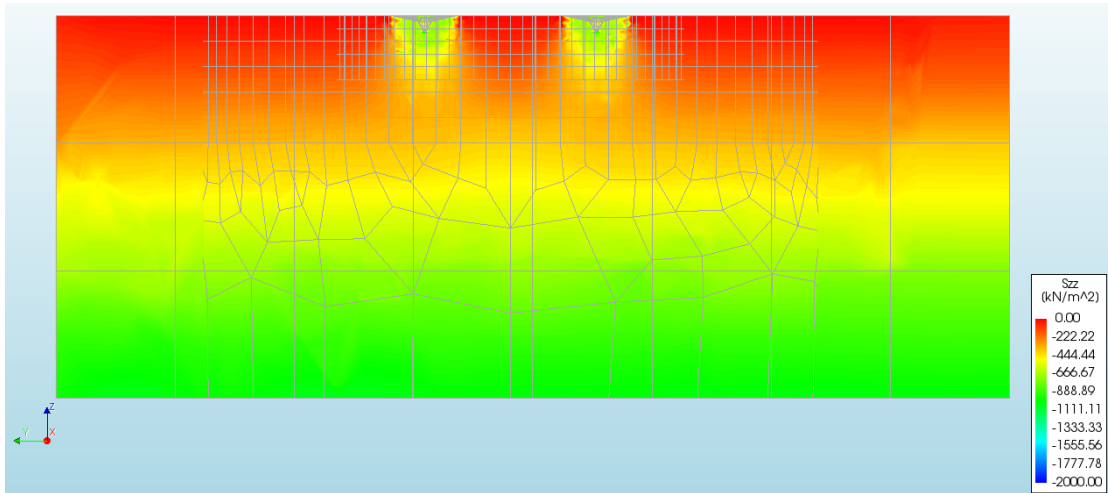


Figure 15: Initial stress conditions in finite element model along a slice of the mesh (see Figure 16)

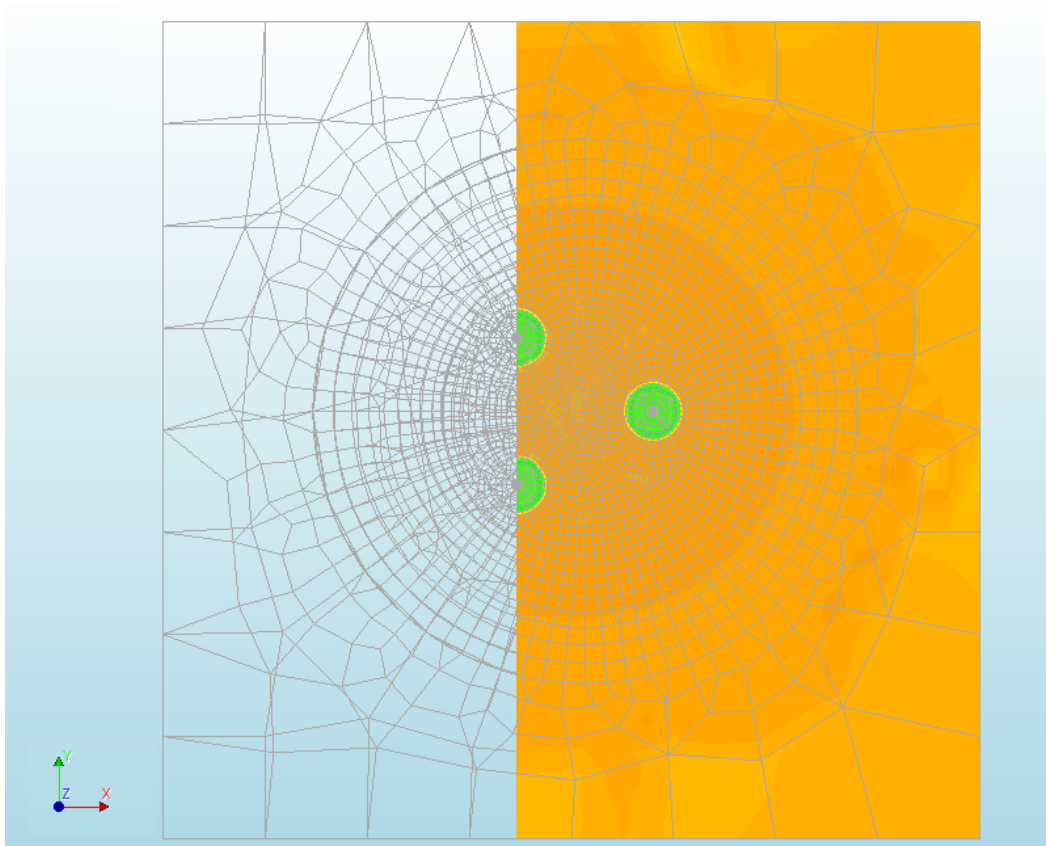


Figure 16: Slice of initial stress conditions in finite element model

Loads

After the initial state definition and the definition of boundary conditions, the finite element model will perform certain loading steps to realistically model the jack-up structure. The following loads are applied in the finite element model:

- Vertical preload: Applied as a force load at the top of the structure, representing the vertical preloading applied to the structure. In reality produced by pumping water in the ballast tanks of the topside structure.
- Vertical unload: Applied as a negative force load at the top of the structure, representing the unloading of the structure. In reality performed by removing water from ballast tanks.
- Horizontal load: Applied at the top of the structure as a:
 - Force load in a force-controlled analysis
 - Prescribed displacement in a displacement-controlled analysis

These loading steps are performed by using specific numerical boundary conditions. The horizontal load application differs between analyses. For a pure lateral push-over analysis, a displacement-controlled analysis is applied, as this control type is very stable. For the non-symmetric pushover analyses, a force-controlled analysis is applied, as the displacement field is not known beforehand.

It should be noted here, that the boundary conditions displayed in Figure 14 apply to all steps. The different loads are applied to the finite element model, together with specific numerical boundary conditions. These numerical boundary conditions are employed to ensure the modelling process is as realistic as possible. The loading stages together with their numerical boundary conditions are displayed in Table 4.

Table 4: Loading stages and their numerical boundary conditions

Loading step	Applied loads	Numerical boundary conditions
Preloading	Preload value	No displacements of total geometry
Unloading	Unload value	No displacements of total geometry
Horizontal load	Horizontal force or; Prescribed horizontal displacement	- Prescribed displacement

Spudcan penetration depth

As described in Table 4, the boundary conditions during the vertical loading steps are no displacement. This leads to an evaluation of stresses, where the vertical and horizontal displacement is zero. These boundary conditions are applied to ensure that the spudcan penetration depth is kept as a constant, thus avoiding installation effects. The spudcan penetration depth of the spudcan tip differs in the research of Bienen and Cassidy (2009) between 2.23 and 2.43 *m* for different loading stages. Although the penetration depth of the spudcan tip after preloading is 2.4 *m* or larger in the research by Bienen and Cassidy (2009), this research uses a penetration depth of the spudcan tip of 2.35 *m* instead. The reason being the spudcan geometry that leads to a numerical instability at larger penetration depths, due to the sharp shape of the spudcan geometry. This is recognized as a shortcoming, although its influence is estimated to be negligible. This penetration depth is taken as a constant throughout the vertical loading steps. During the horizontal loading, the spudcans are capable of showing a push-pull mechanism, allowing for them to separate from or penetrate into the soil.

3.3.4 Geometrical non-linearities in large-deformation framework

Geometrical non-linearities can have a significant influence on the stability of a jack-up structure under loading and can be included in a large-deformation framework (hereafter abbreviated as LDFE). The LDFE allows for the finite element model to experience large displacements, which can lead to second order effects. A large aspect in this specific case are the so-called P- Δ effects. The software package DIANA is capable of taking into account these large deformations. This means that the length, area and stresses of both the structural elements and the soil elements are updated constantly. It is important to note that this framework is a large-displacement small-strain framework, meaning that the constitutive behaviour of the soil model under small-strains is still valid. The governing equations of the LDFE will be described for the DIANA finite element model. The described equations and explanations are taken from Manie (2016a). For further details on the application of a LDFE, the reader is referred to Surana (1986) and Pai et al. (2000).

In the description of the governing equations in the LDFE, a superscript ($^t \dots$) indicates a state of quantity, while a subscript ($_{t \dots}$) indicates the reference coordinate frame for derivatives. A coordinate frame is attached to the material, where the material axes can both rotate and stretch during the transition from one coordinate frame to another (Figure 17).

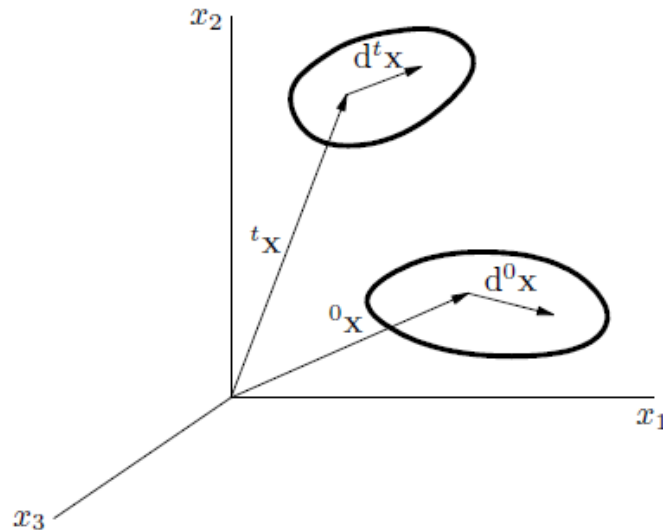


Figure 17: Coordinate frames for LDFE analysis (after Manie (2016a)).

The material point position x and material axis dx are shown for the coordinate frame at state 0 and state t . The displacement u is denoted by

$${}^t u = {}^t x - {}^0 x \quad (11)$$

The deformation gradient F expresses the rotation and stretch of dx . The deformation gradient is

$${}^t_0 F = {}^t x_0 \overleftarrow{\nabla} = \frac{\partial {}^t x}{\partial {}^0 x} \quad (12)$$

with $d^t x = {}^t_0 F d^0 x$. In case of an arbitrary deformation, the rotation matrix R is defined by the polar decomposition of the deformation gradient

$$F = R\dot{U} = V\dot{R} \quad (13)$$

The determinant J of the deformation gradient gives a volume change:

$${}^tV = J {}^0V \quad ; \quad J = \det {}^t_0F \quad (14)$$

the velocity of a point is denoted as

$$\dot{u} = {}^t \dot{x} \quad (15)$$

The velocity gradient is

$$L = \dot{u} \overleftarrow{\nabla} = \frac{\partial {}^t \dot{u}}{\partial {}^t x} \quad (16)$$

The spin Ω and rate of deformation D are defined in terms of the local velocity gradient

$$D = \frac{1}{2}(L + L^T) \quad \text{and} \quad \Omega = \frac{1}{2}(L - L^T) \quad (17)$$

The Green-Lagrange strain is defined as

$${}^t_0E = \frac{1}{2}({}^t_0F^T \cdot {}^t_0F - I) \quad (18)$$

In a LDFE, the stress can no longer be defined as 'force over area', as the area may change in magnitude and/or direction during deformation. The stress in the deformed configuration is defined by a Cauchy stress σ as

$$\sigma n dA = df \quad (19)$$

where df is the force acting on an area dA with a unit normal vector n . Due to the energy principles on which the finite element model is based, the stress measure determines the strain measure and vice versa. The energy conjugate of the Cauchy stress is the linearized strain. The energy variation can be calculated from

$$\delta W = \int_V \sigma \delta \epsilon dV \quad (20)$$

The finite element model in DIANA software offers the choice between a Total Lagrange analysis and an Updated Lagrange analysis. The Total Lagrange analysis typically refers to an undeformed geometry, while an Updated Lagrange analysis has an updated geometry throughout the analysis. The Total Lagrange analysis has been selected for the application in this research. The stress in the Total Lagrange analysis must be related to the undeformed geometry and must be energy conjugated to the Green-Lagrange strain. This stress measure is the 2nd Piola-Kirchhoff stress S and is related to the Cauchy stress by

$${}^t_0S = \det {}^t_0F \cdot {}^t_0F^{-1} \cdot {}^t_i\sigma \cdot {}^t_0F^{-T} \quad (21)$$

All input parameters which indicate a stress are interpreted as 2nd Piola-Kirchhoff stresses in DIANA software. The Jaumann rate is an objective rate, meaning that it transforms properly as a tensor under rigid body motions. The Jaumann derivative of the Cauchy stress is defined as

$$\check{\sigma} = \dot{\sigma} + \sigma \cdot \Omega - \Omega \cdot \sigma \quad (22)$$

Here $\dot{\sigma}$ is the time derivative of the Cauchy stress. The Jaumann stress rate can be considered as the stress rate in the coordinate system that rotates with the material.

For the specific problem of the horizontal loading of a jack-up structure, inclusion of this LDFE typically results in a larger moment at the spudcan footings, during push-over loading. This occurs due to the changes in element lengths, causing a second order effect of the structure's mass. The significance of the large-deformation framework will be discussed in the benchmark study (Section 5.3).

Iterative scheme and convergence criteria

The basic iterative scheme that is used for the calculations is the regular Newton–Raphson scheme. Although the software by DIANA has many iterative schemes available (see Manie (2016b)), the normal Newton–Raphson scheme produces a relatively smooth convergence. Note that the horizontal pushover loading convergences both on force and displacement in the case of a force-controlled analysis, and only on force in the case of a displacement-controlled analysis. The vertical loading stages are always performed through a force-controlled analysis. The convergence criteria for force and displacement are defined as:

$$\text{Force norm} = \frac{\sqrt{g_i^T g_i}}{\sqrt{g_0^T g_0}} \quad (23)$$

$$\text{Displacement norm} = \frac{\sqrt{\Delta u_i^T \Delta u_i}}{\sqrt{\delta u_0^T \delta u_0}} \quad (24)$$

The force norm is the Euclidian norm of the out-of-balance force vector g . The force norm after the current iteration is checked against the norm of initial unbalance g_0 . The displacement norm is a Euclidian norm of the iterative displacement increment. The displacement norm is checked against the norm of displacement increments in the first prediction of the increment. The basic convergence criteria of the finite element model are displayed in Table 5.

Table 5: Control procedure and convergence criteria

Loading step	Control procedure	Convergence tolerances
Gravity loading (initial state)	Force controlled	Force norm = 0.001
Preloading	Force controlled	Force norm = 0.001
Unloading	Force controlled	Force norm = 0.001
Horizontal loading	Force controlled	Force norm = 0.001
		Displacement norm = 0.05
Horizontal loading	Displacement controlled	Force norm = 0.001

Difficulties in the finite element modelling of jack-up structures

As the calculations are performed using a finite element model with iterative procedures, some difficulties can arise, which one must take into account to allow for a smooth modelling process. One important difficulty is the modelling of the spudcan footings. The geometry has to be selected so, that the shape of the spudcan does not lead to large stress singularities in the soil mass below, when loaded. Specifically, a very sharp spigot can have this effect. This can lead to non convergence or even divergence. It is in this case complicated to select a proper geometry, as the modelling process should resemble reality as closely as possible. As the footings are conical and have a relatively sharp point, they have to be meshed in a specific way. The mesh for the footings needs to be relatively fine, to properly describe the complicated three-dimensional shape. The software by DIANA offers guidance here, through an automatic meshing procedure that allows a good representation of the spudcan shape. The user, however, should take into account the importance of avoiding stress singularities and the importance of meshing fine enough, to give a proper description of the footing shape. Another important aspect is the transition of the footing mesh to the soil mesh. Interface elements are meshed in between the nodes of both meshes, allowing for relative displacements. Emphasis should be placed on selecting a proper interface stiffness. Ideally, the interface would be up to a factor of 100 stiffer in normal direction than the soil geometry, to avoid interpenetration of nodes. The application of a so-called no-tension condition can lead to a sudden change in stiffness, especially when no particular care has been taken to avoid stress singularities below the spudcan geometry. This sudden change in stiffness has a large influence on the convergence rate and can lead to large difference in stiffnesses, leading to an ill-conditioned stiffness matrix. Another important aspect is the mesh size of the spudcan footings, relative to the surrounding soil. The automatic meshing procedure in DIANA software allows the element size around the footings to specifically follow the footing mesh size (which is usually the most refined). The mesh will then coarsen outwards, if a more coarse mesh is selected for the surrounding soil. It has been observed in the performed analyses that the mesh size distribution of the footings and the soil directly surrounding the footings has a significant influence on the convergence rate. Typically, a mesh size of the surrounding soil equal to that of the spudcan footings offers the most stable convergence. Finally, the numerical conditions have a significant influence on the modelling process. It is important to select convergence criteria that offer enough accuracy, whilst allowing the model to reach a state of convergence. The size of the load steps also plays a role here. Load steps should be selected so, that the loading path can be properly captured. This means that loading steps can not be too small, or too large.

4 Validation of finite element model

The finite element model will be validated by comparing its results with an experimental test and a macroelement model from literature. These tests are performed for a push-over test. The model will first be benchmarked, after which a series of parametric analyses can be performed.

4.1 The benchmark problem

In a research by Bienen et al. (2009), a model jack-up was designed for experimental investigation in a beam centrifuge. This model jack-up was designed as a representation of an average field jack-up structure. The model jack-up was fabricated from aluminium and consisted of three legs with spudcans, connected to a rigid hull. The centrifuge tests were performed in-flight, at 200 g. The jack-up structure was set down on a bed of (dry) superfine silica sand under its self-weight, and preloaded, after which the model was free to sit under self-weight. After preloading of the jack-up model, a pure lateral push-over was performed, as well as a non-symmetrical lateral push-over. Load reactions at the footings were measured throughout the loading procedure as part of the experimental set-up. The centrifuge tests gave a good insight into the behaviour of a jack-up unit under loading. The response of the experimental jack-up model clearly showed the difference between the behaviour of the model jack-up and the industry guidelines. A more realistic description of jack-up behaviour was given by Bienen and Cassidy (2009), using a macroelement model. In this research, the results from the model jack-up were compared with a macroelement model that was developed. Although somewhat conservative, the macroelement model gave a much better description of the jack-up unit's behaviour under loading, when compared to the linear springs used in the ISO guidelines. The finite element model described in this research will be benchmarked by the research of Bienen and Cassidy (2009) and Bienen et al. (2009). This will be performed by comparing results of a pure lateral push-over, as well as a non-symmetrical lateral push-over (Figure 18). Both loading directions will be simulated in accordance with the tests performed by Bienen et al. (2009), by applying a load at the topside of the structure. The reader should note that in the comparison, references are given to Bienen and Cassidy (2009) for the macroelement and the experimental model, where the experimental model results have been taken from Bienen et al. (2009). Hereafter, the finite element model is abbreviated as FE, the experimental model is abbreviated as EXP and the macroelement model is abbreviated as ME. A sign convention is adopted here, to allow for a uniform description of both the global response of the jack-up unit and the footing responses (Figure 19).

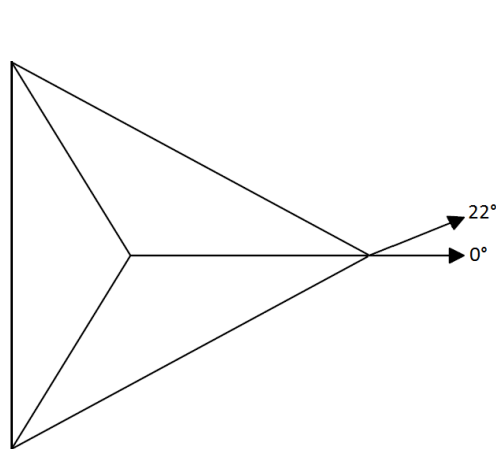


Figure 18: Loading directions used in model validation

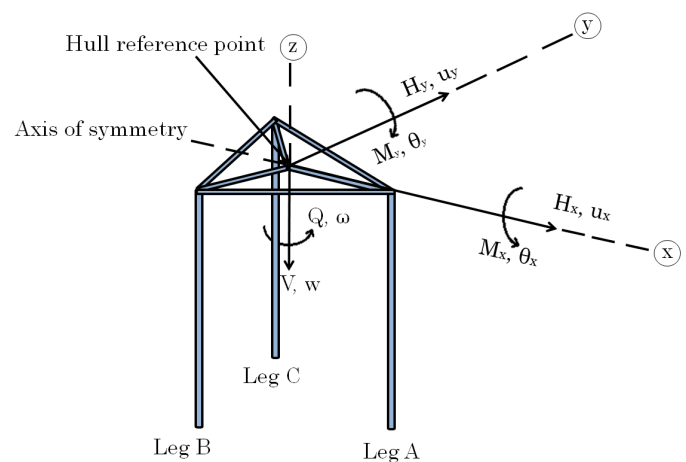


Figure 19: Sign convention adopted in this research

4.1.1 Pure lateral push-over

Figure 20 shows the global response of the jackup structure under loading, where points A, B and C correspond to the loading states for which vertical stresses are displayed in Figure 27. It can be stated that the FE model captures the behaviour of the jack-up structure under loading quite well. Similar to the ME model by Bienen and Cassidy (2009), the global response shows a linear initial response until the model builds up significant plasticity and a non-linear response is observed. The stiffness is then reduced in a non-linear fashion. Where the EXP results from Bienen and Cassidy (2009) show a relatively high stiffness initially, the stiffness of the FE model is significantly lower. This difference in stiffness could be explained when observing the calibration of the soil parameters. It is known that in the EXP model, a relative soil density of 84% is used. The calibration in this research has been performed on the basis of the same soil with a relative density of 75%. This could lead to a less stiff response, initially. As opposed to the ME, the stiffness reduction under loading is quite gradual in the FE model, where the response shows a good fit with the EXP results. Failure of the jack-up system is predicted at an applied horizontal load of 22.7 MN. The predicted horizontal load at failure is relatively high, compared to the ME model and the EXP model, which predict a horizontal load of 18.8 and 22 MN at failure, respectively.

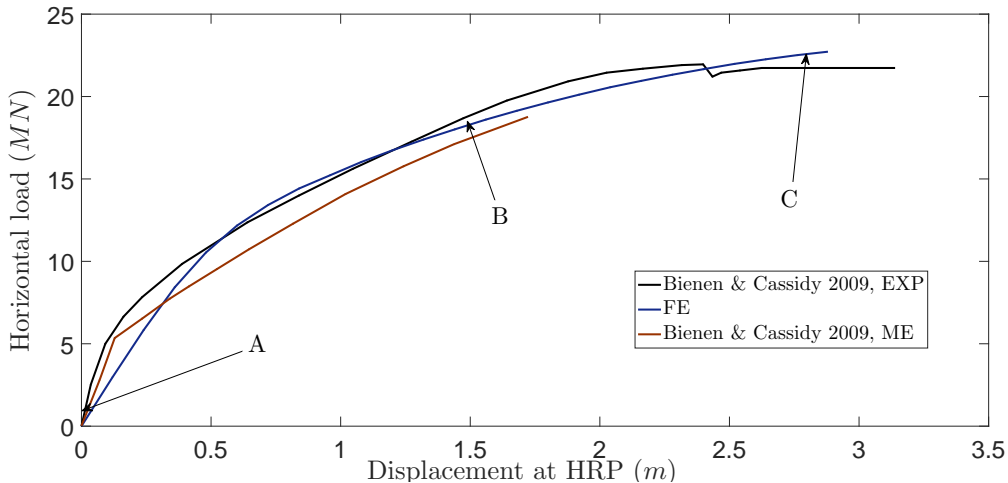


Figure 20: Global response of jack-up structure under pure lateral push-over; HRP, hull reference point.

Figure 21 displays the load-displacement results for the horizontal load and the moments for each individual footing. The EXP results shows an increase of horizontal load in spudcan A, whilst spudcans B and C show a constant, or even a decrease of horizontal load during push-over. A similar response is observed for the moments. An increase in spudcan moment is observed for spudcan A, whilst spudcans B and C show a gradual decrease in moment during push-over. It can be observed that especially the horizontal load and moment response at spudcan A is not modelled accurately in the ME model. The FE model shows a better description of footing response at spudcan A. The ME and FE model show a similar description for response at spudcans B and C. The response for the horizontal load of these spudcans is different from the EXP for both models. The moment loading response of spudcans B and C is captured relatively well, by both the ME and FE model, although not entirely accurate. Some of these differences could be explained by considering the amount of preload at each footing. For the EXP set-up, the amount of preload measured at each footing showed differences between spudcans. Both the ME and the FE model are entirely symmetrical, meaning that the amount of preload at each footing is similar. This results in a similar description of spudcans B and C in both model, whereas the EXP results shows differences between both spudcans.

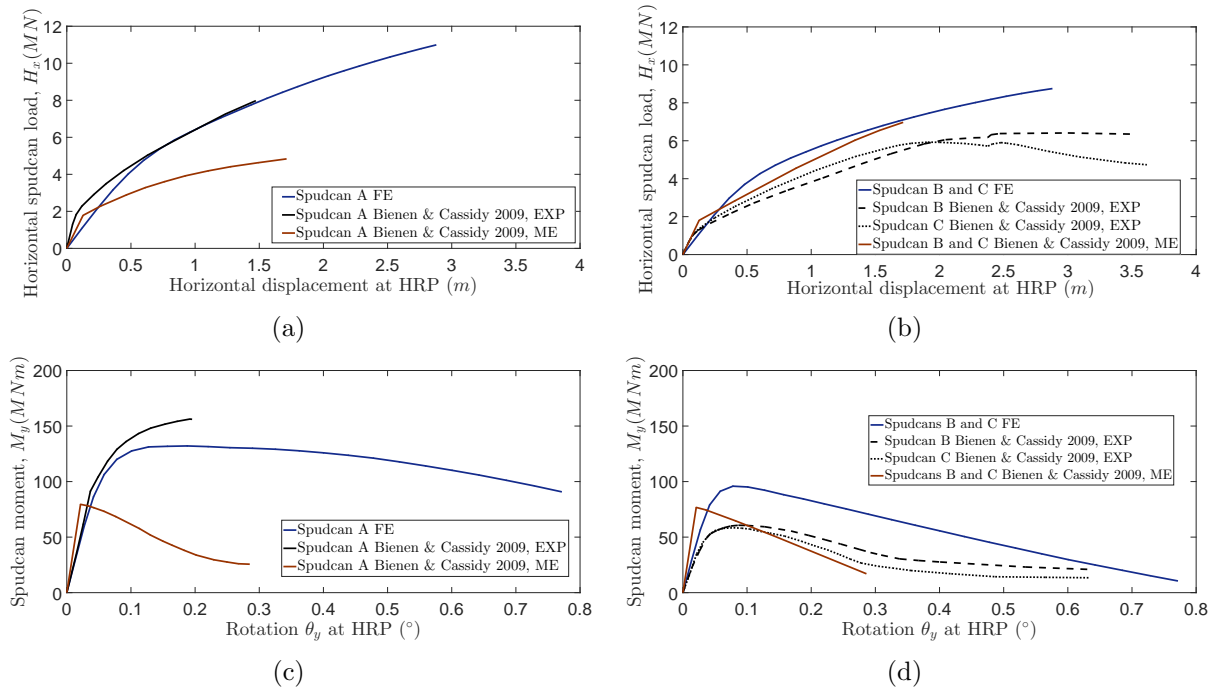


Figure 21: Load-displacement response for pure lateral push-over: (a) horizontal load spudcan A; (b) horizontal load spudcans B and C; (c) moment spudcan A; (d) moment spudcan B and C.; HRP, hull reference point.

Figure 22 shows the normalized footing responses in vertical, horizontal and moment plane. It can be observed that the preload values for the EXP differ for each spudcan. This difference is caused by the installation of the model jack-up, which was not entirely symmetrical. The EXP shows an increase in both vertical, horizontal and moment loading for spudcan A (frontside footing) during push-over. Both the ME model and FE model show a decrease in moment at spudcan A, even under an increasing horizontal and vertical loading. It can be observed that the FE model shows a good description of the response of spudcan A during loading in (V, H, M) plane. The decrease in moment at spudcan A is however only modelled by the ME and the FE model, and is not observed in the EXP results. The FE model shows a better description for the spudcan A footing than the ME model. Both the ME and FE model show a similar response for spudcans B and C during pushover, when compared to the EXP results. It is hard to determine which of the models performs best when looking at spudcans B and C, due to the influence of the preload magnitude at each footing. As these are different in the EXP, it can not be stated that one model does better than the other. It can be stated, however, that both the ME and FE model show a good description of the behaviour of spudcans B and C when compared to the EXP results. It is interesting to see the reduction in moment response at spudcan A for both the ME and FE model. As the jack-up structure shows a stable situation at this point of occurrence, a redistribution of forces is likely the cause.

The stability of the jack-up structure is determined by the behaviour of the foundation as well as the structure. Figure 23 displays a simple representation of the jack-up structure. In an ideal situation, the foundation would be loaded solely by the weight of the structure. The spudcans would then carry this weight load and transfer it to the soil beneath. In a case where a horizontal load is applied to the structure, a moment has to be taken up by the foundation. The horizontal load also leads to a sway of the structure. This leads to a second order effect, causing the weight of the structure to also induce a moment at the foundation. The foundation has two mechanisms

to take up this moment loading: a push-pull mechanism and a moment reaction at the spudcan footing. The push-pull mechanism is controlled by the vertical reaction forces at each spudcan footing. This push-pull mechanism causes a higher vertical reaction force at the front side footing during push-over loading. The vertical reaction force at the back side footings is then decreased. This counteracts partially the induced moments at the foundation. The second type of moment resistance is caused by the spudcan footings in combination with the soil below. Through the penetration of the spudcan footings into the soil, a certain amount of fixity is present. This allows the spudcan to transfer some of its moments to the soil surrounding it. Both mechanisms dictate the behaviour and the stability of the jack-up structure. As observed in Figure 22, a reduction of spudcan moment is observed in the spudcan A at a certain point during push-over loading. To ensure stability of the rig, the moments will need to be accounted for. This happens through the push-pull mechanism as described.

To investigate this, the moments have been computed for the horizontal loading of the structure. These moments will need to be counteracted by the sum of all moments along the spudcan, as well as the moments coming from the vertical push-pull mechanism. The spudcan moments have been taken from the FE model, whilst the moments from the push-pull mechanism have been computed with respect to the hull reference point (HRP). The computed moments are displayed in Figure 24. What can be observed is that the moments at the spudcan footings decrease during the lateral push-over. This decrease in moment is counteracted by the difference in increase in moments from the horizontal loading and the increase in moments coming from the push-pull mechanism. The vertical reactions at the spudcan footings cause the push-pull mechanism, which increases more strongly than the moments coming from the horizontal loading of the topside. It is therefore, that the push-pull mechanism is responsible for counteracting the moment reduction at the footings to ensure stability of the rig.

The vertical displacements of the jack-up structure for a loading state close to failure are displayed in Figure 25. It can be observed that there is compression in the front side (spudcan A) footing, whilst the back side footings show a heave. This causes the back side footings to separate from the soil, locally. This effect can also be observed in the soil stresses, displayed in Figure 27. Here, the stresses are displayed for loading states A to C from Figure 20. The stresses are displayed for a certain cutting plane in the FE model, which is displayed in Figure 26. It can be observed that the stress state prior to the horizontal loading shows a similar state for both footings. During the push-over, as the jack-up rig is displaced horizontally, the total jack-up structure experiences a rotation, as also observed from Figure 25. This causes the front side footing (spudcan A) to receive a larger compression, due to the increased weight loading here. The back side footings (spudcans B and C) are unloaded due to this rotation. This leads to a lower vertical stress in the soil below the back side footings and an increased vertical stress in the soil below the front side footing. When observing a loading situation close to failure, such as point C in fig. 27, it can be observed that the backside footing transfers very little pressure to the soil below, whilst the front side footing experiences a very large compression leading to a large vertical stress in the soil.

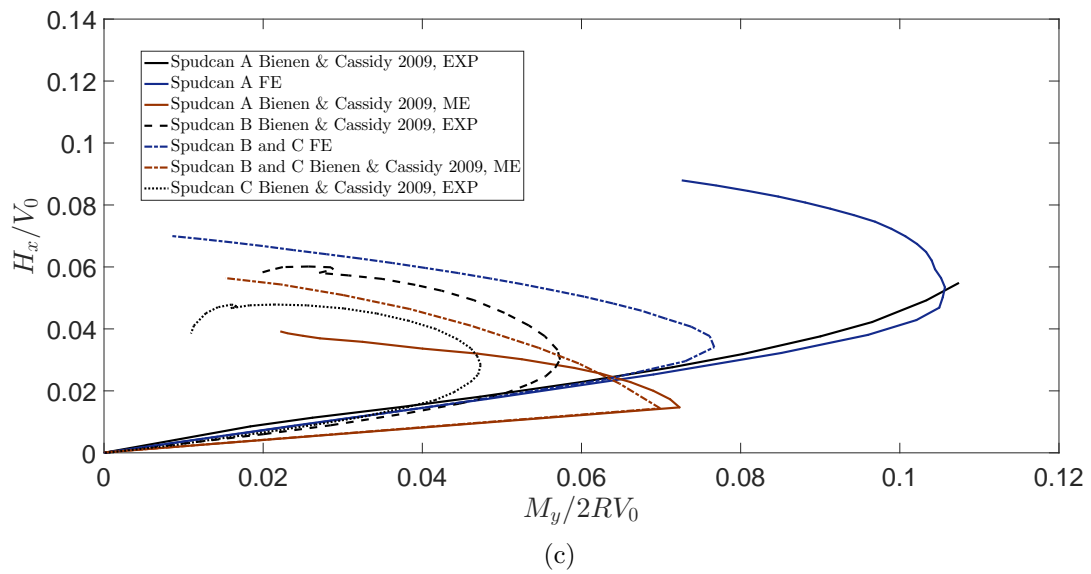
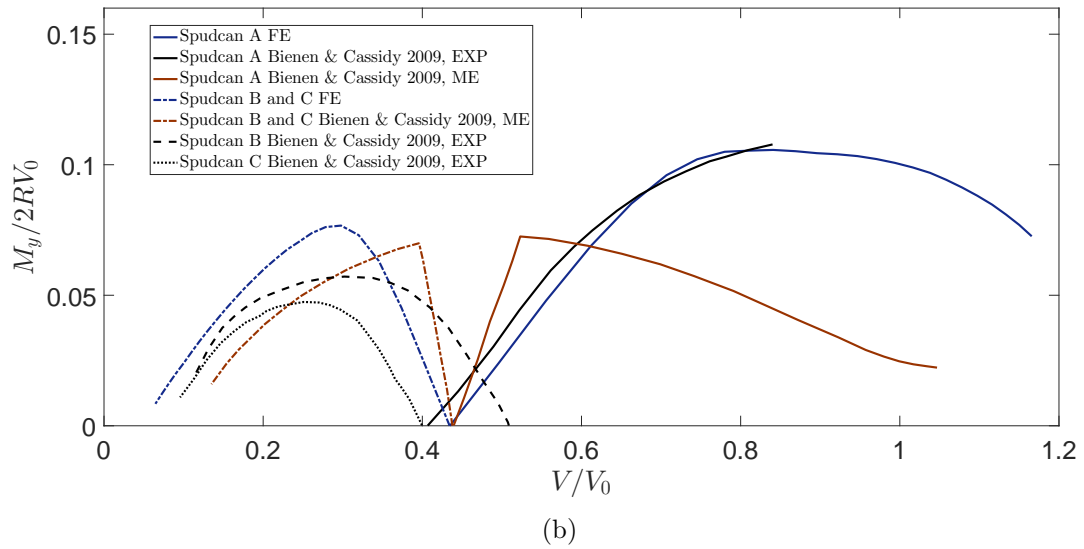
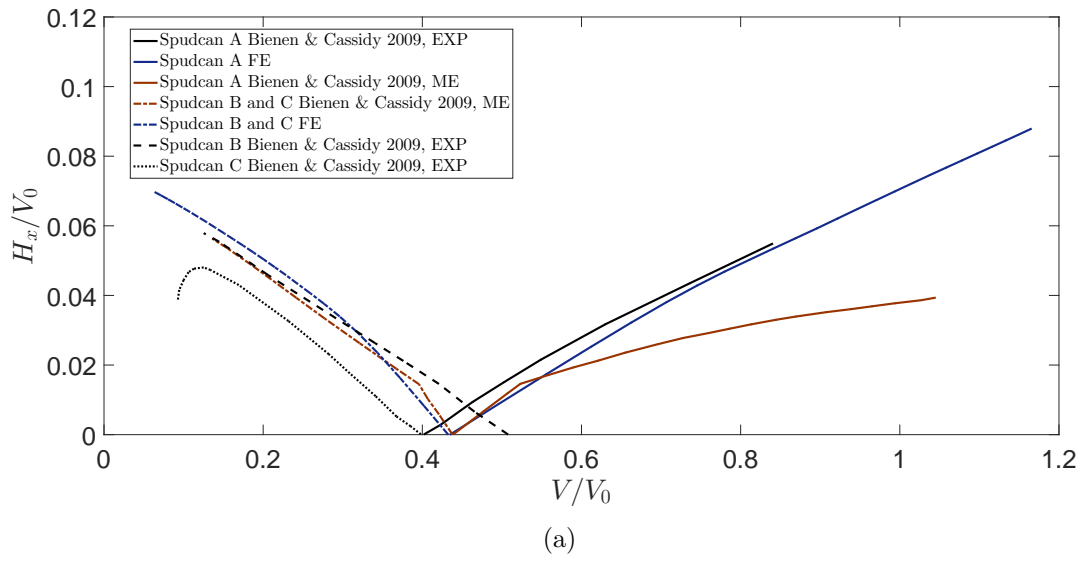


Figure 22: Normalized footing response for pure lateral push-over: (a) vertical-horizontal; (b) vertical-moment; (c) moment-horizontal.

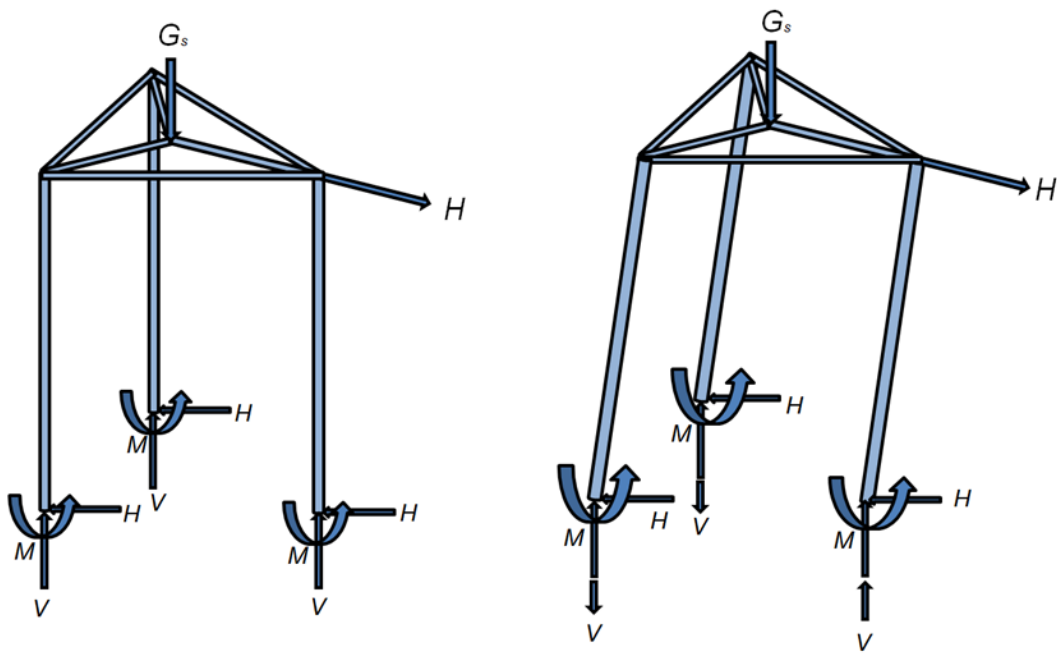


Figure 23: Simplified jack-up structure stability mechanism for pure lateral push-over

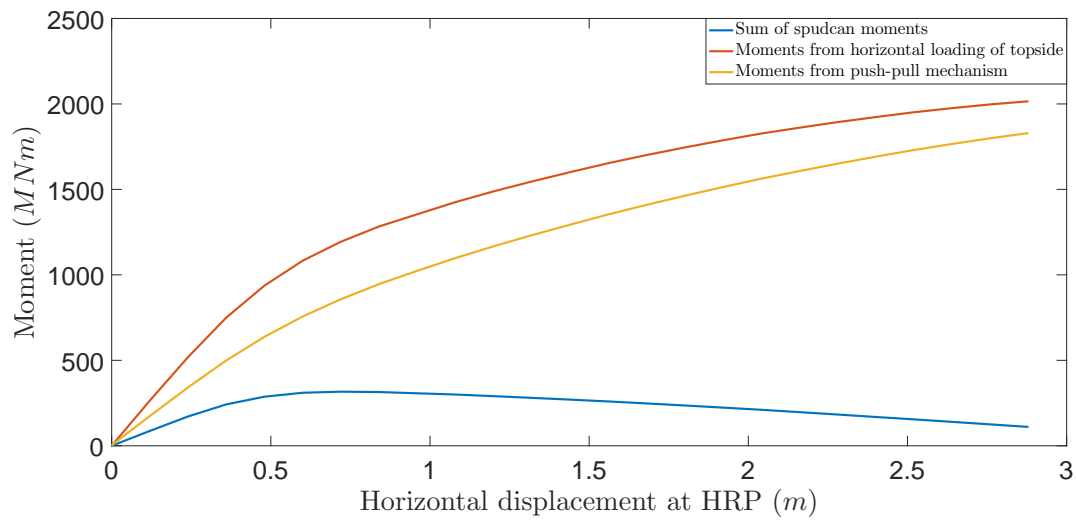


Figure 24: Moments during pure lateral push-over in FE model. HRP, hull reference point.

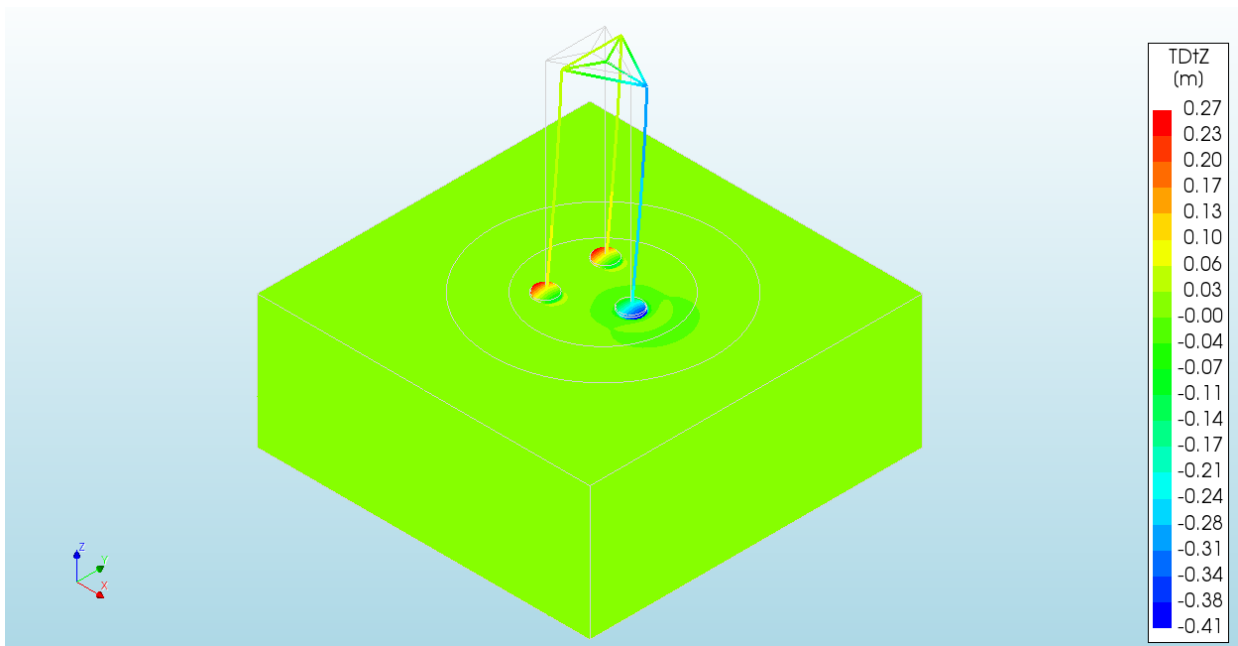


Figure 25: Vertical displacements of jack-up structure close to failure (point C)

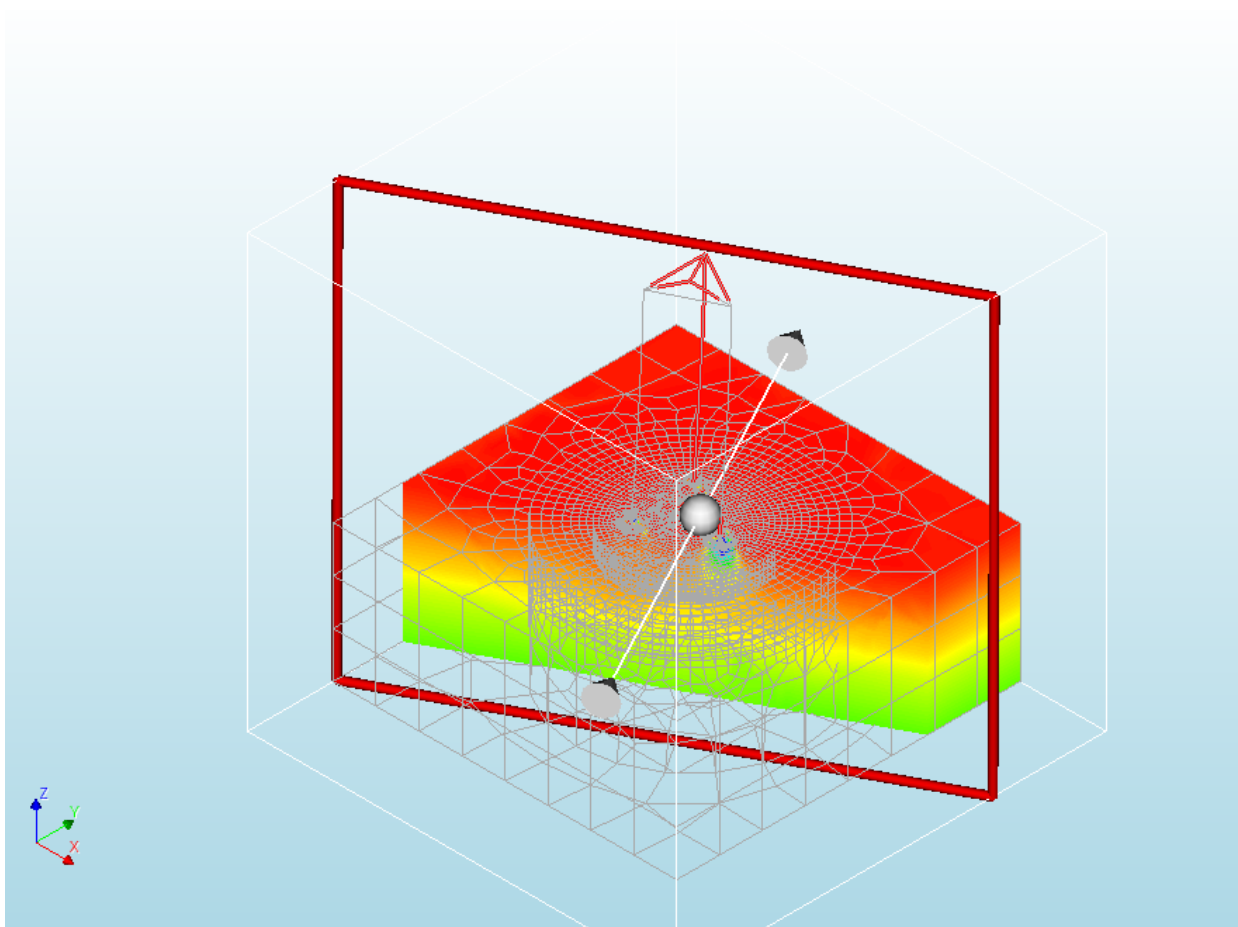
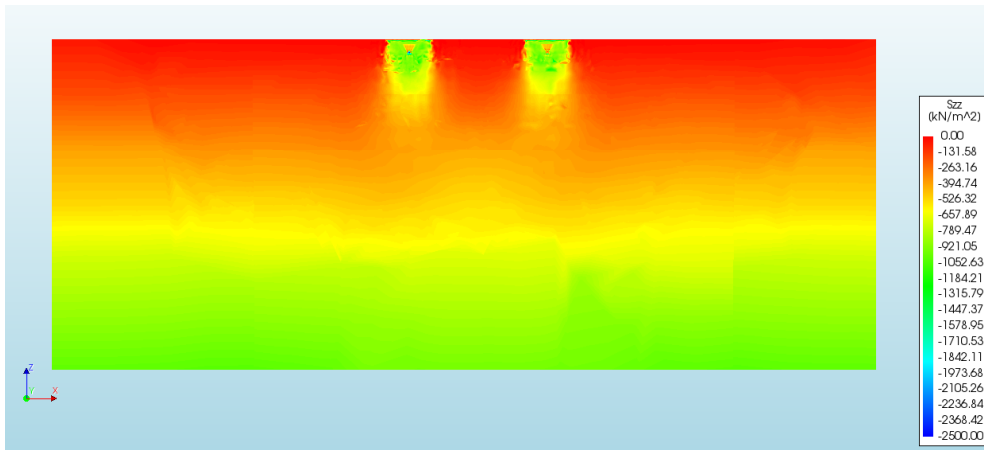
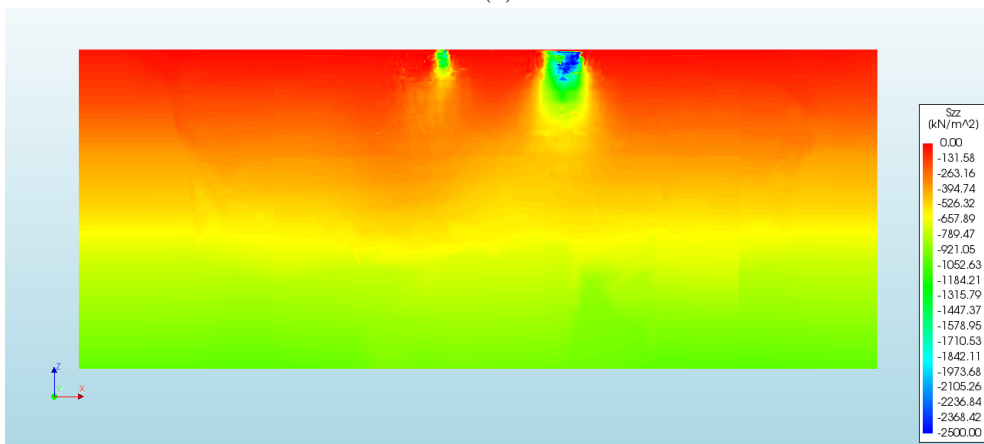


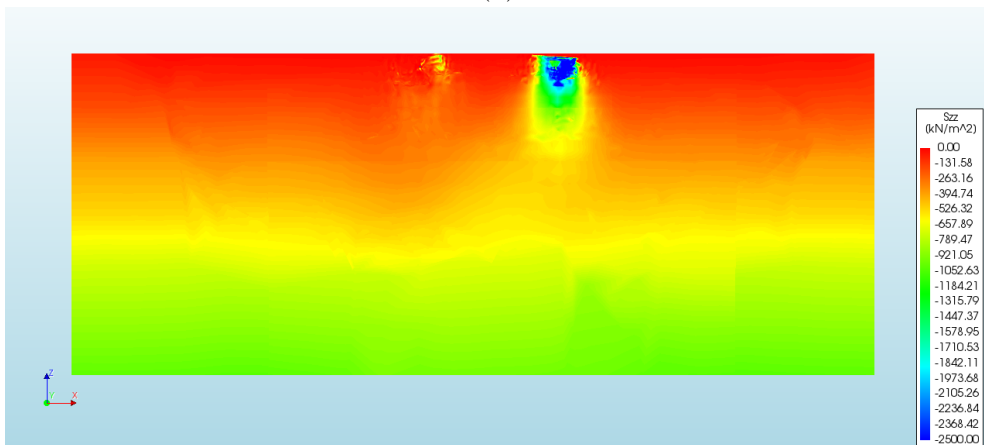
Figure 26: Cutting plane for which stresses are plotted from FE



(a)



(b)



(c)

Figure 27: Vertical soil stresses during pure lateral push-over below spudcan C (back side) and spudcan A (frontside): (a) prior to horizontal loading (point A); (b) during push-over (point B); (c) close to failure (point C)

4.1.2 Non-symmetrical lateral push-over

Next to a pure lateral push-over, the model will also be benchmarked by a non-symmetrical lateral push-over. This analysis is performed in the FE model by means of a force-controlled analysis. The push-over is performed under a 22° loading angle, where the applied load is attached to the topside structure (Figure 28). The same sign convention is adopted here, as for the pure lateral push-over case (Figure 29).

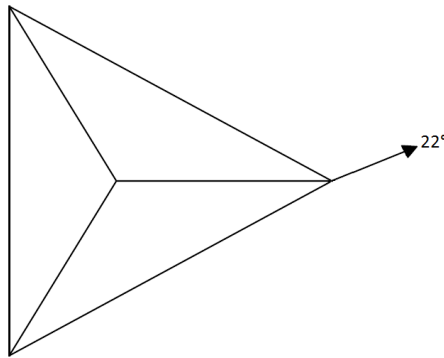


Figure 28: Loading direction applied at topside for 22° non-symmetrical loading

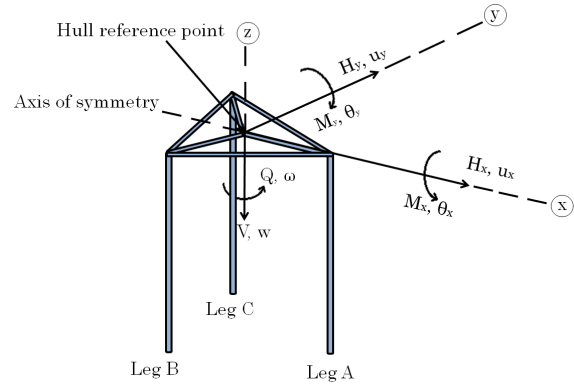


Figure 29: Sign convention adopted in this research

The global response of the jack-up is displayed in Figure 30. It can be observed that the EXP results show a very stiff response initially. Both the ME and FE model underestimate this initial stiffness, similar to the pure lateral push-over. Here, it can be stated again that this could be due to the difference in soil parameter calibration for the FE model. A nonlinear stiffness reduction during loading is observed. This stiffness reduction evolves more gradually in the FE model when compared to the ME model. The overall stiffness during loading is the highest in the FE model. The maximum applied horizontal loads are capture quite well by the FE model. The maximum applied horizontal loads are 17.9, 15.5 and 17.1 MN for the EXP, the ME and the FE model, respectively.

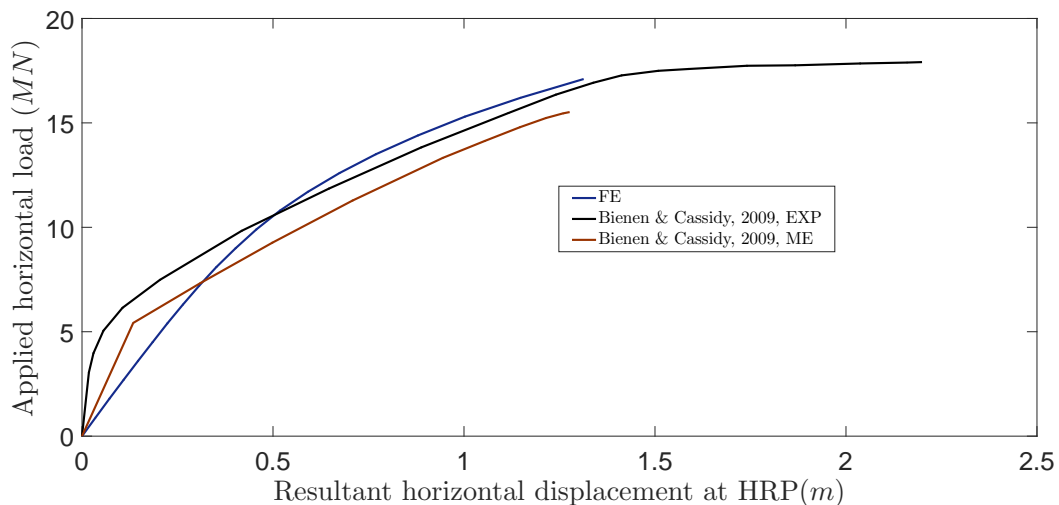


Figure 30: Global response of jack-up structure under 22° lateral push-over; HRP, hull reference point.

Figure 31 displays the load-displacement response for the 22° lateral push-over. It can be observed that the stiffness, initially from the EXP results is significantly higher than the initial stiffness of the FE and ME model. The description of the behavior of the jack-up unit for both the ME and the FE model show some differences with the EXP results. Analogous to the pure symmetrical push-over, the preload magnitudes of the individual spudcans are different for the experimental test, whilst both the ME and the FE model have similar preload magnitudes for all spudcans. Whilst this could cause for some differences in the predicted response, observations can still be made. The description of the load-displacement response at spudcan A is best in direction x, which is the dominant loading direction. Both the ME and the FE model show a similar response as described in the pure lateral push-over here. Both predictions differ from the EXP results in magnitude, but show the same behavior under loading. The description of spudcan A in direction y (secondary loading direction) is less well defined for both the ME and the FE model. Both models show a very similar description for spudcan A in y-direction, which differs substantially from the EXP results. Although the behavior during loading is captured, the magnitude is substantially different between both the ME and FE model and the EXP. The load-displacement response of spudcan B is modelled quite accurately by both the ME and the FE model in both loading direction x and y. The load-displacement response of spudcan C is modelled less well, especially in direction y, where the EXP results show that spudcan B takes virtually no horizontal load. Both the ME and FE model predict a higher horizontal load during push-over here. The load displacement response of spudcan C in direction x is modelled more accurately, although differences between the FE model and the EXP are quite significant for this spudcan. The ME model has a more accurate description for spudcan C in x direction.

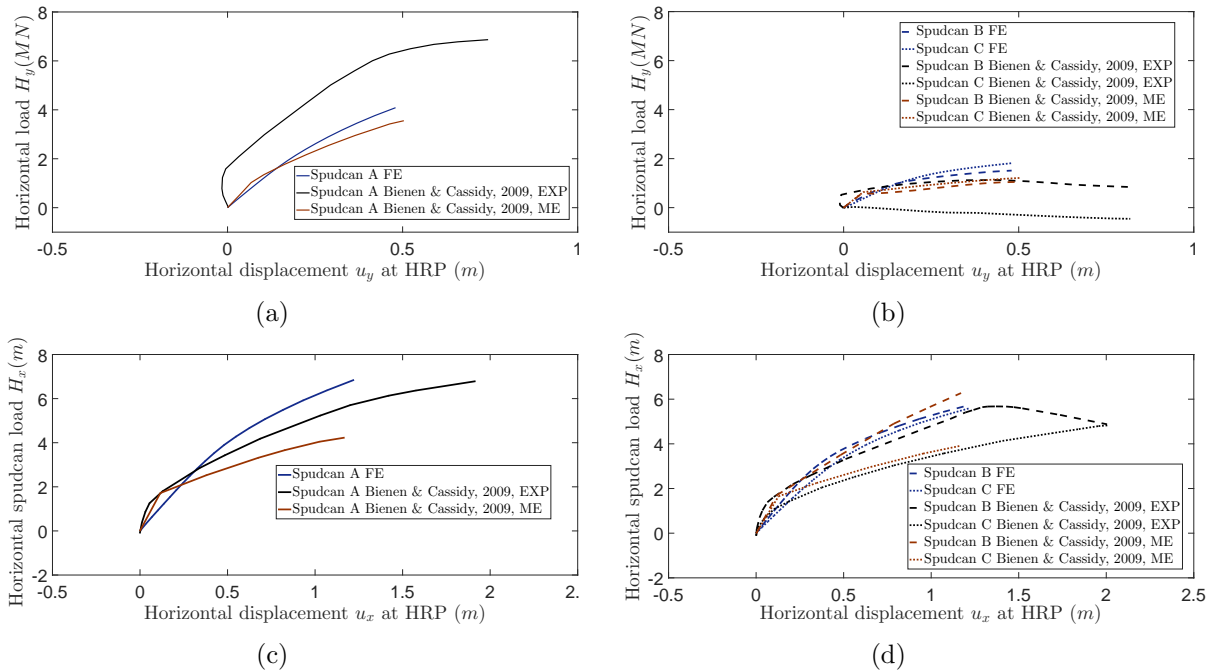
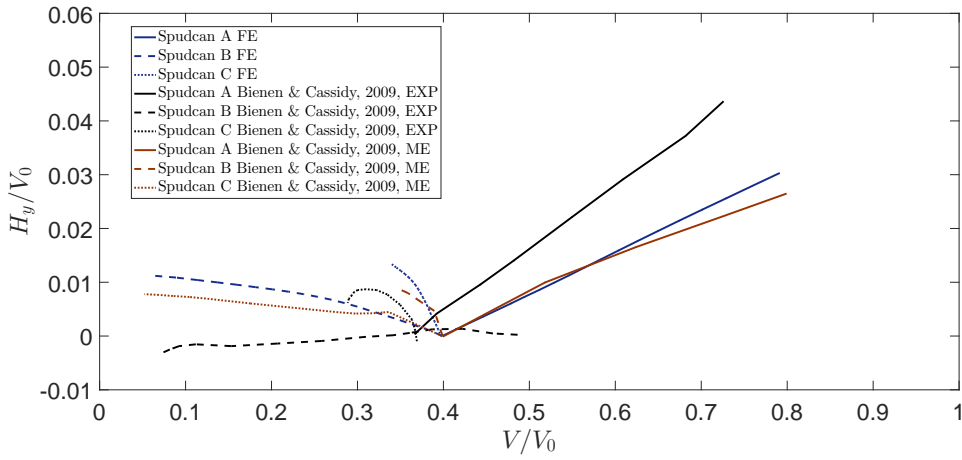
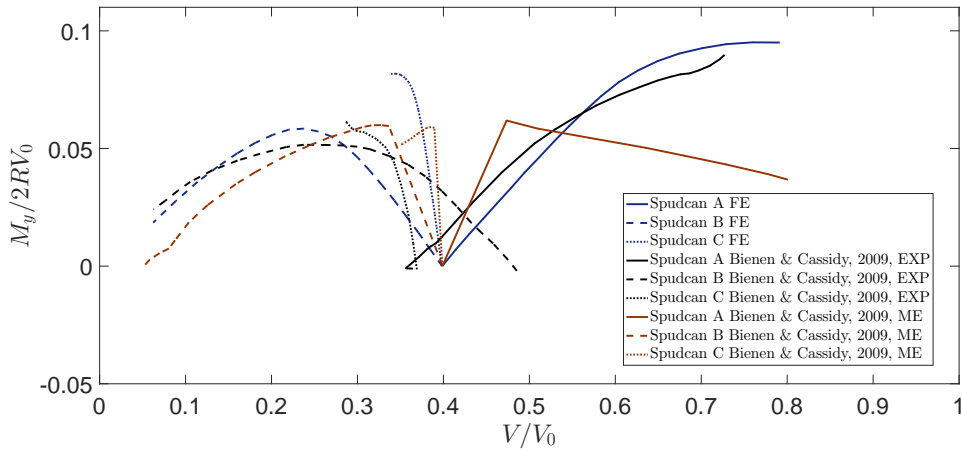


Figure 31: Load-displacement response for 22° lateral push-over: (a) horizontal load H_y spudcan A; (b) horizontal load H_y spudcans B and C; (c) horizontal load H_x spudcan A; (d) horizontal load H_x spudcans B and C; HRP, hull reference point.

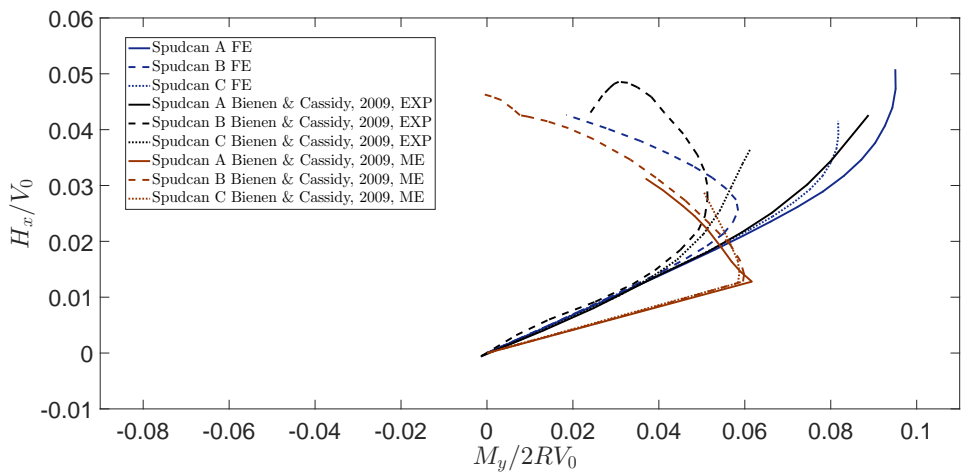
Figure 32 and Figure 33 show the normalized response for the lateral 22° push-over. It can be observed that both the ME and the FE model do fairly well in describing the normalized response when compared to the EXP. When compared to the ME model, the FE model gives a better description of spudcan A. The FE model does well in describing the normalized response of this footing during push-over when compared to the EXP results. The main differences between the FE model and the EXP results are observed in the $M_x - H_y$ and $V - M_x$ plane. It should be stated here, however, that the difference in preload as mentioned previously has an influence on the observed results, making it difficult to judge the accurateness of the prediction of the FE model. The ME model typically shows a response that is elastic initially, and strongly plastic suddenly. The prediction of spudcans B and C for the FE and ME model is quite similar. This prediction is generally quite well matched to the EXP result. Again, the biggest differences here can be observed in the $M_x - H_y$ and $V - M_x$ plane. The overall response of the FE model is typically best in the dominant loading direction (x).



(a)

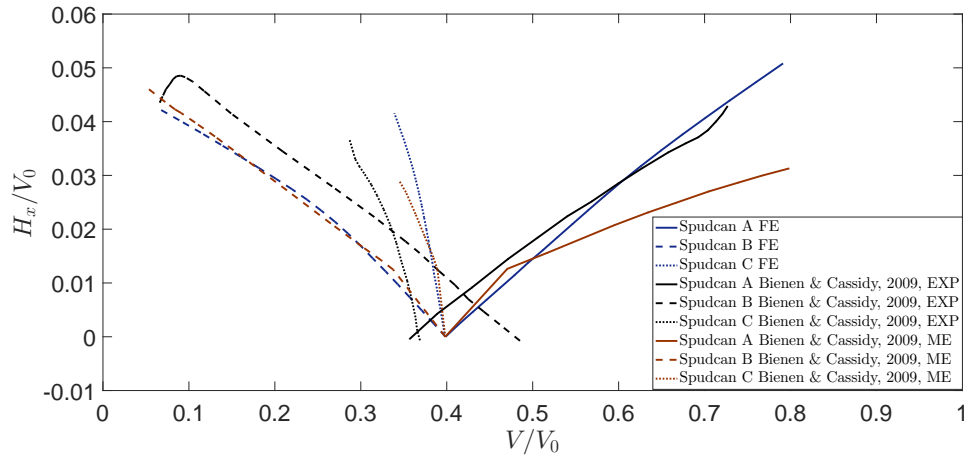


(b)

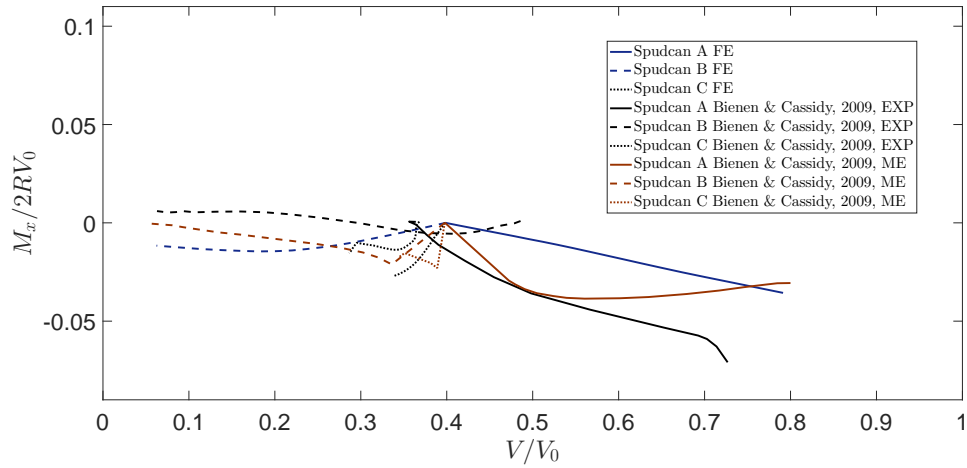


(c)

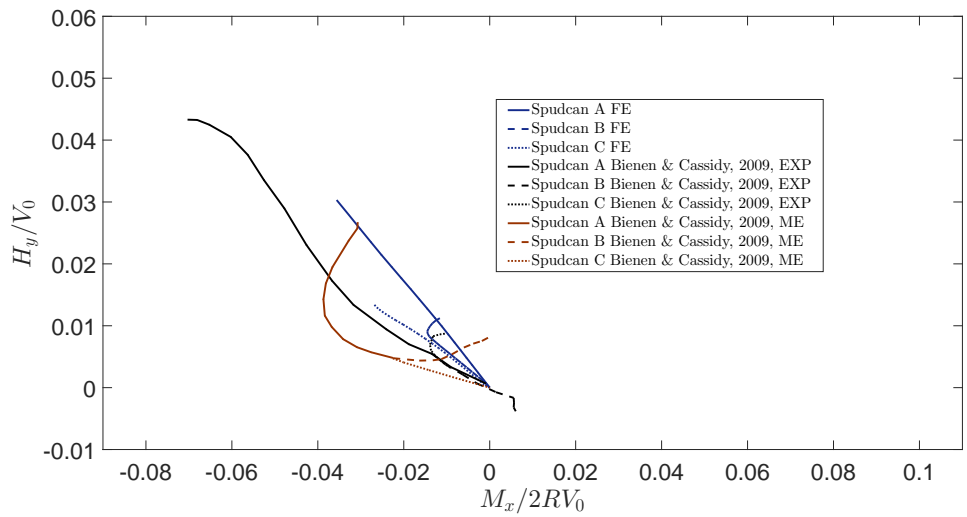
Figure 32: Normalized footing response for non-symmetrical push-over at 22° loading for direction y: (a) vertical-horizontal; (b) vertical-moment; (c) moment-horizontal.



(a)



(b)



(c)

Figure 33: Normalized footing response for non-symmetrical push-over at 22° loading for direction y: (a) vertical-horizontal; (b) vertical-moment; (c) moment-horizontal.

5 Parametric studies

After validation of the finite element model, different parametric studies will be performed. The parametric studies will be performed to investigate the influence of certain parameters on the model behaviour. For each of the parametric analyses, a description of the performed test and the tested parameters will be given.

5.1 Analysis of dilation influence

The soil model used in the validation study used the conservative assumption that the soil displayed no dilative behavior (e.g. $\psi = 0$). This approach is supported by the use of the friction angle at constant volume. As there is no dilative behaviour in the original soil model, the volumetric response of the soil will be contractive under all circumstances. To investigate the influence of the dilation on the model response, the same parameters will be used for the soil model, with the addition of a dilation angle of 10° . This magnitude of the dilation angle does not necessarily represent a real situation. By applying an extreme value, the influence of the dilation angle will be more pronounced. The test performed here, is the same on as the pure lateral push-over test (Section 4.1.1). The push-over is performed through a displacement-controlled analysis, with a prescribed displacement of the topside. The vertical spudcan loads applied in the test are displayed in Table 6 and the soil parameters applied in the test are displayed in Table 7.

Table 6: Vertical spudcan loads

	Spudcan A	Spudcan B	Spudcan C
$V_{sw}[MN]$	54.2	54.2	54.2
$V_0[MN]$	125.1	125.1	125.1

Table 7: Soil parameters applied in dilation parametric study

K_{ref} [MPa]	p_{ref} [kPa]	m	ν	ϕ_0	ϕ_f	α	γ	$\gamma_{soil,dry}$ [kN/m ³]	ψ [deg]
110	100	0.5	0.3	18.5	33.75	120	0.0008	17.36	10

The behaviour of both soil models will differ in their volumetric response. The volumetric response of both models is displayed in Figure 35, taken from a modelled triaxial test in DIANA software. The performed triaxial test was consolidated to a K_0 stress state with $\sigma_1 = 120kPa$ and $\sigma_2 = 60kPa$, analogous to Pucker et al. (2013).

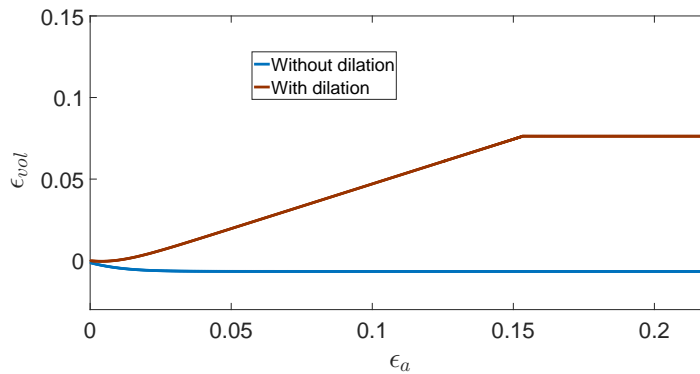


Figure 34: Volumetric response of soil models during triaxial test

It should be noted that the volumetric response shown in Figure 34 for the model including dilation is capped at a certain volumetric strain, based on the void ratio. The void ratio parameters that were used for this cut-off have been taken from Cheong (2002). This is included to avoid the model having a volumetric response that shows a volumetric increase throughout a deviatoric loading path. Furthermore, it can be observed that the model without dilation shows only contractive behaviour under triaxial testing.

The global response of the jack-up unit under a pure lateral push-over including and excluding dilative behavior is displayed in Figure 35. Both analyses display the same initial elastic stiffness. This similarity can be explained by the preload parameters, which are the same for both models. The soil model that includes dilative behaviour shows a larger stiffness under loading than the one that does not. The ultimate capacity of the model that includes dilative behaviour is also significantly higher.

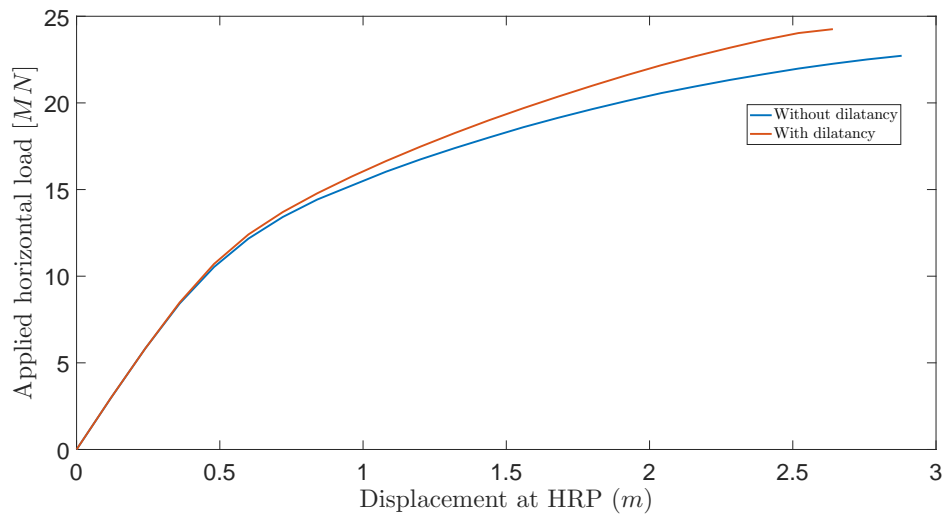
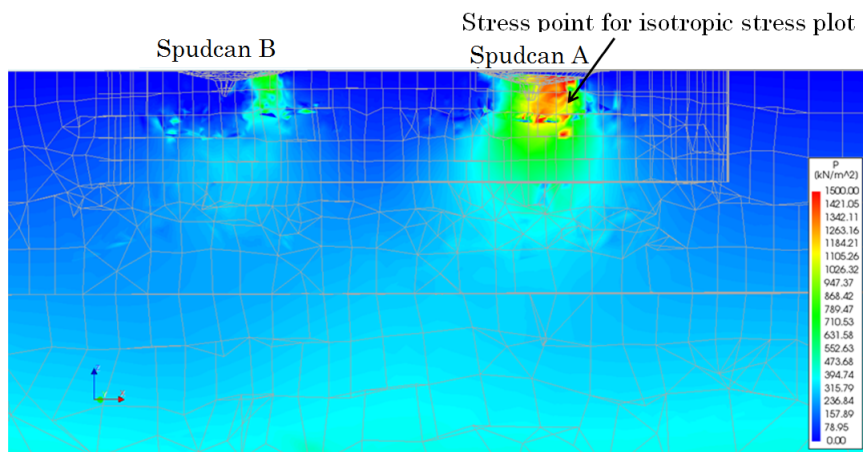


Figure 35: Influence of dilative behaviour on global response of jack-up unit under pure lateral push-over, HRP, hull reference point.

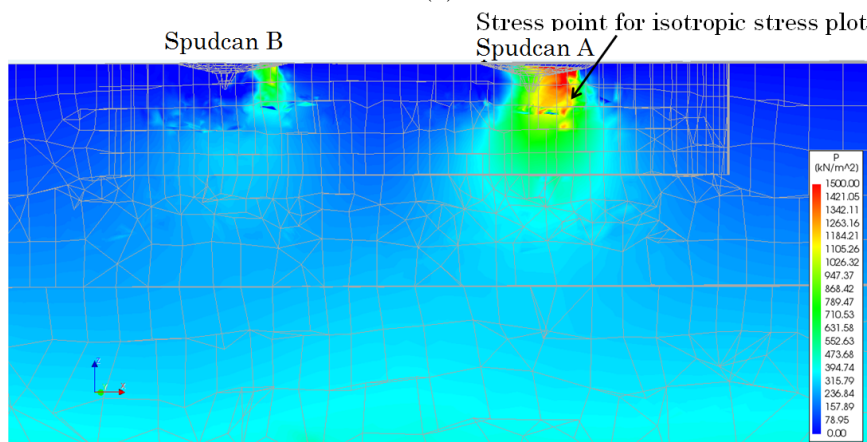
The isotropic effective stress p' of both models below spudcan A and spudcan B have been displayed for the same applied horizontal load in Figure 36. What can be observed, is that the isotropic effective stress is higher in the model that includes the dilative behaviour of the soil. This phenomenon can be explained when considering the effect of a volumetric expansion of the soil, locally. The tendency of the soil to dilate will be counteracted by the surrounding soil particles. This will lead to a higher stress in the soil, when compared to a soil that merely shows contractive behaviour. This causes the isotropic effective stress below both spudcan A and spudcan B to be higher for the case that includes dilatancy. For clarification purposes, the isotropic effective stress is plotted for a point below spudcan A in Figure 37. This plot shows the difference in isotropic effective stress is quite substantial for the observed point below spudcan A. This could be explained by considering that the highest stresses occur around this point, due to the rotation of the jack-up topside leading to a compression of spudcan A. Therefore, a large difference between the soil model that includes dilative behaviour and the one that does not, can be observed. The global response from Figure 35 showed a higher global stiffness during loading and a larger maximum load. The global stiffness can be related to the local stiffness of the soil. A stiffer soil will cause less deformations at the topside structure during loading. This increase in stiffness has a direct

effect on the maximum load, as the LDFE causes the amount of displacements to directly affect the loads at the spudcans. The increase in isotropic effective stresses in the soil also have a direct influence on the capacity. A soil particle with a higher isotropic effective stress, will have a higher capacity during shearing.

Similarly to the original calibrated soil model, the moments acting on the jack-up structure have been computed for the case that includes dilatancy. The results of these computations are displayed in Figure 38. What is interesting to observe from this plot, is that the moment balance is predominantly determined by the moments from the push-pull mechanism. This is very similar to the response of the soil model that disregards dilative behaviour. What stands out in this plot however, is the substantial increase of moments from the push-pull mechanism, whilst the moments at the spudcans are only slightly higher than the case that disregards dilatancy. It can also be observed that the moments from the push-pull mechanism are predominantly determined by the response of spudcan A, the frontside footing. The effect of the dilative behaviour of the soil is more pronounced for this footing, than both backside footings, spudans B and C.



(a)



(b)

Figure 36: Isotropic effective stress p from FE model at 19.7 MN load: (a) without dilatancy; (b) 10° dilatancy.

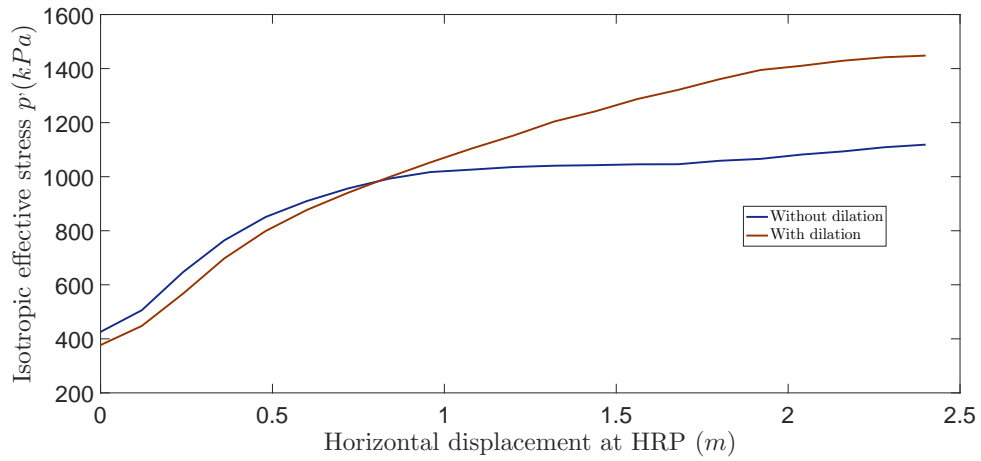


Figure 37: Isotropic stress below spudcan A during push-over

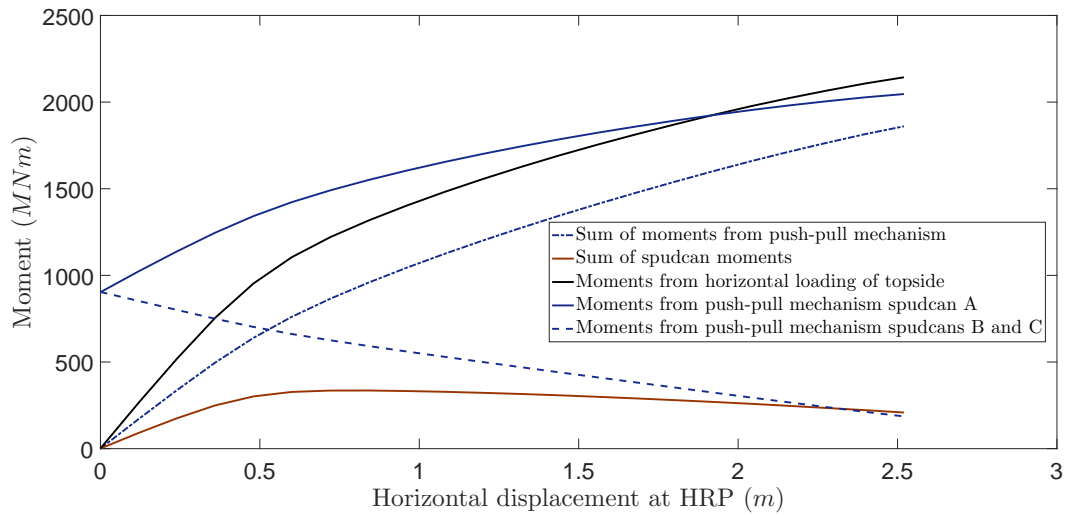


Figure 38: Moments during pure lateral push-over in DIANA model with inclusion of dilatancy.

5.2 Analysis of simple soil model

The soil used in the benchmark study was modelled in the Modified Mohr-Coulomb soil model. This allowed for an accurate description of the soil behaviour for both a triaxial and an oedometer test, allowing for calibration of the soil model. To investigate the influence of the soil model on the behaviour of the jack-up unit under loading, a pure lateral push-over has been performed for three different calibrations of the MMC soil model. The goal for this parametric analysis is to research the influence of the behaviour of the soil under shear and compressional loading on the model performance. This will give an indication of the significance in calibrating the soil model for a shear test or a compression test. The calibrated MMC model is taken as a basis here. A simplified MMC soil calibration is then created. This simplified MMC model will have a similar behaviour during compression, described by a hardening rule and a non-linear elasticity. The behaviour of the simplified MMC model during shear is different from the original calibration of the MMC model. Instead of modelling the behaviour during shear with a complicated hardening rule, a linear approach is taken here. This means that the soil model will be elastic-perfectly plastic during shearing. This should overestimate the capacity of the soil under a shearing test, as the peak is achieved at an earlier stage than for the original calibration. The comparison of these two models will give an indication of the significance of the soil behaviour under shearing.

Finally, a simple MMC model will be calibrated. This calibration will have a stiffer description of the soil during shearing when compared to the simplified MMC model, but will also be modelled elastic-perfectly plastic. The behaviour will be quite different under compression. Under compressional loading, the simple MMC model will behave entirely linear. This shows a large difference with both the original MMC and the simplified MMC model. As the model will perform very different under compression, the influence of this behaviour on the total model can be judged. A very brief description of the three calibrations of the MMC model is given in Table 8.

Table 8: Soil models analyzed in parametric study

Soil model	Behaviour in triaxial test	Behaviour in oedometer test
Original calibration of MMC model	Non-linear behaviour described by hardening rule	Non-linear behaviour described by evolution of preconsolidation pressure (hardening rule) and non-linear elasticity
Simplified MMC model	Linear behaviour	Non-linear behaviour described by evolution of preconsolidation pressure and non-linear elasticity
Simplest MMC model	Linear behaviour	Linear behaviour

All soil models have been used in performing a triaxial as well as an oedometer test. The results of both tests for all three models is displayed in Figure 39 and Figure 40. It can be observed that for the oedometer test, the response of the simplified MMC and the original MMC soil model is similar, apart from a small difference in stiffness at larger stress. The response of the simplest MMC model has been modelled such that the oedometer test response corresponds best with both the simplified and the original MMC model. The simplest MMC soil and the simplified MMC soil model predict the same behaviour in the triaxial test, apart from a very small difference. Both models being approximately linear up until maximum capacity, after which a constant value is found for q .

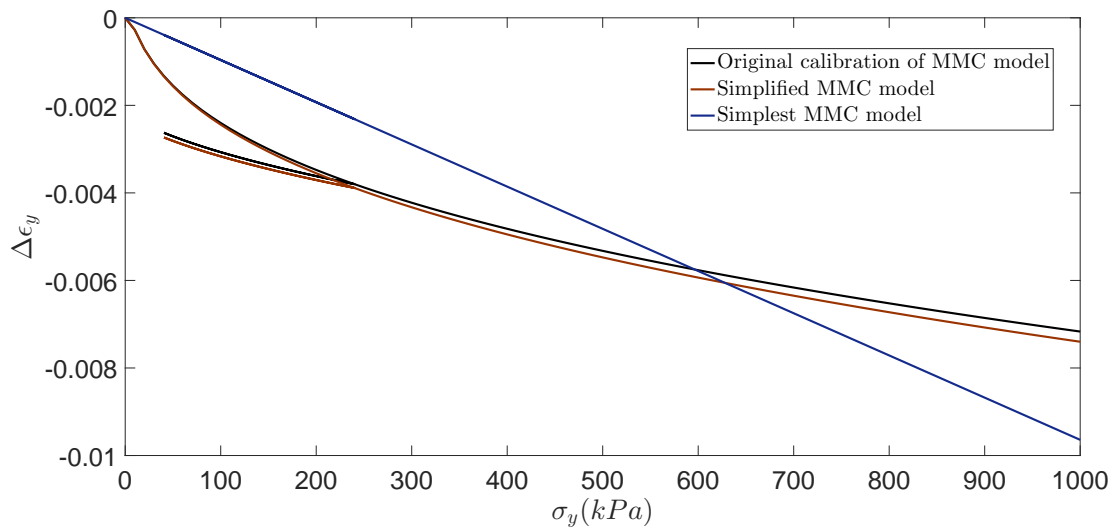


Figure 39: Different soil test simulations for oedometer test

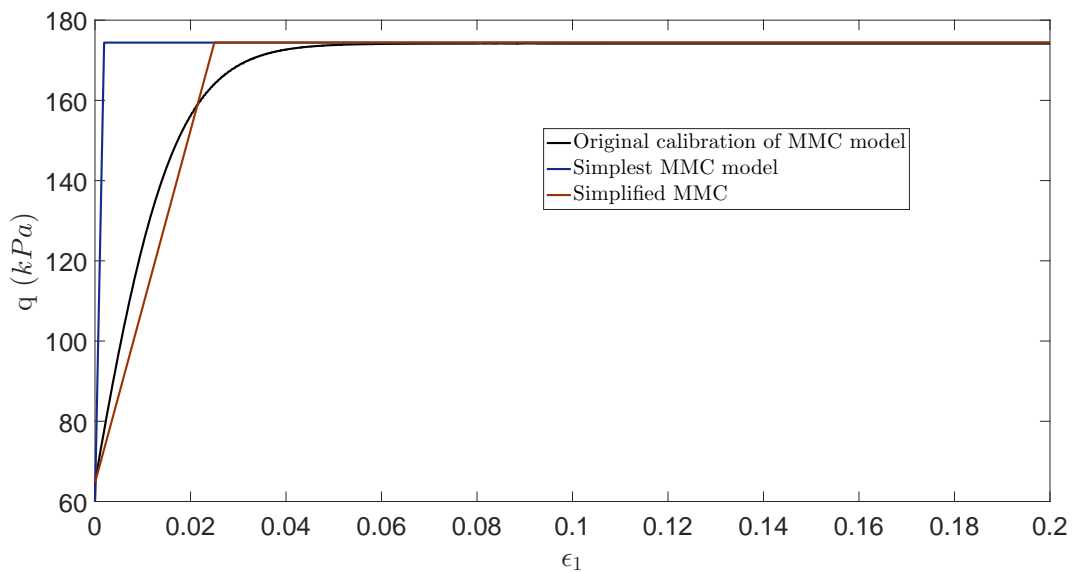


Figure 40: Different soil test simulations for triaxial test

Here it can be observed in Figure 40 that the simplest MMC model performs stiffer under shearing when compared to the simplified MMC model. This difference in stiffness is notable in the strain range up to 3%. The main differences, however, can be observed in the oedometer test. Here, the behaviour at large stresses is quite significantly different between the simplest MMC model and the simplified and original MMC model.

The calibrated parameter sets have been used in performing a pure lateral push-over, similar to the benchmark study described in Section 4.1.1. A displacement-controlled analysis is performed here, where the topside structure experiences a pre-defined translational displacement. This displacement-controlled analysis allows for the model to describe the horizontal load that is to be applied to achieve this deformation value. These results are displayed in Figure 41.

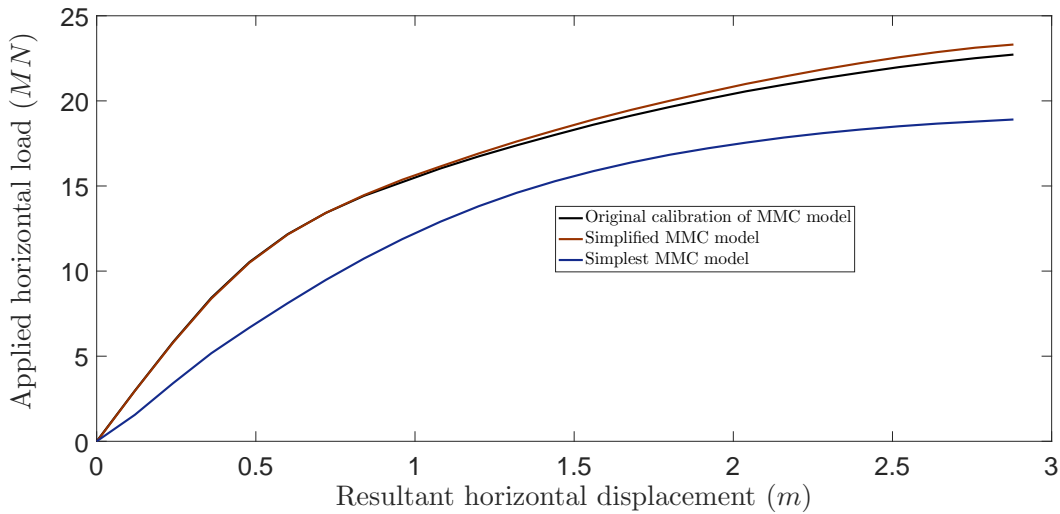


Figure 41: Global response of jack-up structure in a pure lateral push-over for different soil models.

The global response of the jack-up unit for all three soil models is displayed in Figure 41. It can be observed that the response of the soil model used in the validation is matched very well by the simplified MMC soil model. This is striking, as both soil models have a much different response in the triaxial test, although the oedometer test response is similar. The global response shows a significant difference between the simplest MMC model and the simplified MMC model. Although the simplest MMC and the simplified MMC model differ in stiffness during shear loading, the largest differences are observed in compressional loading. The results from the original calibration of the MMC model and the simplified MMC model suggest that the behaviour during shearing has a very small influence on the model behaviour. It can therefore be stated that the large differences between the simplest MMC model and the simplified MMC model are caused by the response of the soil under compression.

The behaviour of the soil in compression will have a significant influence on the push-pull mechanism of the jack-up's legs. As described previously, the push-pull mechanism is dominant in assuring stability of the structure. It is therefore, that the response under compression has such a pronounced influence on the global stiffness during loading, as well as the maximum applied load. As this push-pull mechanism is a compressional phenomenon, the behaviour of the soil under shearing has very little influence on the model behaviour. As known from the push-pull mechanism, the frontside footing (in this case spudcan A) is the most influential on the stability of the structure. This spudcan footing thus receives a large amount of vertical loading, causing the soil to experience large compressional stresses. It can therefore be stated that the behaviour of the soil under compression has a large influence on the model behaviour. Emphasis should be placed on modelling the stiffness of the soil under compression in a correct manner, especially at high stresses.

5.3 Analysis of geometrical non-linearities

The performed push-over tests in the benchmark study have been performed in a LDFE. This framework is capable of taking into account LDFE effects. As such, the model is capable of taking into account second order effects. This framework has a significant influence on both the complexity of the model, as well as the convergence rate of the model. As a LDFE constantly evaluates the problem geometry, it is more computationally heavy. The convergence rate of a LDFE framework is also different from a small-deformation framework (hereafter abbreviated as SDFE). As displacements directly influence the forces in the model, the iterative procedure has more difficulties in reaching a satisfactory equilibrium. It is therefore interesting to study to what extent the LDFE influences the analyses and the produced results. The same tests as in the benchmark problem have therefore been performed: a pure lateral push-over and a non-symmetrical push-over at 22° loading angle. These tests have been performed for both the LDFE and the SDFE framework. The global load-displacement response of the jack-up unit is displayed in Figure 42 and Figure 43, where the benchmark study is also displayed for clarification purposes. It can be observed that the stiffness of the SDFE is larger than that of the LDFE. The SDFE also predicts a larger maximum applied horizontal load. When compared to the experimental test by Bienen and Cassidy (2009), it can be observed that the LDFE provides a much better description of the load-displacement response. than the SDFE does. This large difference can be explained by considering the mass of the topside of the jack-up unit. The large topside mass of the jack-up structure causes the second order effects to have a significant influence on the loads and moments in the structure. Therefore, a large difference between SDFE and LDFE can be observed.

Figure 44 displays the load-displacement and normalized response for both the pure lateral push-over and the 22° lateral push-over for the SDFE and LDFE. It can be observed that the load-displacement response for both the SDFE and LDFE are very similar. An interesting difference between both frameworks can be observed in the vertical-moment plane. Where the LDFE framework predicts a reduction of the front footing moment (spudcan A), the SDFE predicts an increase throughout the push-over. The LDFE shows a redistribution of moments as described in the model validation. Due to the geometrical linear behaviour of the SDFE, the push-pull mechanism has a less pronounced influence on the stability when compared to the LDFE.

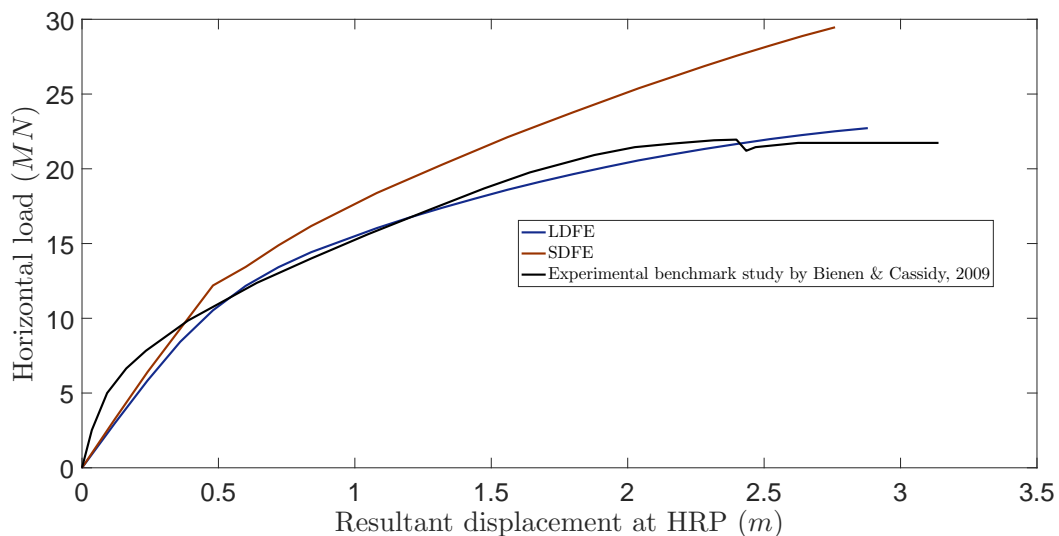


Figure 42: Load-displacement response in LDFE and SDFE for pure lateral push-over; HRP, hull reference point.

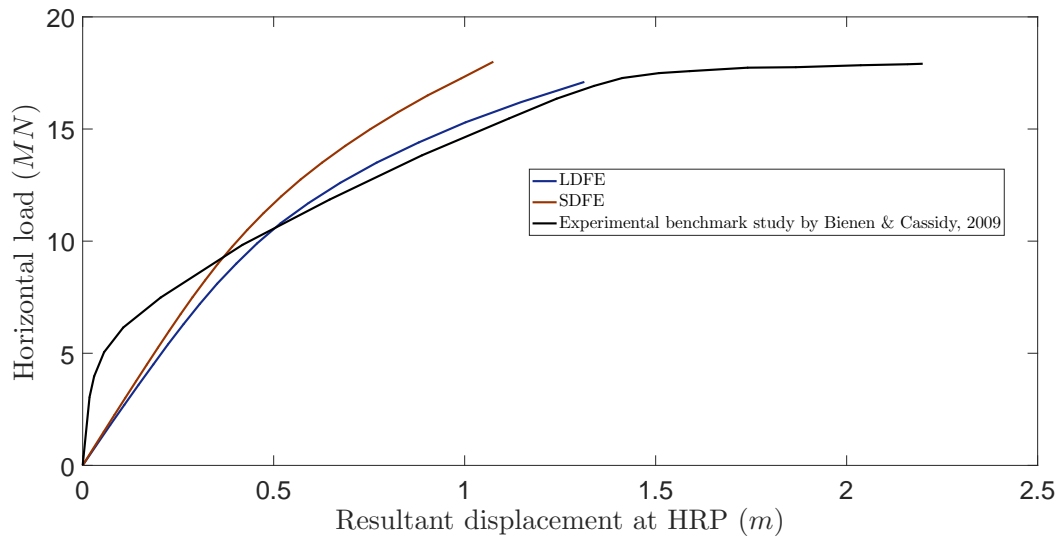


Figure 43: Load-displacement response in LDFE and SDFE for non-symmetrical lateral push-over; HRP, hull reference point.

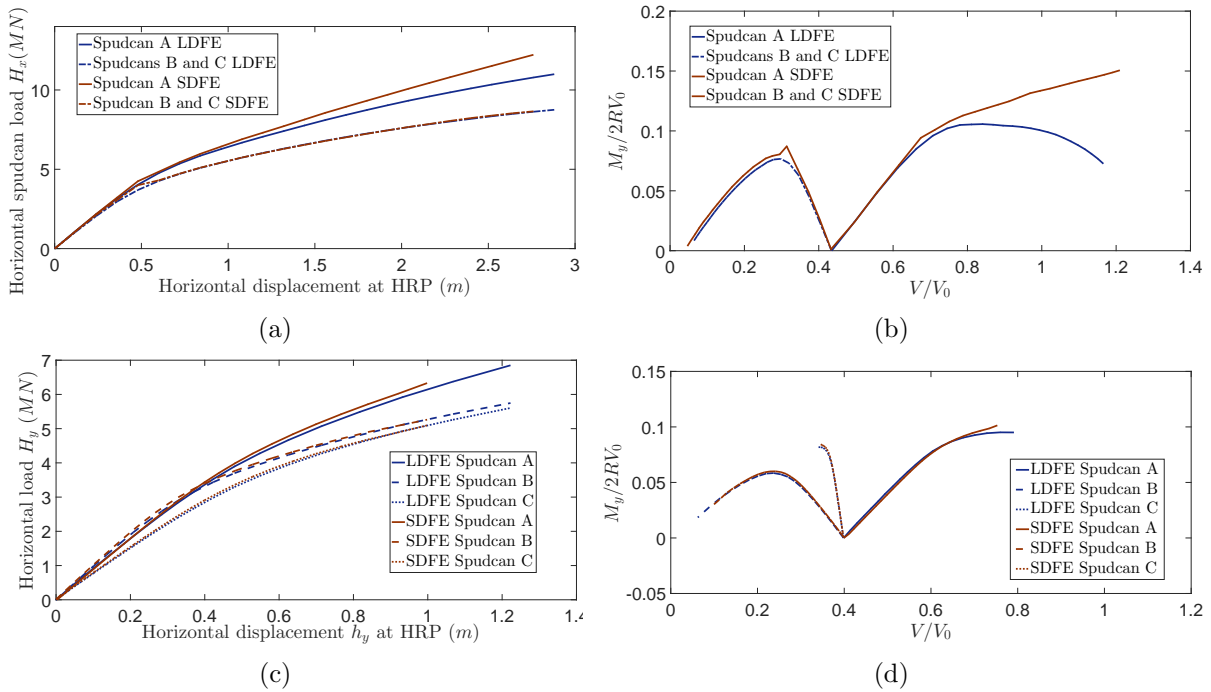


Figure 44: Load-displacement response and normalized response for lateral push-over: (a) pure lateral push-over load-displacement response (b) pure lateral push-over normalized response vertical-moment; (c) 22° lateral push-over load-displacement response; (d) 22° lateral push-over normalized response vertical-moment; HRP, hull reference point.

The computed moments of both the horizontal loading, as well as the push-pull mechanism and the spudcan moments are displayed in Figure 45. It can be observed that the moments at the spudcans are decreasing during loading, however the moments at spudcan A remain at a similar level throughout the push-over. The push-pull mechanism ensures the stability of the jack-up rig, similar to the large-deformation case, displayed in Figure 24. It can be observed that the moment loads show a very linear increase during push-over, especially when compared to Figure 24. This is

the effect of the SDFE, as second order effects are not taken into account. It can also be observed that the computed moments are significantly higher than for the LDFE case.

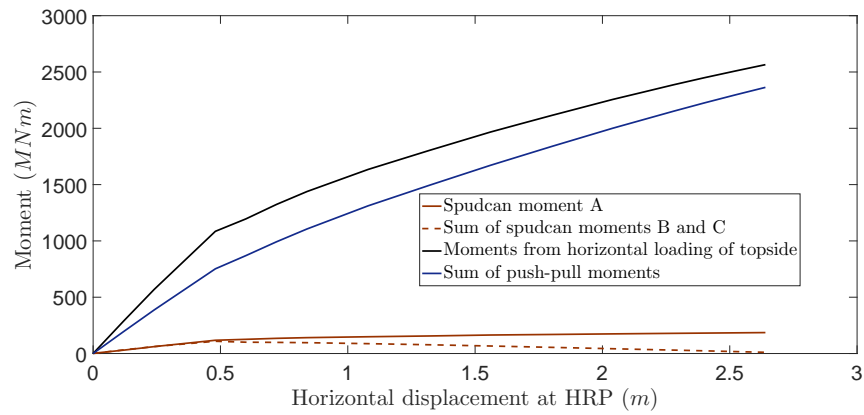


Figure 45: Moments during pure lateral push-over in DIANA model in SDFE. HRP, hull reference point.

5.4 Analysis of preload influence

The preload applied to jack-up structure typically has a double effect: it allows for a larger penetration of the spudcans, as well as proof loading the jack-up foundation to storm conditions. The stress history of the soil below the spudcans should lead to a different response under different preload magnitudes. To investigate the influence of the preload magnitude on the jack-up unit behaviour, a pure lateral push-over will be performed under varying preload. The push-over will be performed in a displacement-controlled analysis, similar to the benchmark study. The preload magnitude is defined as:

$$L = \frac{V - V_{sw}}{V_0 - V_{sw}} \quad (25)$$

with V as the current vertical load, V_{sw} as the vertical load under self-weight and V_0 as the vertical load during preloading from the benchmark study. The preload parameters used in the preload analysis are displayed in Table 9. The global response of the jack-up unit under loading is displayed in Figure 46.

Table 9: Preload parameters for parametric analysis

Description	Preload factor L [-]
Half preload	0.5
Normal preload	1
One and a half preload	1.5

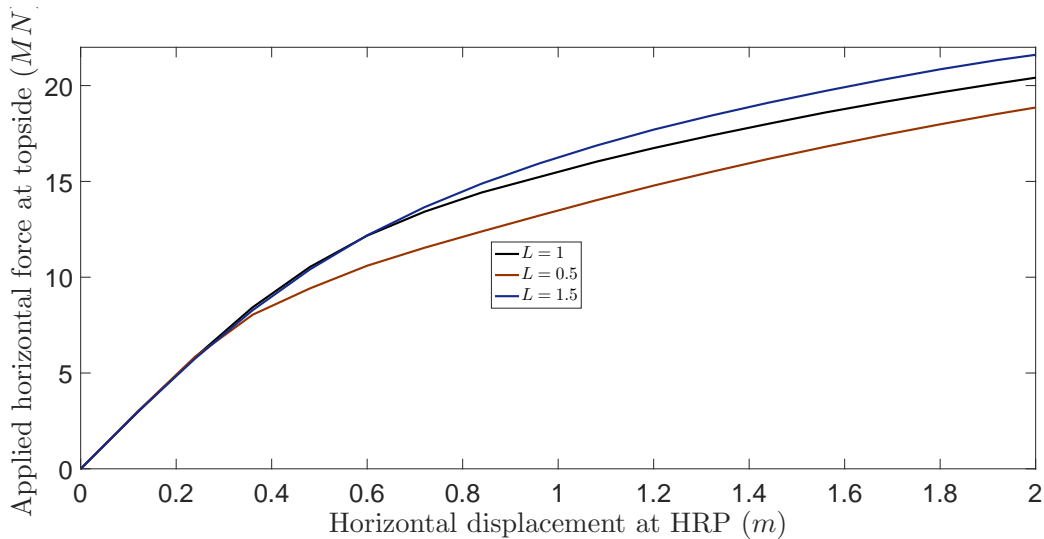


Figure 46: Parametric analysis of preload influence in DIANA FEA model

As can be observed in Figure 46, the amount of preload has a significant influence on the maximum applied horizontal load at failure. It can be observed that the stiffness reduction under loading is observed at a lower horizontal loading for a lower preload value. For the highest amount of preloading, the linear behavior is shown to be up to a significantly higher load than for the lowest amount of preloading.

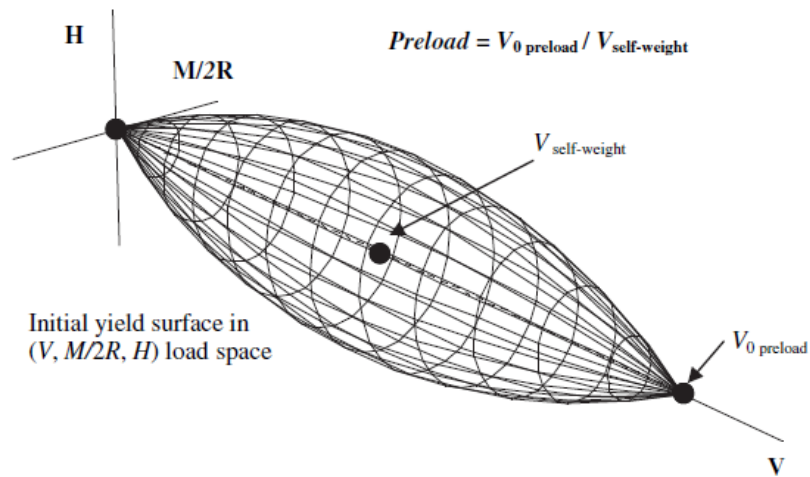


Figure 47: Yield surface in (V, H, M) space (after Cassidy et al. (2010))

The influence of the preload can be understood by considering the yield surface of the foundation in (V, H, M) space (Figure 47). The amount of preload determines the size of the initial yield surface. The loading state at self-weight will be inside the yield surface, producing elastic strains, until the stress state is such that yielding and plastic deformations occur. For a larger preload value, the size of the initial yield surface will be larger, leading to more elastic deformations until yielding. As the elastic stiffness is stiffer than the stiffness under yielding, a higher stiffness will thus be achieved. This explains the results from Figure 46, as a larger preload will lead to more elastic deformations and thus a higher stiffness. As the analyses are performed in a large-deformation framework, the stiffness of the response has a direct influence on the maximum applied horizontal load, leading to a larger capacity for the highest preload.

5.5 Analysis of different loading directions

Under operational conditions, jack-up structures are loaded from different angles through a combination of wind and wave loading. The angle at which the structure is loaded can have an influence on both the stiffness of the jack-up during loading, as well as the capacity. The influence of the loading angle will be researched by performing a push-over analysis that is non-symmetrical. The push-over will be modelled such, that the applied load does not lead to a torque in the structure. This has been performed by performing the push-over loading at the center of gravity of the topside structure, using a force-controlled analysis. This eliminates the effect of the torque on the overall behaviour, and allows the analysis to focus solely on the influence of the loading angle. A 60° loading angle will thus be compared to a pure lateral push-over. An overview of the applied loading directions and their application point is displayed in Figure 48.

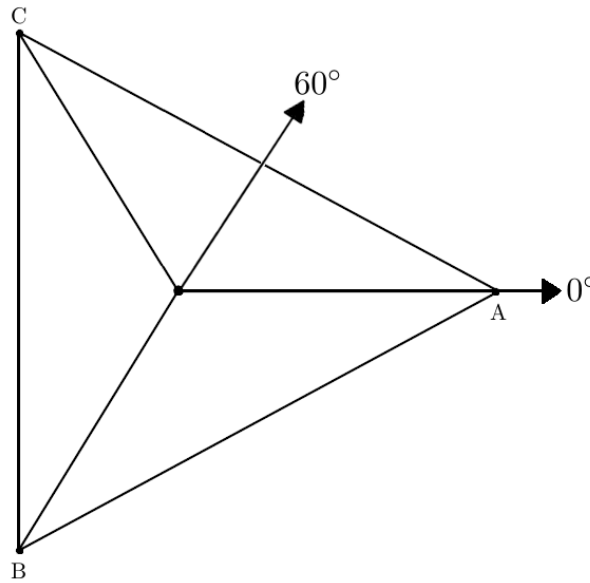


Figure 48: Topside loading of parametric analysis of loading directions

The global response of the jack-up unit is displayed in Figure 49. The reader should note that the displacement is plotted as a resultant displacement, rather than a directional displacement.

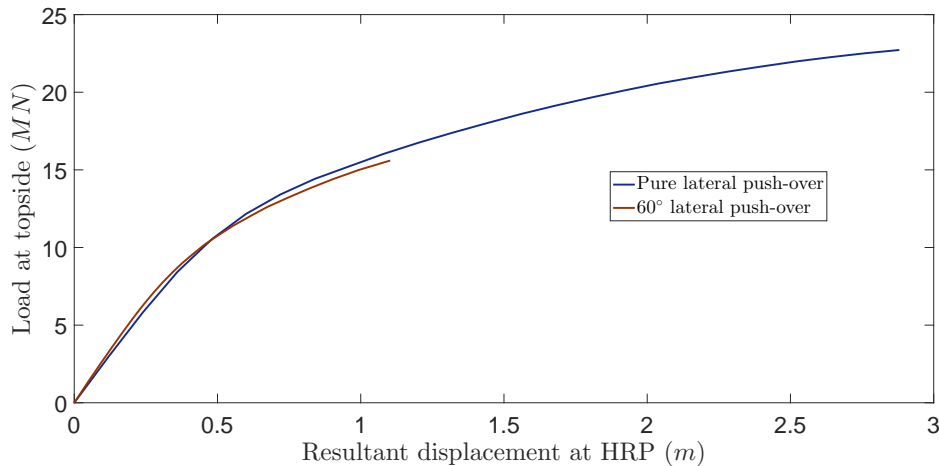


Figure 49: Global response of jack-up structure under push-over

It can be observed that the maximum applied load at the topside decreases significantly for a loading direction of 60° . The maximum applied load at the topside is 22.7MN and 15.6MN for the symmetrical and non-symmetrical pushover, respectively. The global stiffness under loading is also lower for a non-symmetrical loading angle, with stiffness reduction during loading occurring at an earlier stage. Judging from the loading angle of 60° as displayed in Figure 48, it is likely that the difference in capacity is caused by the different in loading of the footings. To observe this, the normalized response is displayed in Figure 51 for both loading angles.

As can be observed from the normalized responses at the footings, the behaviour of spudcan A under loading is generally the same, although lower values in (V, H, M) plane are found. The main difference can be observed in the response of footings B and C. Where the pure lateral push-over predicts a similar response for both footings, the 60° push-over model predicts a different response for both footings. In this model, spudcan C is under compression, whilst spudcan B receives a tensional loading. The response of spudcan B shows a reduction in vertical load, almost reaching tension at ultimate capacity. This suggests a different response of the jack-up structure when compared to the pure lateral push-over test. This difference in response can be understood when considering the loading states at the individual legs (Figure 50).

For the pure lateral push-over test, leg A will be under compression while both back side legs receive a tensional force. For the 60° push-over test, both legs A and C receive a compression, whilst leg B receives a tensional force. The reduction in vertical load at spudcan B here suggests a failure caused by a pull-out of spudcan B. The failure of the jack-up rig under pure lateral push-over loading is caused by overturning. The difference in response leads to a difference in push-pull mechanism, causing a lower capacity and lower stiffness of the rig under loading for a non-symmetrical push-over test.

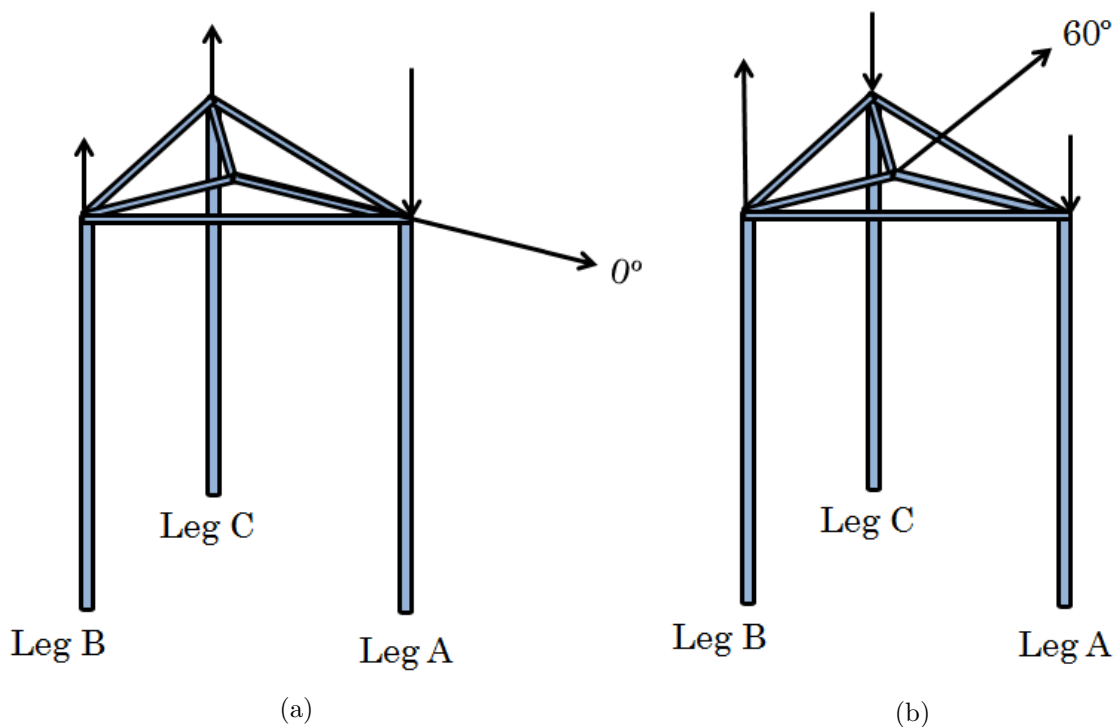


Figure 50: Footing response in lateral push-over; (a) pure lateral push-over; (b) 60° push-over

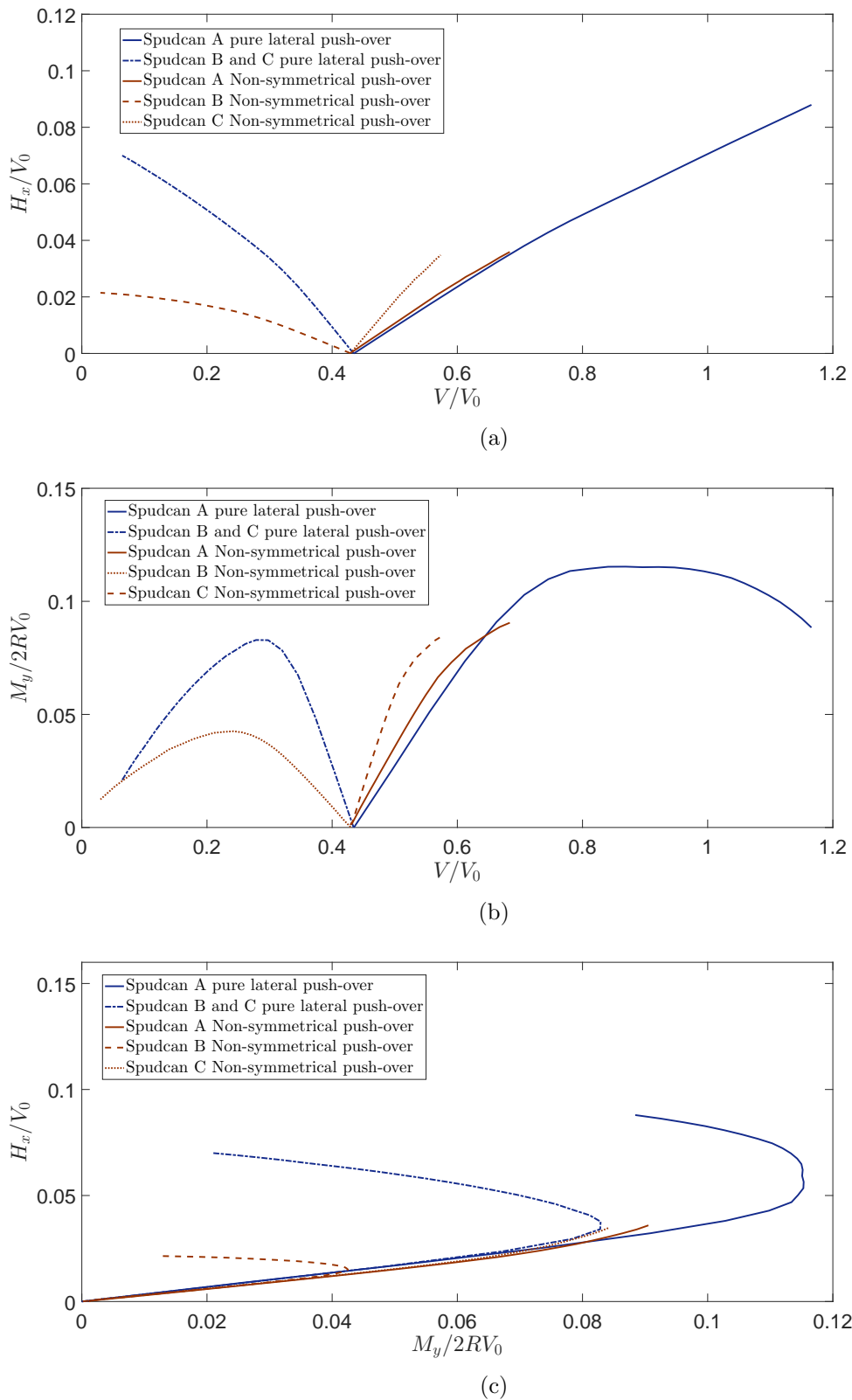


Figure 51: Normalized footing response for parametric analysis of push-over load angle: (a) vertical-horizontal; (b) vertical-moment; (c) moment-horizontal.

5.6 Analysis of pure torsional loading of topside

Under the influence of wave and wind loads, a jack-up structure is loaded with a torsional, as well as a lateral load. The relationship between torsion at the hull of a jack-up structure and the torsion at the footings of a jack-up structure is poorly investigated in literature. This relationship will be investigated by performing an analysis for which the jack-up structure is loaded solely under torsion. This torsion will be applied at the hull reference point (Figure 52).

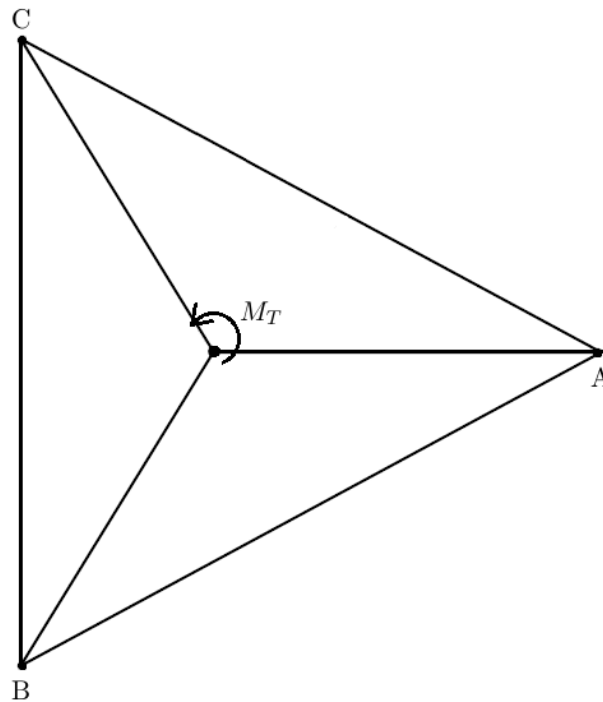


Figure 52: Torsional loading of jack-up structure

Under the influence of a torsional loading, the legs of the jack-up structure experience a deformation. This leads to a rotation of the topside with respect to its original position. Part of the moments from the topside will be taken up by the rotational deformation of the jack-up's legs. Figure 53 displays the rotation of the top side as well as the legs under loading. The rotational deformation of the jack-up legs has an influence on the spudcans of the jack-up. Part of the rotational moment will be taken up by the deformation of the legs. The spudcans will also experience a rotational moment. The load combination leads to a rotation of the spudcans and thus a separation between soil and spudcan. As it is hard to judge from Figure 53 what the actual torsional displacement of the spudcans is, a vector field is plotted for the individual spudcans, showing more clearly their rotational displacement in Figure 59. In this plot, the vector field shows a rotation along a center point at the spudcan. It can be observed that the soil also experiences a displacement locally, due to the rotation of the spudcans.

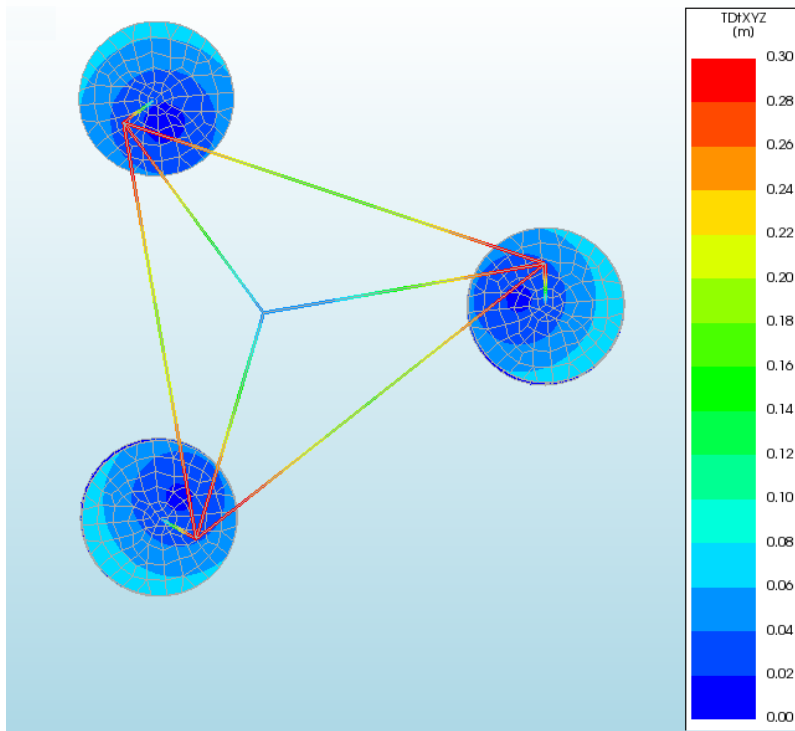


Figure 53: Response of jack-up structure to torsional loading

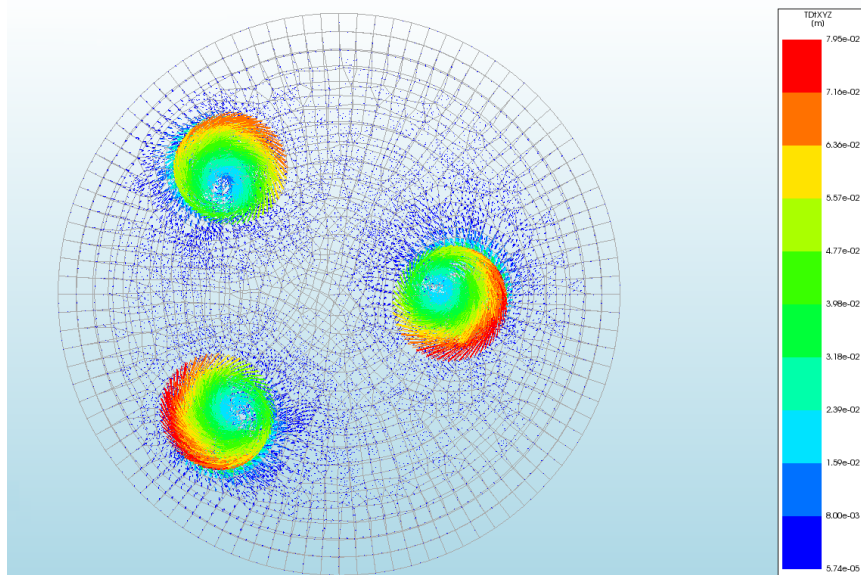


Figure 54: Rotation of spudcans under torsional loading of topside

The rotation of the spudcans is a result of the moments transferred from the topside. Each individual spudcan will experience a different rotation field, based on the moments at the individual spudcan. These rotations together with the moments at the spudcans are displayed in Figure 55, Figure 56 and Figure 57 for each individual spudcan. From these plots, it can be observed that spudcan A receives the highest amount of rotation in torsional direction, where the bending rotation is quite low. Spudcans B and C show a more gradual rotation in torsion and bending directions. The amount of torsional moment is the highest at spudcan A, and lowest at spudcan B.

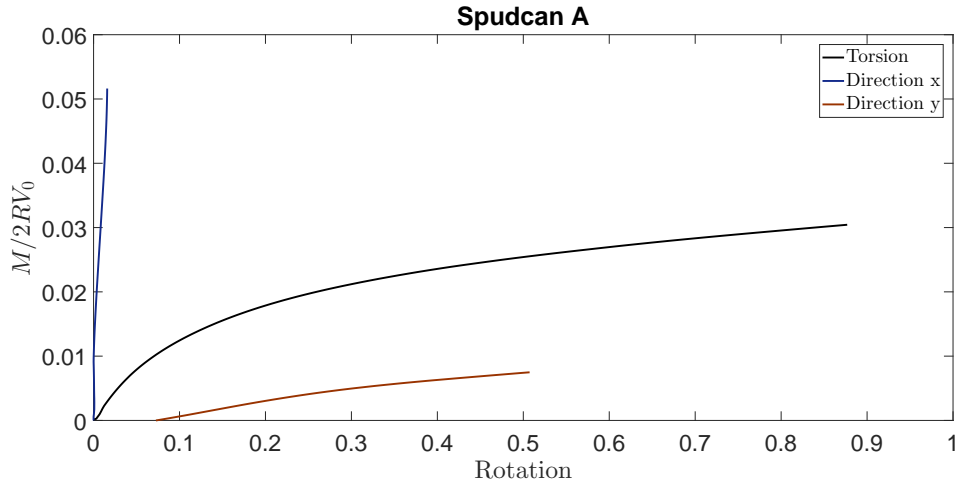


Figure 55: Rotation of spudcan A under torsional loading of topside

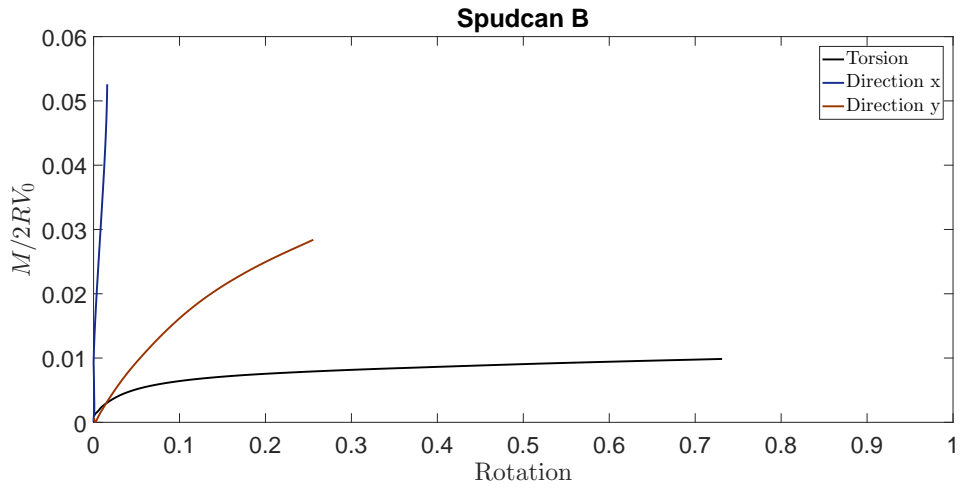


Figure 56: Rotation of spudcan B under torsional loading of topside

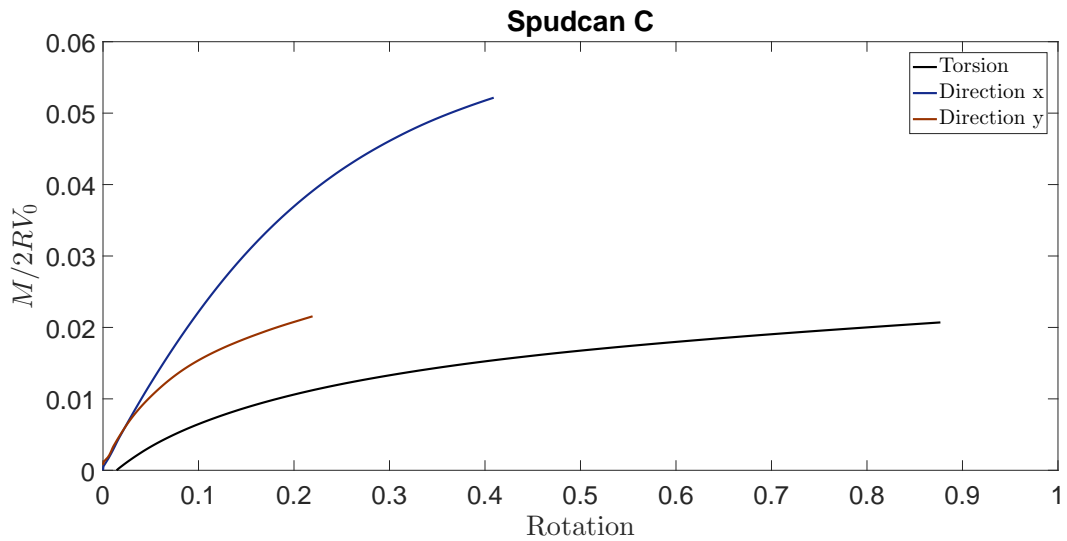


Figure 57: Rotation of spudcan C under torsional loading of topside

The amount of torsional moment at each individual spudcan is plotted as a function of the bending moments in Figure 58. Here, it can be clearly observed that spudcan A receives the highest amount of torsional moment, whereas spudcan C receives a large bending moment. It can also be observed that in relation to the bending moments at the footings, the torsional moments are of significant magnitude.

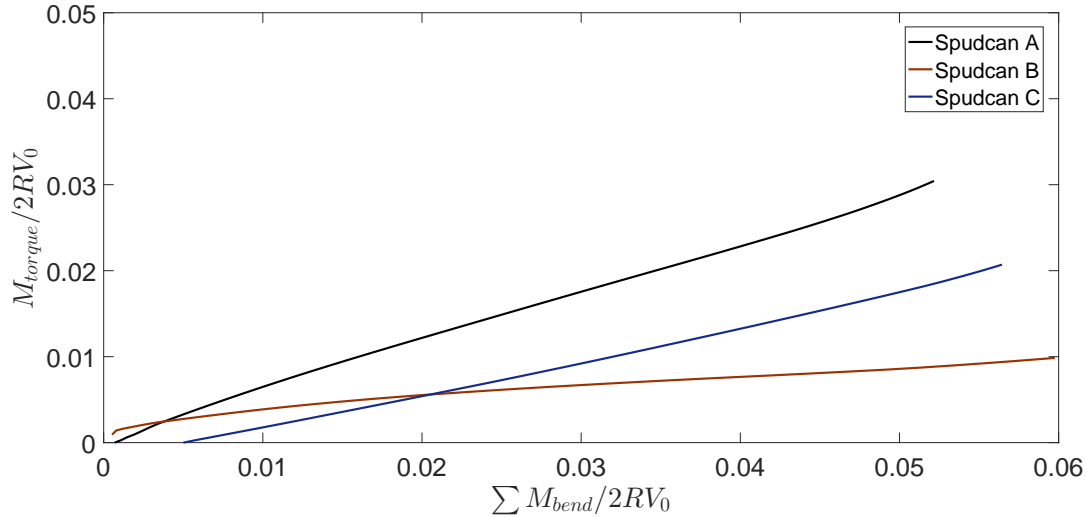


Figure 58: Torsional and bending moments at spudcan footings due to torsional loading of topside structure

The amount of torsional moment at the spudcans together with the shear forces in the jack-up's legs ensures stability under torsional loading. In its current state, the torsion at spudcan footings is disregarded in the calculation of the bearing capacity envelope. It is therefore important to consider the sum of torsional moments at the spudcans. The moments from the loading, shear and the moments at the spudcans are displayed in Figure 59.

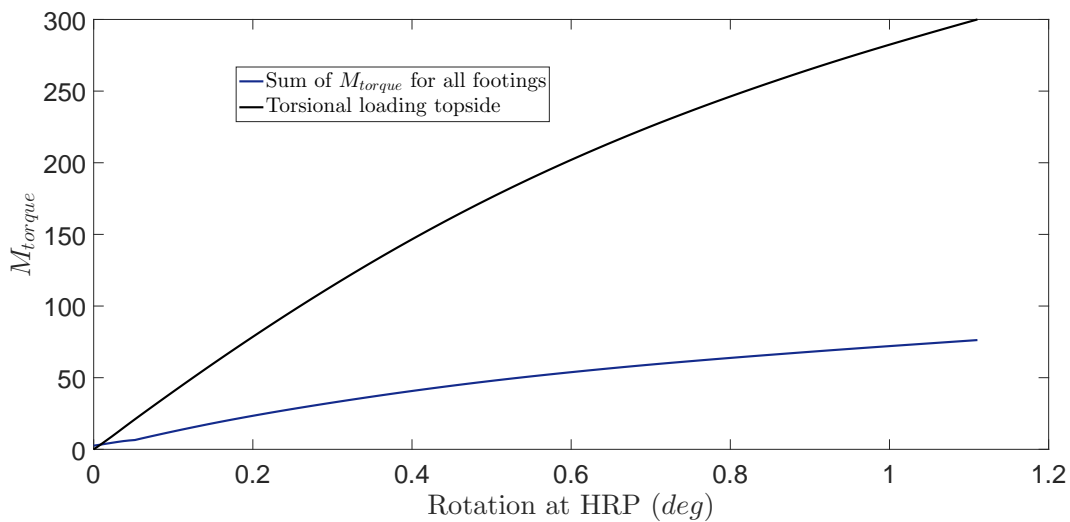


Figure 59: Torsional moments at spudcan footings due to torsional loading of topside structure

It can be observed that a substantial amount of torsional loading is taken up by the rotational

moments at the spudcans. The difference between the applied torsional moment and the torsional moment at the spudcans is taken up by the shear forces in the structure. When comparing the magnitude of the applied rotational moment, it can be observed that the torsional moment at the spudcans is as high as 25% of the applied torsional moment.

To study the influence of the spudcan rotations on the global behaviour, the torsional analysis has also been performed for a condition where rotations are fixed at the leg-to-spudcan connection, in torsional direction. This allows for the model to simulate the case where the rotation of spudcans is not included. The results of this analysis are displayed in Figure 60

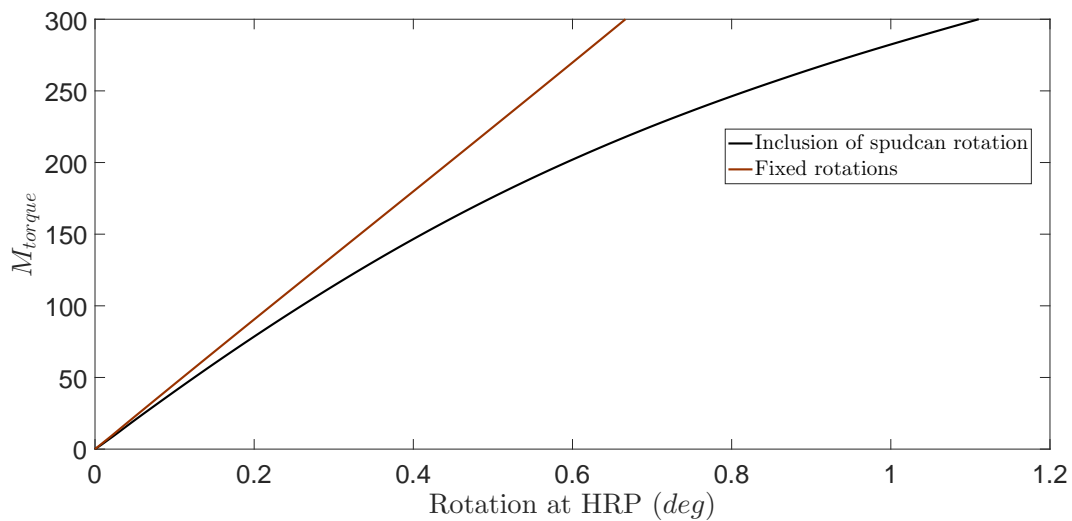


Figure 60: Rotation of topside structure for inclusion of spudcan rotation and fixation at spudcans

It can be observed that the model that disregards the rotation of the spudcans has a far lower predicted rotation of the hull. This fixed rotation condition will lead to the torsional moments to be taken up fully at the leg-to-spudcan connection. Effectively, this leads to the foundation behaviour under torsion to be linear. From Figure 60 it can thus be observed that the current practice, to disregard the rotation of the spudcans leads to a different behaviour of the jack-up structure, globally.

It should be stated here that the pure torsional loading of a structure does not occur in real-life situations, as a combination of wind- and wave loading would always be present. However, it can be observed that the rotational moments at the footings are substantial in magnitude. Even though the model is not validated for a torsional loading of the structure with a benchmark test, the results of the torsional loading suggest that the rotational moments at the spudcans are of such magnitude that they should be taken into account when considering the bearing capacity of the foundation.

6 Concluding remarks

From the model validation and parametric analyses it can be concluded that the FE model is capable of describing both the global behaviour of the jack-up structure during loading, as well as the behaviour of the individual spudcan footings. The application of a large-deformation framework is a prerequisite in the finite element modelling of a jack-up structure. The stability of the jack-up structure is strongly dependent on the vertical footing reactions. Consequently, emphasis should be placed on the calibration of soil parameters under compression, especially at high stresses. The response of the soil to shear loading has a far lower influence on the model performance. Due to the swaying of the jack-up structure, the global stiffness of the rig during loading has an influence on the load capacity. The amount of preload applied to the structure therefore has an influence on the capacity of the rig, as an increase in preload leads to a generally stiffer response during loading. The dilative behaviour of the soil has a positive influence on both the global stiffness during loading, as well as the load capacity of the jack-up rig. The failure mechanism of the jack-up structure has a significant influence on both the global stiffness during loading as well as the capacity. The largest capacity and stiffness can be observed under a pure lateral push-over, due to the push-pull mechanism. The analysis of the torsional loading of the structure indicates that substantial rotational moment can be expected at the foundation. Though the torsional prediction of the model is not validated, the magnitude of the torsional moments at the foundation suggest that the torsional loading of the foundation should be taken into account in a bearing capacity analysis.

7 Recommendations for further research

The different parametric analyses, as well as the benchmark study have shown that the finite element model is capable of capturing the complicated non-linear response of the jack-up structure during loading. The macroelement model by Bienen and Cassidy (2009) gives a good description of the global behaviour of the jack-up unit under loading, although the individual footing responses are not entirely accurate. The macroelements attached to each individual spudcan in this macroelement model have the same yield surface, hardening rule and flow rule. The individual footing responses show a good description for unloading conditions, but do not give an entirely accurate representation under compressional loading. It is therefore recommended that the compressional behaviour of the spudcans is researched in more detail. Furthermore, the parametric analyses have shown the significance of different loading types, preload values and soil parameters. It is recommended that the influence of the compressional behaviour of the soil underneath the spudcan footings is researched in more detail. Experimental modelling could provide a better insight of this influence. The loading direction also has a significant influence on the behaviour of the individual spudcan footings. As the macroelement model does not describe entirely accurate this behaviour and very limited variation of the loading direction is analyzed, further research in the influence of different loading directions on the jack-up behaviour is recommended. Lastly, the influence of torsional loading is shown to be significant in this research. As currently, this effect is not taken into account in the modelling of jack-up structures, it is advised that the influence of torsional loading is to be observed. Experimental tests could be used to research this phenomenon. The knowledge coming from these recommendations could be used to further improve the macroelement modelling of jack-up structures.

As this research has focused on the static loading of a jack-up structure in a dry soil, dynamic effects and the partial drainage of the soil is not taken into account. These effects, combined with different loading directions of both wind and wave loading could have a pronounced influence on the stability of the jack-up unit in real conditions. Although research on the static loading of

jack-up structures is still needed, these effects could be analyzed in the future, for the description of a real jack-up unit during operation.

Acknowledgements

The work that was presented in this paper has been performed in-house at DIANA FEA BV. I would like to take this opportunity to thank its staff for the support and feedback throughout my research. Special thanks go out to Federico Pisanó who has been very involved in my research. I am sure that without your feedback and hands-on supervision this work would not have been what it is today. My appreciation goes out to Gerd-Jan for giving me this opportunity and being involved, even under a busy time schedule. The other members of my graduation committee are also much appreciated for their input and feedback. I would like to thank my friends and family for taking my mind off things when needed and for their encouragement throughout my studies. Last but not least, I thank Marlieke for her support through these past years and look forward to our future together.

References

- Bienen, B. and Cassidy, M. (2006). Advances in three-dimensional fluid-structure-soil interaction analysis of offshore jack-up structures. *Marine Structures*, 19(2-3):110–140.
- Bienen, B. and Cassidy, M. (2009). Three-dimensional numerical analysis of centrifuge experiments on a model jack-up drilling rig on sand. *Canadian Geotechnical Journal*, 46:208–224.
- Bienen, B., Cassidy, M., and Gaudin, C. (2009). Physical modelling of the push-over capacity of a jack-up structure on sand in a geotechnical centrifuge. *Canadian Geotechnical Journal*, 46:190–207.
- Butterfield, R., Houlsby, G., and Gottardi, G. (1997). Standardized design conventions and notation for generally loaded foundations. *Géotechnique*, 47(5):1051–1054.
- Cassidy, M., Vlahos, G., and Hodder, M. (2010). Assessing appropriate stiffness levels for spudcan foundations on dense sand. *Marine Structures*, 23:187–208.
- Cheong, J. (2002). Physical testing of jack-up footings on sand subjected to torsion. B.E. thesis. Centre for Offshore Foundation Systems, The University of Western Australia, Crawley, Australia.
- Gottardi, G., Houlsby, G., and Butterfield, R. (1999). Plastic response of circular footings on sand under general planar loading. *Géotechnique*.
- Groen, A. (1997). *Three-dimensional elasto-plastic analysis of soils*. PhD thesis, Delft University of Technology.
- Houlsby, G. (2016). Interactions in offshore foundation design. *Géotechnique*, pages 1–35.
- Houlsby, G. and Cassidy, M. (2002). A plasticity model for the behaviour of footings on sand under combined loading. *Géotechnique*, 52(2):117–129.
- Hoyle, M., Stiff, J., Hunt, R., and Morandi, A., editors (2006). *Jack-up assessment - past, present and ISO*, volume Proceedings of the Sixteenth International Offshore and Polar Engineering Conference, San Francisco, California.
- ISO (2012). Petroleum and natural gas industries - sitespecific assessment of mobile offshore units - part 1: Jack-ups (iso 19905-1:2012,idt). Technical report, International Organization for Standardization.
- Manie, J. (2016a). Diana fea bv material library - release 10.0. Technical report, DIANA FEA BV.
- Manie, J. (2016b). Diana fea bv theory - release 10.0. Technical report, DIANA FEA BV.
- Martin, C. (1994). *Physical and numerical modelling of offshore foundations under combined load*. PhD thesis, Oxford: University of Oxford, UK.
- Ng, T. and Lee, F. (2002). Cyclic settlement behaviour of spudcan foundations. *Géotechnique*, 52(7):469–480.
- Nova, R. (2012). *Soil mechanics*. John Wiley & Sons.
- Pai, F., Anderson, T., and Wheeler, E. (2000). Large-deformation tests and total-lagrangian finite-element analyses of flexible beams. *International Journal of Solids and Structures*, 37:2951–2980.

- Pucker, T., Bienen, B., and Henke, S. (2013). Cpt based prediction of foundation penetration in siliceous sand. *Applied Ocean Research*, 41:9–18.
- Randolph, M. and Gourvenec, S. (2011). *Offshore Geotechnical Engineering*. Abingdon, Oxon: Spon Press.
- Reardon, M. (1986). Review of the geotechnical aspects of jack-up unit operations. *Ground Engineering*, 19(7):21–26.
- Rowe, P. (1962). The stress-dilatancy relation for static equilibrium of an assembly of particles in contact. In *Proceedings of the Royal Society of London A: Mathematical, Physical and Engineering Sciences*, volume 269, pages 500–527. The Royal Society.
- SNAME (2002). Guidelines for site specific assessment of mobile jack-up units. Technical report, Society of Naval Architects and Marine Engineers.
- Surana, K. (1986). A generalized geometrically nonlinear formulation with large rotations for finite elements with rotational degrees of freedoms. *Computers and Structures*, 24(1):47–55.
- Vlahos, G., Cassidy, M., and Martin, C. (2008). Experimental investigation of the system behaviour of a model three-legged jack-up on clay. *Applied Ocean Research*, 30:323–337.
- Zhang, Y., Bienen, B., and Cassidy, M. (2014). Jack-up push-over analyses featuring a new force resultant model for spudcans in soft clay. *Ocean Engineering*, 81:139–149.

A Calibration of MMC soil parameters

The available soil data is quite limited. The model will be calibrated based on a super fine silica sand, which has been compacted to reach a relative density D_r of 84%. Unfortunately, triaxial and oedometer tests on this soil are not available. To perform the calibration, an oedometer test from the research by (Pucker et al., 2013) on the same soil with a relative density D_r of 75% will be used, together with data from (Cheong, 2002), which includes soil classification, as well as a direct shear test on the same soil at the correct relative density of 84%.

Oedometer test

The oedometer test has been calibrated to the results from a research by (Pucker et al., 2013), which uses the silica sand generally used at the University of Western Australia with a relative density of 75%. The results of the oedometer test have been digitized and will be compared to the oedometer test that is predicted by DIANA software for the calibrated soil. As displayed in

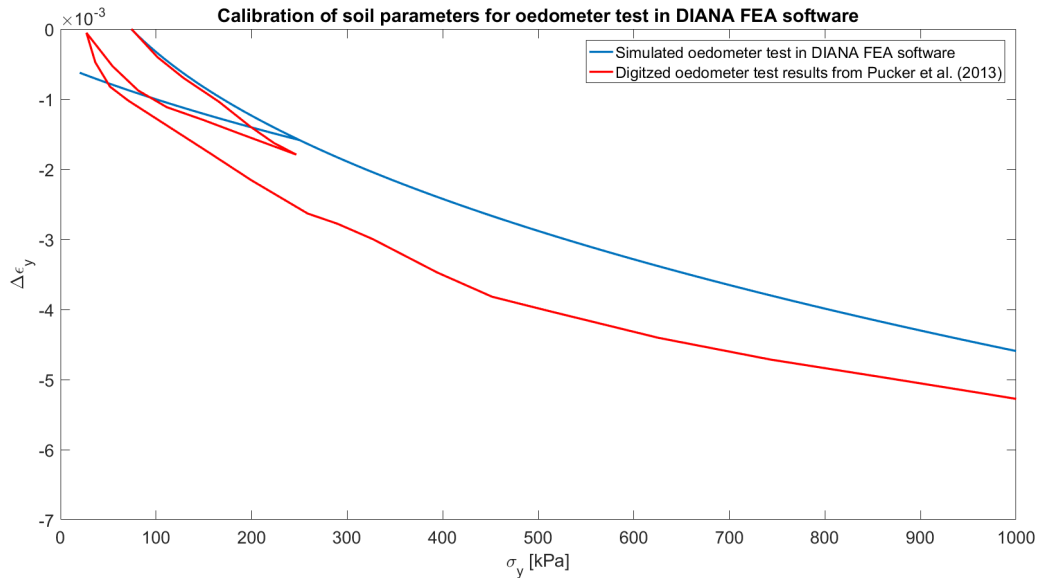


Figure 61: Oedometer test simulation of calibrated soil parameters in DIANA

Figure 61, the prediction of the behavior of the soil in an oedometer test using DIANA software is performed quite well. It should be noted that Figure 61 displays incremental vertical strains, rather than total strains. The reason behind this, is that the oedometer test from (Pucker et al., 2013) showed some installation effects, which influenced the strains. To filter out the installation effects, the first part of the loading has been disregarded. Incremental strains are then plotted for comparison purposes. It can be observed that the initial compression is modeled quite well, where the DIANA model overestimates the stiffness slightly. As the soil model is based on the Hardening Soil model, the unload-reload stiffness is elastic. The stiffness under larger loads is modeled quite well by the soil in the DIANA model. As the stresses below the spudcans are in the range of 1500 kPa, it is necessary that the ultimate stiffness is modeled properly, rather than the initial stiffness. This has been achieved by the calibration of the soil parameters.

It should be mentioned that the oedometer results from a soil with a relative density of 84% would be stiffer than the response displayed in Figure 61. However, as an oedometer test has not been performed on the 84% relative density sample, the calibration has been made on the relative density of 75% sample instead.

Triaxial test

Analogous to the oedometer test, a triaxial test has not been performed on the 84% relative density sample. Results from (Cheong, 2002) on a direct shear test will be used to determine the friction angle of the soil. There is however, no information about the behavior under loading. The calibration of the triaxial test have been performed based on the friction angle of (Cheong, 2002), together with typical calibration values for sandy soils. The friction angle used in the calibration is the sand-on-sand direct shear test friction angle at residual strength (see Cheong (2002)). The results of the triaxial test are displayed in Figure 62.

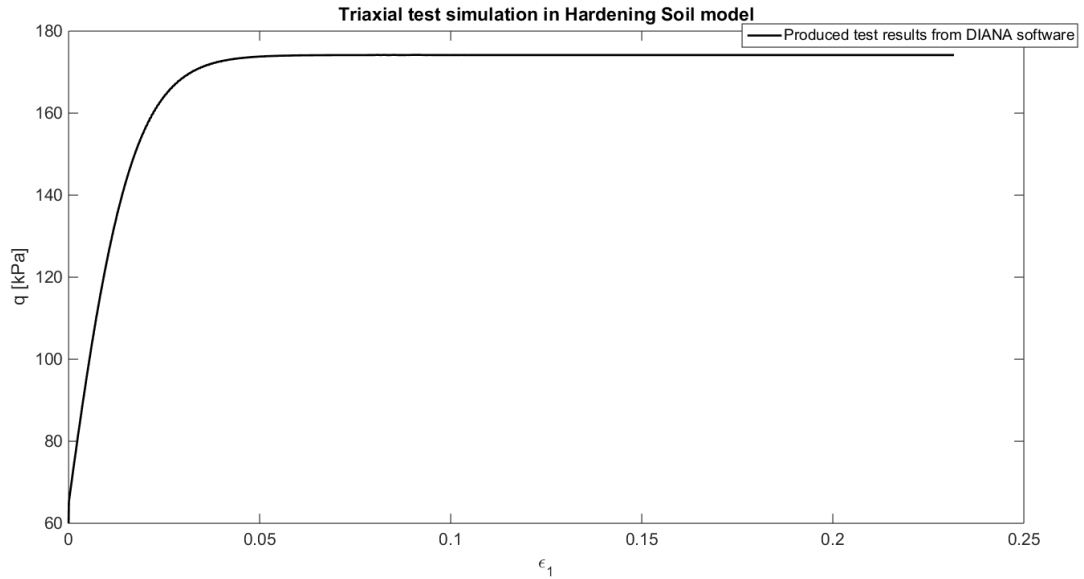


Figure 62: Triaxial test simulation of calibrated soil parameters in DIANA

B Interface elements in DIANA software

The interfaces can be modelled in several ways in DIANA software. The different interfaces will be discussed briefly, after which results of two selected interfaces will be displayed and compared. On the basis of the comparison, the final interface parameters will be selected.

Interface types

The simplest of interfaces is the linear elastic interface. The elasticity matrix of these interfaces can be defined as

$$D_{el} = \begin{bmatrix} K_n & 0 & 0 \\ 0 & K_t & 0 \\ 0 & 0 & K_s \end{bmatrix} \quad (26)$$

In which K_n is the stiffness in normal direction and K_t and K_s is the stiffness under shearing. An alternative to linear interfaces are the interfaces with a nonlinear elasticity. This means that these interfaces contain the same elastic parameters as displayed in eq. (26) with the inclusion of a stiffness reduction factor under tension. The user can select an interface opening displacement for which the reduction factors are applied. The reduction factors are then applied to the elastic parameters under compression, to create the interface properties under tension. When the stiffness under tension is reduced to zero, these interfaces can be used to model the separation of two elements with respect to each other. The linear no-tension interfaces are a numerically stable way to model relative displacements and opening under tension.

Next to interfaces that behave linearly, DIANA also has the possibility to model the interfaces in a nonlinear way. These interfaces are so-called Coulomb friction interfaces (Figure 63). The interfaces have a linear behavior under compression. Under tension or deviatoric loading, a frictional sliding together with a tensile strength is available.

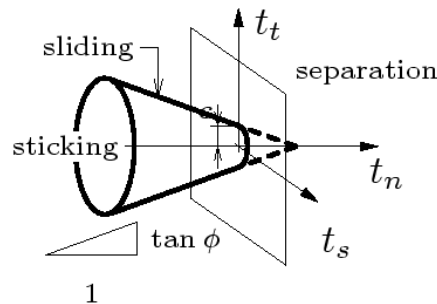


Figure 63: Mechanics of the Coulomb friction interface in DIANA (adopted from (Manie, 2016a))

The sliding is set up according to the failure surface formulated as

$$f_1 = \sqrt{t_t^2 + t_s^2} + \tan \phi t_n - c > 0 \quad (27)$$

with c as the cohesion of the interface, ϕ as the friction angle along the interface and t_s as the tensile strength of the interface. The behavior under compression is described according to Equation (26). For tension behavior, the assigned tensile strength allows for a gap opening. The Coulomb friction interfaces are especially useful when modeling the sliding behavior between elements.

Interface parameters

As stated by the DIANA user manual (see (Manie, 2016a)), it is necessary to specify a relatively high normal stiffness to the interface elements, to avoid interpenetration of the structural element nodes into nodes of the soil elements. The user manual states some general guidelines on assessing these stiffnesses.

The interface stiffnesses are defined as (see (Manie, 2016a))

$$D_{tt} = D_{ss} = \frac{A^2}{t} \frac{E_{soil}}{2(1 + \nu_{soil})} \quad ; \quad D_{nn} = f \times D_{tt} \quad (28)$$

where the Coulomb friction parameters are determined as

$$c = A c_{soil} \quad ; \quad \tan \phi = A \tan \phi_{soil} \quad (29)$$

where A is a reduction factor to render the soil-structure interface weaker and more flexible than the surrounding soil formation, with a range of $0.5 \leq A \leq 1$, t is a small length that represents the virtual thickness of the interfaces, f is a multiplication factor with a range of $10 \leq f \leq 100$ and E_{soil} and ν_{soil} are the Young's modulus and Poisson's ratio of the soil, respectively, c is the cohesion and ϕ is the friction angle.

Interface selection

The selection of the interface can have an influence on the results of the finite element model. In general, the Coulomb friction interfaces are the most sophisticated in describing the behavior of the soil-structure interaction. The stability of the numerical model, however, is also influenced by the interface elements. It can be generally stated that under tension conditions, the Coulomb friction is less stable than the nonlinear elastic interfaces. It is therefore necessary to compare the interface elements for the specific problem, in terms of realistic behavior, as well as numerical stability. The results of a pure lateral push-over are displayed for both interfaces in Figure 64.

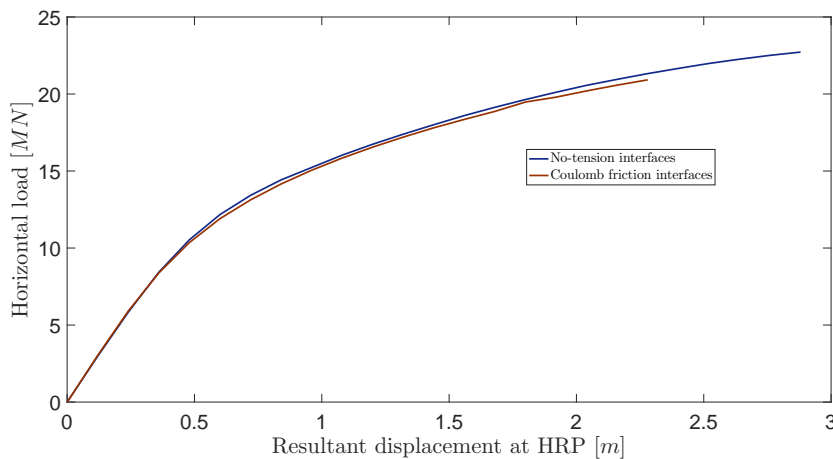


Figure 64: Global response of jack-up unit for pure lateral push-over; interface comparison

It can be observed that both interfaces produce very similar results. This can be explained by considering the loading state of the jack-up foundation. The main difference between both interfaces is the addition of a sliding failure in the Coulomb Friction model. As the foundation is loaded with a high vertical load, and has a significant penetration, it is likely that the horizontal loads applied are taken up by the passive resistance of the soil. This means that the frictional

sliding of the interface is not a large influence. The Coulomb friction interface is less stable than the no-tension interfaces. It shows a divergence at a stage where a failure of the jack-up rig is not expected. The no-tension interfaces perform better in this sense, showing a realistic push-over response during loading. As the results are very similar and the no-tension interface is more stable, the no-tension interface has been selected as a proper way of modelling the interfaces between soil and structure.

C Mesh comparison

The refinement of the mesh used in the finite element model has an influence on the results. In general, it can be stated that a more refined mesh provides a more accurate description. However, as the amount of elements strongly influences computational efforts, a consideration should be made between computational efforts and numerical accuracy. In order to investigate the mesh that is best capable of providing accurate results, in a combination with reasonable computational efforts, a mesh comparison has been made. Three mesh types have been selected, which will be compared: a coarse mesh, an intermediate and a fine mesh. The mesh has been refined in DIANA software in a circular manner, where the mesh coarsens outwards (Figure 65). It should be noted by the reader that the different meshes have been created by making use of quadratic elements in DIANA software, which typically provide better numerical accuracy than standard linear elements.

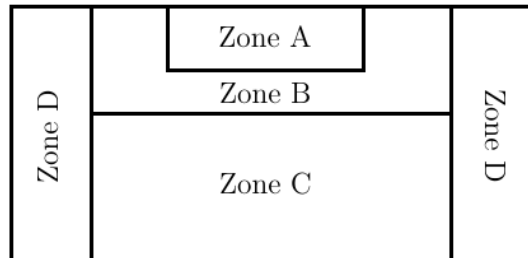


Figure 65: Cross-section of mesh refinement in DIANA

The element sizes of the three meshes that will be compared are displayed in Table 10.

Table 10: Mesh sizes in mesh comparison

Mesh type	Footing element size [m]	Element size [m]			
		Zone A	Zone B	Zone C	Zone D
Coarse	2	4	8	20	20
Intermediate	1	2	4	15	20
Fine	1	1.5	2	15	20

These meshes have been used to perform a pure lateral push-over, using a displacement controlled analysis in DIANA software. The results of the mesh comparison will be displayed using a force-displacement curve (Figure 66). The displacements are shown for the hull reference point (abbreviated as HRP), which is the gravitational center of the topside of the jack-up structure. What can be observed, is that stiffness of the response decreases with mesh refinement. The intermediate mesh offers a large increase in terms of accuracy, when compared to the coarse mesh, whilst the fine mesh shows a small difference with the intermediate mesh. All mesh types show a similar response for the elastic part of the loading. When substantial plasticity is observed, the results of the mesh types differ. For computational convenience, the analyses in this research will be performed using the intermediate mesh. Detailed pictures of the mesh are displayed in Figure 68, Figure 70 and Figure 72.

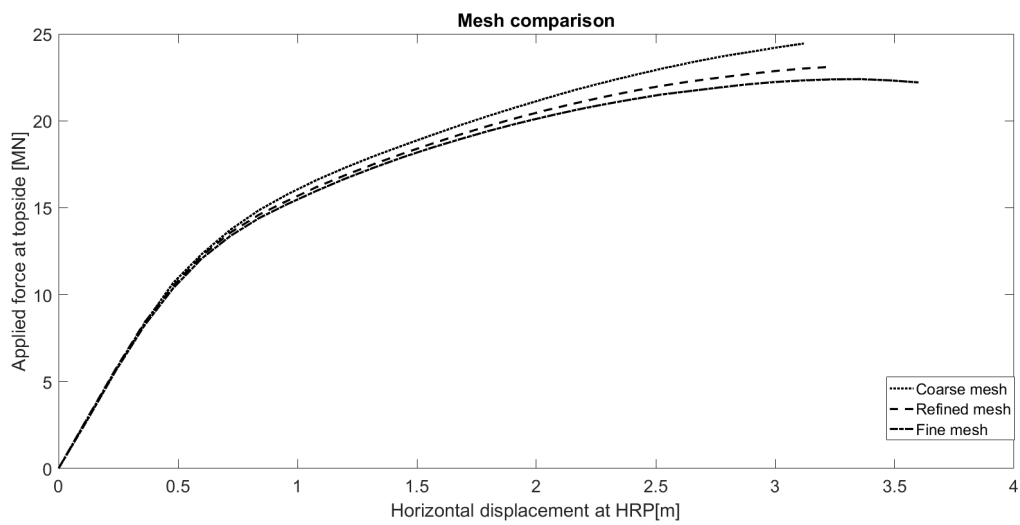


Figure 66: Mesh comparison results from pure lateral push-over using DIANA software

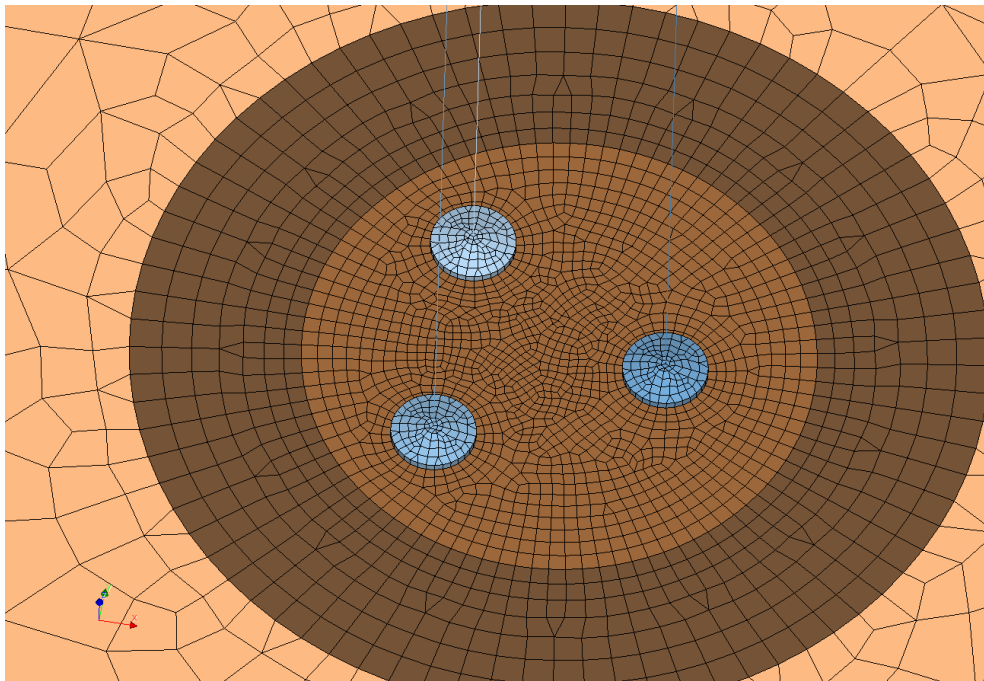


Figure 67

Figure 68: Overview of mesh in DIANA software

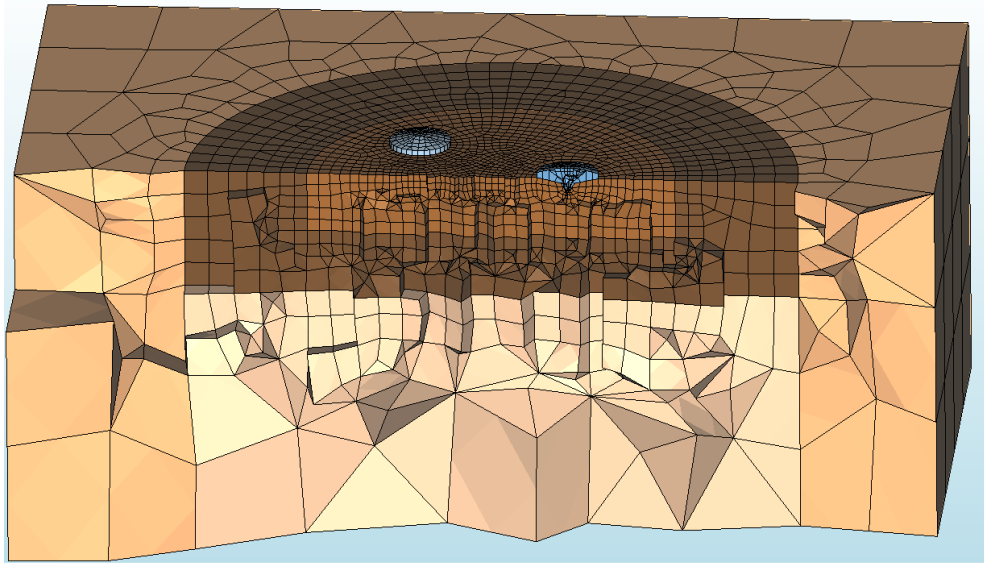


Figure 69

Figure 70: Slice of mesh in DIANA software

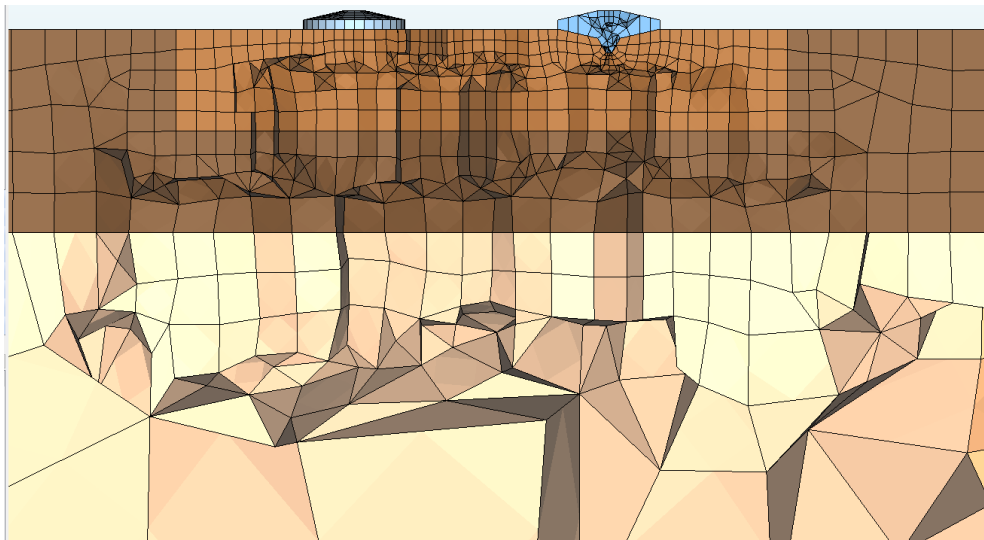


Figure 71

Figure 72: Detailed mesh below spudcans in DIANA software